Boundary Layer Flows and Heat

Transfer of Cross Fluid

By

Mehwish Manzur

Department of Mathematics
Quaid-I-Azam University
Islamabad, Pakistan
2019

Boundary Layer Flows and Heat Transfer of Cross Fluid

By

Mehwish Manzur

Supervised

By

Prof. Dr. Masood Khan

Department of Mathematics
Quaid-I-Azam University
Islamabad, Pakistan
2019

Boundary Layer Flows and Heat Transfer of Cross Fluid

By

Mehwish Manzur

A THESIS SUBMITTED IN THE PARTIAL FULFILLMENT OF THE REQUIREMENT FOR
THE DEGREE OF
DOCTOR OF PHILOSOPHY
IN
MATHEMATICS

Supervised by

Prof. Dr. Masood Khan

Department of Mathematics
Quaid-I-Azam University
Islamabad, Pakistan
2019

Boundary Layer Flows and Heat Transfer of Cross Fluid
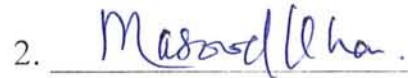
By

Mehwish Manzur

CERTIFICATE

A DISSERTATION SUBMITTED IN THE PARTIAL FULFILLMENT OF THE REQUIREMENTS FOR THE DEGREE OF THE DOCTOR OF

PHILOSOPHY

We accept this dissertation as conforming to the required standard

1. _____
Prof. Dr. Sohail Nadeem
(Chairman)

2. _____
Prof. Dr. Masood Khan
(Supervisor)

3. _____
Prof. Dr. Saleem Asghar
Department of Mathematics
COMSATS University
Park Road Chak Shahzad,
Islamabad

4. _____
Dr. Nasir Ali
Associate Professor
Department of mathematics & Statistics
International Islamic University, Sector
H-10 Islamabad

Department of Mathematics
Quaid-I-Azam University
Islamabad, Pakistan
2019

Certificate of Approval

This is to certify that the research work presented in this thesis entitled **Boundary Layer Flows and Heat Transfer of Cross Fluid** was conducted by Mrs. **Mehwish Manzur** under the kind supervision of **Prof. Dr. Masood Khan**. No part of this thesis has been submitted anywhere else for any other degree. This thesis is submitted to the Department of Mathematics, Quaid-i-Azam University, Islamabad in partial fulfillment of the requirements for the degree of Doctor of Philosophy in field of Mathematics from Department of Mathematics, Quaid-i-Azam University Islamabad, Pakistan.

Student Name: **Mehwish Manzur**   Signature: _____

External committee:

a) **External Examiner 1**:   Signature: _Saleem Asghar_
   Name: **Prof. Dr. Saleem Asghar**
   Designation: Professor
   Office Address: Department of Mathematics, COMSATS University Park road Chak Shahzad, Islamabad.

b) **External Examiner 2**:   Signature: _____
   Name: **Dr. Nasir Ali**
   Designation: Associate Professor
   Office Address: Department of mathematics& Statistics, Faculty of Basics Applied Sciences International Islamic University, Islamabad.

c) **Internal Examiner**   Signature: _Masood Khan._
   Name: **Dr. Masood Khan**
   Designation: Professor
   Office Address: Department of Mathematics, QAU Islamabad.

Supervisor Name: Signature: _Masood Khan._
Prof. Dr. Masood Khan

Name of Dean/ HOD   Signature: _Nadeem_

Prof. Dr. Sohail Nadeem

Author's Declaration

I **Mehwish Manzur** hereby state that my PhD thesis titled **Boundary Layer Flows Heat Transfer of Cross Fluid** is my own work and has not been submitted previously by me for taking any degree from the Quaid-I-Azam University Islamabad, Pakistan or anywhere else in the country/world.

At any time if my statement is found to be incorrect even after my graduate the university has the right to withdraw my PhD degree.

Name of Student: **Mehwish Manzur**

Date: **26-07-2019**

Plagiarism Undertaking

I solemnly declare that research work presented in the thesis titled **"Boundary Layer Flows Heat Transfer of Cross Fluid"** is solely my research work with no significant contribution from any other person. Small contribution/help wherever taken has been duly acknowledged and that complete thesis has been written by me.

I understand the zero tolerance policy of the HEC and **Quaid-i-Azam University** towards plagiarism. Therefore, I as an Author of the above titled thesis declare that no portion of my thesis has been plagiarized and any material used as reference is properly referred/cited.

I undertake that if I am found guilty of any formal plagiarism in the above titled thesis even afterward of PhD degree, the University reserves the rights to withdraw/revoke my PhD degree and that HEC and the University has the right to publish my name on the HEC/University Website on which names of students are placed who submitted plagiarized thesis.

Student/Author Signature: _____

Name: **Mehwish Manzur**

Dedication

To my Parents...

Mr. and Mrs. Manzur Ahmed

and

To my Husband...

Dr. Masood ur Rahman

Acknowledgement

All praise to **ALLAH**, the almighty for providing me this opportunity and granting me the capability to proceed successfully. Peace and Blessing be upon the holy prophet Mohammad (ﷺ), whose way of life has been a continuous guidance for me.

I realized though only my name appears on the cover of this dissertation, a great many people including my family members and my well-wishers have contributed to accomplish this huge task. I would therefore like to offer my sincere thanks to all of them.

First of all I pay my sincere gratitude and a very special thanks to my parents for showing faith in me and giving me liberty to choose what I desired. I salute both of you for the selfless love, care, pain and sacrifice you did to shape my life. I would never be able to pay back the love and affection showered upon by my parents.

I want to express my deep thanks to my esteemed Supervisor **Prof. Dr. Masood Khan** for accepting me as a PhD student and for his warm encouragement, thoughtful guidance, critical comments, and correction of the thesis. I have been extremely lucky to have a supervisor who cared so much about my work, and who responded to my questions and queries so promptly. It would never have been possible for me to take this work to completion without his incredible support and encouragement.

I also dedicate this thesis to my two lovely daughters, *Maryaa Masood Qureshi* and *Maheen Masood Qureshi* who are the pride and joy of my life. I appreciate all your patience and support during mommy's PhD studies. Words would never say how grateful I am to both of you. And finally, I do not know how to begin with saying thank you to my soul mate, my dearest husband

and my best friend, *Dr. Masood ur Rahman*, for being so understanding and for putting up with me through the toughest moments of my life. I thank Allah for enlightening my life with your presence. I consider myself the luckiest in the world to have such a lovely and caring family, standing beside me with their love and unconditional support.

I acknowledge the people who mean a lot to me my sister *Tehmina* and my brothers *Shuaib* and *Awais*, my brother in law *Col. Dr. Naeem* and my sister in law *Sumaira*. Thanks for your selfless love, care and dedicated efforts which contributed a lot for completion of my thesis. My heart felt regard goes to my mother in law for her love and moral support. I can just say thank you for everything and may Allah give you all the best in return.

I thank the Almighty for giving me the strength and patience to work through all these years so that today I can stand proudly with my head held high.

Sincere Regards,

Mehwish Manzur

Dated: 11-07-19.

Table of Contents

Abstract

The study of generalized Newtonian fluid (GNF) is a topic of practical interest in fluid mechanics. The GNF is non-Newtonian in nature, although its constitutive equation is generalized form of Newtonian fluid. Researchers are devoting their studies to explore different subclasses of GNF. Despite of the abundant research work in this field, an important subclass of GNF namely the Cross fluid has not been given due attention. The objective of this research work is to concentrate on the flow and heat transfer characteristics of Cross fluid. The inaugural work has been presented in this thesis by bestowing the boundary layer equations of Cross fluid in different coordinate systems. This has opened new doors for researchers to carry out further research in this direction. In this thesis, a theoretical study is done to explore the flow and heat transfer characteristics of Cross fluid. The reported work presents the modelling of the boundary layer equations of GNF using the Cross viscosity model and further bestows the numerical solution regarding these equations. The current research work covers the flow of Cross fluid past a planer as well as radially stretching sheet and stretching cylinder. Moreover, investigations are done on the mixed convection flow, Falkner-skan flow, nano boundary layer flow and stagnation point flow of Cross fluid. Several effects are taken into consideration including the impact of activation energy, melting phenomenon, linear and non-linear radiation, heat generation/absorption, multiple slip effects, variable thermal conductivity, Newtonian heat and mass conditions. The modelled problems are numerically handled by two numerical techniques namely the shooting method and bvp4c in MATLAB. The results presented in this thesis are verified by making comparison with already available results in literature for reduced cases and excellent compatibility is achieved. From the obtained results, it is observed from that the

progressive value of the local Weissenberg number reduces the velocity distribution while the temperature of the fluid rises. However, quite an opposite trend is exhibited by velocity and temperature profiles for growing values of the power-law index.

Chapter 1

Research Context and Outline

The present chapter being the introductory chapter of this thesis provides a theoretical foundation for the present research work. A precise literature about the subject matter has been mentioned which paves the way for better understanding of the phenomenon of flow together with heat transfer aspects of non-Newtonian fluid particularly the Cross fluid. The basic conservation laws are stated which contributed in constructing the governing equations mentioned in the disquisition. In addition, boundary layer equations of Cross fluid are introduced in Cartesian as well as in cylindrical polar coordinates which will facilitate the future research in fluid mechanics. The numerical methodologies are also described which are exploited for attaining solutions. Moreover, a brief layout of the thesis is also presented with a chapter wise short description.

1.1   Research Background

The generalized Newtonian fluids have attained prominence on account of their abundant practicalities in mechanisms of industrial and technological importance. In the generalized Newtonian fluids (GNF) $[1 - 2]$ the viscosity is shear dependent as a result of which a new constitutive relation is defined by making modifications in Newton's law of viscosity to account for change in viscosity with varying shear rate. One of the simplest type of GNF is the power-law fluid [3] which tenders a simplest

representation of the shear-thinning/thickening behaviors of several fluids. Despite of abundant process engineering applications, the main limitation of the power-law fluid is that it cannot describe the behavior of the fluid for very low along with very high shear rates but only for limited range of shear rate called power-law region. If deviation from power-law model is notable solely at very low shear rate, Ellis model [4] is utilized. Likewise, Sisko model [5] characterizes the flow of fluids in the power-law and very high shear rate region. The problems which were showed up by above mentioned rheological models were tackled by a broader sub-class of the generalized Newtonian fluids namely the Cross model, introduced by Cross [6] in 1965. This model is competent of depicting the flow in the power-law region as well as the zones of very low together with very high shear rates. In contrast with power-law fluid, the viscosity would not become undefined even when shear rate gets zero ($\dot{\gamma} = 0$) and in addition to that due to the involvement of a time constant it is greatly employed in engineering calculations. Cross model is widely used in the synthesis of various polymeric solutions like 0.35% aqueous solution of Xanthan gum, blood, aqueous solution of polymer latex sphere, 0.4% aqueous solution of polyacrylamide [7]. The Cross rheology equation [8, 9] for viscosity in terms of shear rate is provided by:

$$\eta^* = \eta_\infty + (\eta_0 - \eta_\infty)\left[\frac{1}{1 + (\Gamma\dot{\gamma})^m}\right], \tag{1.1}$$

or equivalently,

$$\frac{\eta_0 - \eta^*}{\eta^* - \eta_\infty} = (\Gamma\dot{\gamma})^m, \tag{1.2}$$

where η_0 and η_∞ are limiting viscosities at low and high shear rates, respectively, Γ is the material Cross time constant, m the dimensionless constant, commonly known as the flow behavior index and $\dot{\gamma} = \sqrt{1/2\,\Pi}$ the shear rate with Π the second invariant strain rate tensor. In 1965 Cross [6] presented an experimental data for many systems by using a simple value $m = 2/3$ but he clearly stated that there is no hindrance in treating m as an adjustable parameter [10]. This model predicts the usual Newtonian fluid if $\Gamma = 0$.

It is interesting to note that by making certain approximation to the Cross equation, we can achieve various other popular viscosity models like the well-known power-law model, the Sisko model and even Bingham model. When $\eta^* \ll \eta_0$ and $\eta^* \gg \eta_\infty$, the Cross equation (1.2) reduces to

$$\eta^* = K_1/(\dot{\gamma})^m, \tag{1.3}$$

which is the well-known power-law model with K_1 the consistency index while m the power-law index.

Furthermore, if $\eta^* \ll \eta_0$, we get

$$\eta^* = \eta_\infty + K_1/(\dot{\gamma})^m, \tag{1.4}$$

which is the renowned Sisko rheological model.

Further, by setting $m = 1$ in Sisko model and by slight redefinition of parameters

we attain

$$\eta^* = \mu_B + \sigma_0\dot{\gamma}, \tag{1.5}$$

which represents the Bingham model [11] such that μ_B is the Bingham plastic viscosity and σ_0 is the Bingham yield stress.

In the last two decades experimental based study is done on the Cross model by several investigators. An experimental analysis was performed by Escudier *et al.* [12] by adjusting the Cross model for non-Newtonian liquid specifically the Xanthan gum (XG). Xie and Jin [13] used Cross rheology equation to explore the free surface flow of widely known non-Newtonian fluids. The Cross equation was handled by numerical method namely the WC-MPS method to analyze the four rheology parameters of the Cross model.

The problems referring to boundary layer flow together with transfer of heat in view of stretching surfaces have been highly acknowledged by investigators due to their occurrence in mechanisms of great technological importance. The wide spread applications include the drawing of plastic sheets and copper wires, glass-fiber manufacturing, polymer as well as food processing, geothermal energy extraction, drawing of rubber, melting-spinning processes, polymer melts, hot rolling and abundant other pertinence. The amount of cooling and stretching renders significant part in monitoring the features of the final product. Boundary layer flow in consideration of moving surface with constant speed was first implemented by Sakiadis [14]. After that, Crane [15] extended the concept of boundary layer flow by taking into account the stretching surfaces. A closed form solution is presented for viscous fluid over a planar stretching sheet. The outcomes of boundary layer problem

of power-law fluid for the stretching wall problem were presented by Banks [16]. After these pioneering attempts, the research in the direction of stretching surfaces was immensely done by various investigators [17 − 19]. An overlook of the literature reveals that much work is reported on the subject of boundary layer flows past planar stretching sheet in comparison with radially stretching sheet. However, with each passing decade the process of axisymmetric flow over a radially stretching sheet is emerging as a topic of eminent interest among researchers. Ariel [20] made an initial attempt in this direction by considering an axisymmetric flow in fluid by incorporating partial slip at the boundary. The work bestowed by Sajid et al. [21] is associated with the axisymmetric flow in viscous fluid by considering stretching boundary and gave analytical solution of concerned problem. Shahzad et al. [22] explored exact solution owning to boundary layer flow together with heat transfer of MHD viscous fluid over a non-linearly radially porous stretching sheet. Further work in the respect of radially stretching sheet by taking the Sisko model in consideration was reported by Khan et al. [23].

During last few years, nanotechnology has been widely enchanted by scientists due to its peculiar physical and chemical properties. A nanofluid comprises of nanometer sized particles $(1 − 100\ nm)$ held in base fluid. Nanofluid generally includes up to 5% by volume fraction of nano-scale particles to ensure high thermal conductivity of fluid. The principal advantage of practicing nanotechnology is that fluids thermal conductivity is enriched by including nanoparticles. Moreover, the blocking in flow passage is also insubstantial. Additionally, nanofluids are endowed with long lasting stability and homogeneity. Due to these noteworthy features,

boundary condition for the modified second grade fluid model and computed stretching sheet solutions by the help of a numerical technique.

Magnetohydrodynamic (MHD) is substantial in multitudinous physical situations since the applications of applied magnetic field regulate the mechanics of the system but also influences the thermodynamics extensively. Its wide scale applications in the field of medicine includes the magnetic resonance imaging, decreasing the blood loss in severe injuries, tumor treatment and abundant other. The industrial and technological applications include the MHD power generators, crystal growth process, cooling of fission reactors, electronic packages, oil exploration, sunspot development and abundant other applications in plasma studies, aerodynamics and thermal engineering. Sarpkaya [32] did pioneering work on the implication of magnetic field on account of non-Newtonian fluids. Pavlov [33] explored the magnetohydrodynamic flow of viscous fluid by considering deformation of a plane surface. Andersson [34] examined flow of viscoelastic by considering transverse magnetic field. Vajravelu and Prasad [35] examined a hydromagnetic flow together with transfer of heat in power-law fluid by viewing a stretching surface.

Stagnation point is regarded as a point at the surface of object at which fluid particles attain zero velocity with respect to the object. The static pressure is highest at the stagnation point due to zero velocity which is guaranteed by Bernoulli equation. Stagnation point flow is involved in number of appealing phenomena like the blood flow within in the junction inside arteries, cooling of papers, glass blowing, cable covering, flows at the tips of spaceships and many more. The very first attempt on

this subject was done by Heimenz [36]. Homann [37] extended this work for the axisymmetric case. Chiam [38] presented his work on the stagnation point flow in viscous fluid which was further extended by Mahapatra [39] by taking the heat transfer analysis in account. Later, Mahapatra et al. [40] explored stagnation point flow of MHD power-law fluid and presented analytical solutions of the problem. Noreen et al. [41] examined stagnation point flow of MHD nanofluid affected by thermal radiation and convective boundary.

In recent times, notable attention has been imparted on the flow situations involving the simultaneous effect of forced and free convection, that is, the mixed convection. It is a heat transfer mechanism which emerges as a result of some external applied forces and by the difference in fluid temperature at various locations. Mixed convection heat transfer has secured pertinence in science and technology due to its multitudinous applications including nuclear reactors, solar energy systems, heat exchangers and so on. Abundant work has been compiled by various researchers on mixed convective heat transfer by considering various fluid models and different geometries. However, before granting new work in this field it is informative to present a brief literature review. Wang [42] performed the numerical computations in order to analyze mixed convection of power-law fluid and computed non-similar results of the considered problem. Mixed convective flow beyond a vertical stretching sheet was explored by Chen [43] and thus presented the numerical solution by finite difference method. The same author [44] also probed the issue of magneto-hydrodynamic mixed convection flow of well-known power-law model making allowance of heat generation/absorption. Turkyilmazoglu [45] analytically solved the

problem of mixed convective transfer of heat in MHD viscoelastic fluid over a vertically stretching sheet in a porous medium. Recent investigations that emphasize on the concept of mixed convective heat transfer are witnessed in literature [46 − 48].

The application of convective boundary condition in heat transfer analysis has found diversified applications in technology embodying thermal energy storage, petroleum processing, material drying etc. Recently, various heat transfer problems are revised by incorporating convective boundary condition instead of usual conditions of constant temperature together with constant flux at boundary. Aziz [49] worked on the flow towards a flat plate along with convective boundary condition and calculated the similarity solution. A comprehensive work on hydromagnetic mixed convection flow over a vertical plate by incorporating convective heat exchange on the surface was performed by Makinde and Aziz [50]. Notable attempts are made on convective boundary condition until now and a few of them could be seen in references [51 − 53].

Newtonian heating process takes place in conjugate convective flows in which heat transportation occurs via boundary surface of finite heat capacity to local surface temperature. It has gained the attention of numerous researches owning to the fact that it plays significant role in many mechanisms like conjugate heat transport, heat exchangers, nuclear turbines and petroleum industry. Merkin [54] was the pioneer who inspected the Newtonian heating effect on boundary layer flow past a vertical surface. Salleh et al. [55] studied the consequence of Newtonian heating condition by

exploring the phenomenon of flow along with transfer of heat in viscous fluid. Recently, Rahman et al. [56] probed the consequence of homogenous-heterogenous reactions in modified second grade by considering the Newtonian heating effect. The combine Newtonian heat and mass condition was utilized by Qayyum et al. [57] for stagnation point flow by taking Walters-B nanofluid. Hayat et al. [58] examined Newtonian heating on a nanofluid past a permeable cylinder.

The traditional no-slip boundary condition suggests zero velocity of the fluid near solid walls with respect to the solid boundaries. Although, no-slip boundary condition was efficiently invoked by researchers in many significant problems, but it becomes ineffective for many non-Newtonian fluids like polymers melts, emulsions, gels, slurries, foams, particularly in highly confined geometries. Moreover, the no-slip boundary is inadequate for investigation of micro-scale fluid dynamics. Such problems were overcome by suggestion of slip flow model by Navier [59] which was an efficient replacement to conventional no slip boundary condition. According to which, the amount of slip at solid surface is directly proportional to the tangential stress. It founds abundant applications in electrochemical and polymer industry. The initial experimental work in account of slip was done by Schnell [60]. Andersson [61] investigated the slip flow on account of a stretching surface. Turkyilmazoglu [62] computed the exact solution related to heat along with mass transfer processes in MHD nanofluid in view of slip condition. Ellahi and Hameed [63] worked on the non-Newtonian flows and also on heat transfer aspects by considering slip effects. Ibrahim and Shankar [64] examined the velocity, thermal and also solutal slip boundary conditions to MHD flow in nanofluid.

Melting heat transfer is nowadays a field of chief consideration on account of its immense role in processes like welding, crystal growth, extrusion of metals and polymers, phase change material, magma solidification, freeze treatment of sewage, the melting of permafrost, frozen ground thawing etc. Robert [65] did the initial work on the melting heat process by considering the ice slab situated in a hot air stream. Epstein and Cho [66] worked on the steady laminar flow and melting heat transfer across a flat plate. Chen *et al.* [67] discussed the free convection melting of a solid immersed in a hot dissimilar solution. Bakier [68] considered mixed convection flow past a vertical flat plate embedded in a porous medium by contemplating the effects of melting heat transfer. Ishak *et al.* [69] researched on the melting phenomenon on the laminar flow and computed the dual solutions by the help of numerical technique. The impact of the melting heat transfer in consideration of stagnation point flow has been explored for various fluid models [70 – 71]. Recently, Hashim *et al.* [72] numerically solved the issue of melting heat transfer while considering the Carreau fluid past a stretching cylinder.

In majority of problems including the heat transfer phenomenon, the thermophysical properties of fluids are supposedly treated as constant, although many quantities possess variable behavior in more realistic situations. Thermal conductivity is one such property which characterizes the ability of a substance to conduct heat but for majority of the problems it is usually assumed to be constant. However, in practical cases it changes by varying temperature in nearly linear mode. Chiam [73] presented his work on heat transfer analysis on stagnation point flow by incorporating variable thermal conductivity. Chiam [74] further worked on the variable thermal

conductivity by investigating the behavior of Newtonian fluid near a porous stretching sheet with blowing/suction. Vajravelu *et al.* [75] performed numerical investigation on unsteady convective flow considering viscous fluid by taking variable fluid properties.

The inclusion of heat generation or absorption phenomenon play remarkable role in heat transfer investigation as they alter the temperature distributions prominently. It plays eminent role in numerous applications like electronic chips, metal waste, rocket engine, nuclear fuel, fire and combustion studies. Vajravelu and Nayfeh [76] contemplated heat generation or absorption in a viscous fluid near a cone and a wedge. Sheikh and Abbas [77] computed the MHD flow past an oscillatory stretching surface together with heat generation/absorption and chemical reaction. Hayat *et al.* [78] calculated analytic solution regarding magnetohydrodynamic Oldroyd-B nanofluid by taking note of heat generation/absorption.

The role of thermal radiation in heat transfer analysis is effective in many technological and engineering fields including thermal engineering, propulsion engineering, mechanical engineering, aeronautics and much more. It is practically employed in the designing of gas turbines, heat exchangers, space vehicles and nuclear power plants. Mohammadein and Amin [79] investigated the effect of thermal radiation during the buoyancy induced flow of power-law fluid past a flat plate in a porous media. Khan [80] invoked thermal radiation in a viscoelastic flow by considering suction/blowing. Cortell [81] devoted his study to investigate the flow along with transfer of heat by considering power-law fluid across a semi-infinite

porous flat plate subject to suction. He examined the energy equation by including both the thermal radiation along with viscous dissipation effects and solved the related problem numerically. Literature survey discloses that abundant work has been done in last few decades on the thermal radiation by incorporating the linearized Rosseland approximation but the main drawback of this linearized form is that it is not effective for the situation involving a high temperature difference among the fluid and plate. In order to overcome this barrier, the non-linear Rosseland approximation is employed by scientists due to its peculiar characteristics. The usage of non-linear form of Rosseland approximation results in the appearance of three dimensionless parameters in the heat equation namely the Prandtl number, temperature ratio parameter and the radiation parameter. Pantokratoras and Fang [82] invoked the non-linear Rosseland approximation for the first time to examine the Sakiadis flow along with transfer of heat along a moving plate. Following this work, Cortell [83] did a numerical analysis on the flow and also on heat transfer towards a stretching surface by incorporating the non-linear thermal radiation effects. Mushtaq *et al.* [84] numerically handled stagnation point flow together with heat transfer by considering viscous nanofluid by using non-linear thermal radiation effects.

Recently, considerable attention has been bestowed on the theoretical as well as experimental work based on diffusion of species in chemical reactions. The analysis on chemical reactions found substantial pertinence in various chemical industries and technological innovations. A few of the major applications can be listed as energy transfer in cooling tower, geothermal reservoir, dispersion of fog, cleaning and processing of materials, oil recuperation, nuclear reactor cores and underground

energy transport. Chemical reactions are generally grouped as either heterogeneous or homogeneous reactions provided they occur at an interface or in the form of a single-phase volume reaction. The reaction rate of a chemical reaction relies on concentration of specie itself. In first order chemical reaction, the rate at which the chemical reaction occurs is directly proportional to species concentration [85]. Das [86] contemplated the topic of heat along with mass transfer of magneto-micropolar fluid and made conclusions about the role of chemical reaction and thermal radiation too. In the same year, Bhattacharyya [87] computed dual solutions for viscous fluid by checking the effect of chemically reactive species.

The study of Arrhenius activation energy subject to mass transfer analysis finds important applications in chemistry, physics and engineering fields. In fact activation energy serves as the least amount of energy necessary to initiate a chemical reaction. A few of many applications include the cooling of nuclear reactors, geothermal reservoirs and recovery of thermal oil, food processing, thermal insulation and many more. Despite of its wide scale applications in fluid mechanics not much work has been reported in this regard. The pioneering work in this field was done by Bestman [88]. He computed the natural convection flow, heat and also mass transfer in porous medium for quite simple model embodying binary chemical reaction along with Arrhenius activation energy. Makinde et al. [89] examined the unsteady convection by incorporating n^{th} order chemical reaction besides with Arrhenius activation energy over a flat porous plate. Maleque [90, 91] worked on Arrhenius activation energy during mass transfer by taking different effects. Awad et al. [92] scrutinized the problem in which he considered activation energy in an unsteady rotating fluid.

Mustafa *et al*. [93] established the results regarding enforcement of activation energy in MHD nanofluid flow.

In the present world of technology, the Falkner-Skan flow has amassed tremendous fame due to its practicality in hydrodynamics as well as in aerodynamics. The usance of flows past wedge shaped geometries appears to be requisite in variant fields which include enriched oil recoveries, geothermal industries, storage of nuclear waste, and sundry other applications. Falkner and Skan [94] presented the Falkner-Skan boundary layer equation with stream-wise pressure gradient. Hartree [95] scrutinized the dependence of the solutions of these equations on the parameter of stream-wise pressure gradient. Rajagopal [96] probed the Falkner-Skan wedge flow of second grade fluid in which wedge was placed symmetrically to the direction of flow. The MHD flow together with transfer of heat over a static moving wedge saturated in a nanofluid was explored by Nadeem *et al*. [97]. Hashim *et al*. [98] performed several computations on the unsteady flow of Williamson nanofluid across a wedge geometry and explored the heat as well as mass transfer characteristics.

Fluid flow along cylinder body has secured special attention in fluid mechanics. Generally, the flow over a cylinder is regarded two-dimensional when the radius of the cylinder overshoots in contrast with the boundary layer thickness. However, if we take the case of thin or slender cylinder the flow is termed as axisymmetric since the cylinder radius together with boundary layer thickness are taken of same order. The usage of slender bodies offer lesser drag as a result they are applicable in mechanisms like hot rolling, polymer spinning, fiber drawing liquid coating in photography films,

heat exchangers, etc. Initially, the work in the direction of stretching cylinder for viscous fluid case was specified by Wang [99]. Ishak *et al.* [100] investigated the flow and also heat transfer in electrically conducting fluid outside stretching cylinder. Numerical investigations are made by Ishak and Nazar [101] to examine the axisymmetric flow of viscous fluid towards a stretching cylinder. Kaya [102] efficiently described the issue of heat along with mass transfer over a horizontal slender cylinder subjected to transverse magnetic field.

1.2 Basic Conservation Equations of Fluid Mechanics

1.2.1 Equation for Mass Conservation

Mathematically, mass conservation law can be stated as:

$$\frac{\partial \rho}{\partial t} + \nabla.\left(\rho V\right) = 0. \tag{1.6}$$

In the above equation, ρ stands for the density of fluid while V represents the velocity field.

If the fluid is considered as incompressible then Eq. (1.6) turns into:

$$\nabla.V = 0. \tag{1.7}$$

1.2.2 Equation for Momentum Conservation

The law governing the conservation of linear momentum is formulated as:

$$\rho \frac{dV}{dt} = \nabla.\tau + \rho b, \tag{1.8}$$

where τ denotes the Cauchy stress tensor, $\frac{d}{dt}$ the material time derivative and $\boldsymbol{b}$ the body force.

For steady flow and in the absence of body force, above expression reduces to:

$$\rho[(\boldsymbol{V}.\nabla)\boldsymbol{V}] = \nabla.\tau. \tag{1.9}$$

1.2.3 Equation for Energy Conservation

We can formulate the law of conservation of energy as:

$$\rho c_p \frac{dT}{dt} = \tau.\boldsymbol{L} - \nabla.\boldsymbol{q} - \nabla.\boldsymbol{q}_r, \tag{1.10}$$

where T symbolizes fluids temperature, c_p the specific heat at constant pressure and $\boldsymbol{q}_r$ the radiative heat flux. Moreover, $\boldsymbol{L}$ stands for velocity gradient and $\boldsymbol{q}$ denotes thermal heat flux defined as:

$$\boldsymbol{L} = \nabla \boldsymbol{V}, \boldsymbol{q} = -k\,\nabla T, \tag{1.11}$$

such that k is used for thermal conductivity of fluid.

Relation (1.10) can be reduced for steady flow as:

$$\rho c_p[(\boldsymbol{V}.\nabla)T] = \tau.\boldsymbol{L} + k\,\nabla^2 T - \nabla.\boldsymbol{q}_r. \tag{1.12}$$

1.2.4 Equation for Concentration Conservation

The law of conservation of concentration can be mathematically written as:

$$\frac{dC}{dt} = -\nabla.\boldsymbol{J} + \boldsymbol{R}. \tag{1.13}$$

In aforementioned equation, C constitutes fluids concentration, R the chemical reaction while J the normal mass flux given by Fick's first law as:

$$J = -D\nabla C, \tag{1.14}$$

where D is the mass diffusivity.

For steady flow and in the absence of chemical reaction, Eq. (1.13) becomes

$$(V.\nabla)C = D\nabla^2 C. \tag{1.15}$$

1.2.5 Equation for Energy Conservation of Nanofluid

Mathematically, the law for conservation of energy considering an incompressible nanofluid is:

$$\rho c_p \frac{dT}{dt} = -\nabla.q - h_p\nabla.J_p. \tag{1.16}$$

where h_p is the specific enthalpy for nanofluid. While q and J_p denote the thermal flux for nanofluid and nanoparticle diffusive mass flux, respectively, given by:

$$q = -k\,\nabla T + h_p J_p, \qquad J_p = -\rho_p D_B \nabla C - \rho_p D_T \frac{\nabla T}{T_\infty}, \tag{1.17}$$

such that C represents the nanoparticle volume fraction, ρ_p the density of nanoparticles, D_B and D_T, respectively, imply the Brownian motion parameter and thermophoretic diffusion coefficient.

Using Eq. (1.17) in Eq. (1.16) and for the case of steady flow we obtain:

$$\rho c_p [(V.\nabla)T] = k \nabla^2 T + \rho_p \rho c_p \left[D_B \nabla C. \nabla T + D_T \frac{\nabla T. \nabla T}{T_\infty} \right]. \qquad (1.18)$$

1.2.6 Equation for Concentration Conservation of Nanofluid

The law of conservation of concentration for an incompressible nanofluid can be written as:

$$\frac{dC}{dt} = -\frac{1}{\rho_p} \nabla. J_p. \qquad (1.19)$$

On using relation (1.17) and for steady flow case we get:

$$(V.\nabla)C = D_B \nabla^2 C + D_T \frac{\nabla^2 T}{T_\infty}. \qquad (1.20)$$

1.3 Mathematical Modelling

1.3.1 Boundary Layer Equations for Cross Fluid in Cartesian Coordinates

We model boundary layer equations concerning two-dimensional flow for an incompressible Cross fluid in Cartesian coordinates (x, y, z). We choose the velocity and stress field such that:

$$V = [u(x, y), v(x, y), 0], \qquad (1.21)$$

where (u, v) are velocity components in (x, y) directions, respectively.

The Cauchy stress tensor for the four parameter fluid model is:

$$\tau = -p\mathbf{I} + \eta^* A_1, \qquad (1.22)$$

where $\mathbf{I}$ the identity tensor and p is pressure while the constitutive relation for apparent viscosity η^* in Cross fluid provided by:

$$\eta^* = \eta_\infty + (\eta_0 - \eta_\infty)\left[\frac{1}{1 + (\Gamma\dot{\gamma})^m}\right]. \tag{1.23}$$

The first Rivlin-Ericksen tensor $\mathbf{A_1}$, the shear rate $\dot{\gamma}$ with Π being the second invariant strain rate tensor are, respectively, defined as:

$$\mathbf{A_1} = \mathbf{L} + \mathbf{L^T}, \ \dot{\gamma} = \sqrt{^1/_2\,\Pi}, \ \Pi = tr(\mathbf{A_1^2}). \tag{1.24}$$

The infinite shear rate viscosity η_∞ is frequently set equal to zero [103] in Eq. (1.23) and accordingly Eq. (1.22) becomes:

$$\tau = -p\mathbf{I} + \eta_0\left[\frac{1}{1 + (\Gamma\dot{\gamma})^m}\right]\mathbf{A_1}. \tag{1.25}$$

The shear rate $\dot{\gamma}$ can be determined by the help of Eq. (1.21) as:

$$\dot{\gamma} = \left[\left(\frac{\partial v}{\partial x} + \frac{\partial u}{\partial y}\right)^2 + 4\left(\frac{\partial u}{\partial x}\right)^2\right]^{\frac{1}{2}}. \tag{1.26}$$

The continuity equation (1.7) and momentum equation (1.9) in the absence of body force are given by:

$$\frac{\partial u}{\partial x} + \frac{\partial v}{\partial y} = 0, \tag{1.27}$$

$$\rho\left(u\frac{\partial u}{\partial x} + v\frac{\partial u}{\partial y}\right) = \frac{\partial \tau_{xx}}{\partial x} + \frac{\partial \tau_{xy}}{\partial y}, \tag{1.28}$$

$$\rho\left(u\frac{\partial v}{\partial x} + v\frac{\partial v}{\partial y}\right) = \frac{\partial \tau_{yx}}{\partial x} + \frac{\partial \tau_{yy}}{\partial y}, \tag{1.29}$$

where the stress components τ_{xx}, τ_{xy}, τ_{yx} and τ_{yy} can be calculated by the help of

Eq. (1.25) as:

$$\tau_{xx} = 2\eta_0 \frac{\partial u}{\partial x} \left[\frac{1}{1 + \left\{ \Gamma^2 \left(4\left(\frac{\partial u}{\partial x}\right)^2 + \left(\frac{\partial v}{\partial x} + \frac{\partial u}{\partial y}\right)^2 \right) \right\}^{\frac{m}{2}}} \right], \qquad (1.30)$$

$$\tau_{xy} = \tau_{yx} = \eta_0 \left(\frac{\partial v}{\partial x} + \frac{\partial u}{\partial y} \right) \left[\frac{1}{1 + \left\{ \Gamma^2 \left(4\left(\frac{\partial u}{\partial x}\right)^2 + \left(\frac{\partial v}{\partial x} + \frac{\partial u}{\partial y}\right)^2 \right) \right\}^{\frac{m}{2}}} \right], \qquad (1.31)$$

$$\tau_{yy} = 2\eta_0 \frac{\partial v}{\partial y} \left[\frac{1}{1 + \left\{ \Gamma^2 \left(4\left(\frac{\partial u}{\partial x}\right)^2 + \left(\frac{\partial v}{\partial x} + \frac{\partial u}{\partial y}\right)^2 \right) \right\}^{\frac{m}{2}}} \right]. \qquad (1.32)$$

Substitution of the stress components mentioned in Eqs. $(1.30 - 1.32)$ in Eqs. (1.28)

and (1.29) yield:

$$\rho \left(u \frac{\partial u}{\partial x} + v \frac{\partial u}{\partial y} \right) = -\frac{\partial p}{\partial x} + 2\eta_0 \frac{\partial}{\partial x} \left[\frac{\frac{\partial u}{\partial x}}{1 + \left\{ \Gamma^2 \left(\left(\frac{\partial v}{\partial x} + \frac{\partial u}{\partial y}\right)^2 + 4\left(\frac{\partial u}{\partial x}\right)^2 \right) \right\}^{\frac{m}{2}}} \right]$$

$$+ \eta_0 \frac{\partial}{\partial y} \left[\frac{\left(\frac{\partial v}{\partial x} + \frac{\partial u}{\partial y}\right)}{1 + \left\{ \Gamma^2 \left(\left(\frac{\partial v}{\partial x} + \frac{\partial u}{\partial y}\right)^2 + 4\left(\frac{\partial u}{\partial x}\right)^2 \right) \right\}^{\frac{m}{2}}} \right], \qquad (1.33)$$

$$\rho\left(u\frac{\partial v}{\partial x}+v\frac{\partial v}{\partial y}\right)=-\frac{\partial p}{\partial y}+\eta_0\frac{\partial}{\partial x}\left[\frac{\left(\frac{\partial v}{\partial x}+\frac{\partial u}{\partial y}\right)}{1+\left\{\Gamma^2\left(\left(\frac{\partial v}{\partial x}+\frac{\partial u}{\partial y}\right)^2+4\left(\frac{\partial u}{\partial x}\right)^2\right)\right\}^{\frac{m}{2}}}\right]$$

$$+2\eta_0\frac{\partial}{\partial y}\left[\frac{\frac{\partial v}{\partial y}}{1+\left\{\Gamma^2\left(\left(\frac{\partial v}{\partial x}+\frac{\partial u}{\partial y}\right)^2+4\left(\frac{\partial u}{\partial x}\right)^2\right)\right\}^{\frac{m}{2}}}\right]. \quad (1.34)$$

The above equations of motion are made dimensionless through the following relations:

$$(x,y)=L(x^*,y^*),(u,v)=U(u^*,v^*)\text{ and }p=\rho U^2 p^*. \quad (1.35)$$

Writing aforementioned equations based on dimensionless variables, we achieve:

$$\frac{\partial u^*}{\partial x^*}+\frac{\partial v^*}{\partial y^*}=0, \quad (1.36)$$

$$\rho\left(u^*\frac{\partial u^*}{\partial x^*}+v^*\frac{\partial u^*}{\partial y^*}\right)=-\frac{\partial p^*}{\partial x^*}+2\epsilon_1\frac{\partial}{\partial x^*}\left[\frac{\frac{\partial u^*}{\partial x^*}}{1+\left\{\epsilon_2\left(4\left(\frac{\partial u^*}{\partial x^*}\right)^2+\left(\frac{\partial v^*}{\partial x^*}+\frac{\partial u^*}{\partial y^*}\right)^2\right)\right\}^{\frac{m}{2}}}\right]$$

$$+\epsilon_1\frac{\partial}{\partial y^*}\left[\frac{\left(\frac{\partial v^*}{\partial x^*}+\frac{\partial u^*}{\partial y^*}\right)}{1+\left\{\epsilon_2\left(4\left(\frac{\partial u^*}{\partial x^*}\right)^2+\left(\frac{\partial v^*}{\partial x^*}+\frac{\partial u^*}{\partial y^*}\right)^2\right)\right\}^{\frac{m}{2}}}\right], \quad (1.37)$$

$$\rho\left(u^*\frac{\partial v^*}{\partial x^*} + v^*\frac{\partial v^*}{\partial y^*}\right) = -\frac{\partial p^*}{\partial y^*} + \epsilon_1\frac{\partial}{\partial x^*}\left[\frac{\left(\frac{\partial v^*}{\partial x^*} + \frac{\partial u^*}{\partial y^*}\right)}{1 + \left\{\epsilon_2\left(4\left(\frac{\partial u^*}{\partial x^*}\right)^2 + \left(\frac{\partial v^*}{\partial x^*} + \frac{\partial u^*}{\partial y^*}\right)^2\right)\right\}^{\frac{m}{2}}}\right]$$

$$+2\epsilon_1\frac{\partial}{\partial y^*}\left[\frac{\frac{\partial v^*}{\partial y^*}}{1 + \left\{\epsilon_2\left(4\left(\frac{\partial u^*}{\partial x^*}\right)^2 + \left(\frac{\partial v^*}{\partial x^*} + \frac{\partial u^*}{\partial y^*}\right)^2\right)\right\}^{\frac{m}{2}}}\right], \quad (1.38)$$

where the dimensionless parameters are defined as:

$$\epsilon_1 = \frac{\eta_0/\rho}{LU} \text{ and } \epsilon_2 = \frac{\Gamma^2}{\left(L/U\right)^2}. \quad (1.39)$$

Using the standard boundary layer assumptions, where x, u, p are of order 1 while v and y are of order δ. The dimensionless parameters ϵ_1 and ϵ_2 are of order δ^2.

Keeping in view the boundary layer analysis, we attain:

$$\frac{\partial u}{\partial x} + \frac{\partial v}{\partial y} = 0, \quad (1.40)$$

$$u\frac{\partial u}{\partial x} + v\frac{\partial u}{\partial y} = -\frac{1}{\rho}\frac{\partial p}{\partial x} + \vartheta\frac{\partial}{\partial y}\left[\frac{\frac{\partial u}{\partial y}}{1 + \left\{\Gamma\left(\frac{\partial u}{\partial y}\right)\right\}^m}\right], \quad (1.41)$$

$$0 = -\frac{1}{\rho}\frac{\partial p}{\partial y}, \quad (1.42)$$

where $\vartheta\left(= \eta_0/\rho\right)$ gives the kinematic viscosity.

1.3.2 Boundary Layer Equations for Cross Fluid in Cylindrical Polar Coordinates

Here we derive boundary layer equations considering Cross fluid in cylindrical polar coordinates (r, θ, z). We model the equation for two-dimensional axisymmetric flow and because of rotational symmetry all physical quantities will be regarded independent of θ.

We take velocity and stress field of the type:

$$V = [u(r,z), 0, w(r,z)], \qquad \tau = \tau(r,z), \tag{1.43}$$

where u and w are velocity components along radial and axial directions, respectively.

In view of Eq. (1.43), we can formulate $\dot{\gamma}$ as:

$$\dot{\gamma} = \left[4 \left(\frac{\partial u}{\partial r} \right)^2 + 4 \left(\frac{u}{r} \right)^2 + 4 \frac{u}{r} \left(\frac{\partial u}{\partial r} \right) + \left(\frac{\partial w}{\partial r} + \frac{\partial u}{\partial z} \right)^2 \right]^{\frac{1}{2}}. \tag{1.44}$$

The leading equations for present case are given by:

$$\frac{\partial u}{\partial r} + \frac{u}{r} + \frac{\partial w}{\partial z} = 0, \tag{1.45}$$

$$\rho \left(u \frac{\partial u}{\partial r} + w \frac{\partial u}{\partial z} \right) = \frac{1}{r} \frac{\partial (r\tau_{rr})}{\partial r} + \frac{\partial \tau_{rz}}{\partial z} - \frac{\tau_{\theta\theta}}{r}, \tag{1.46}$$

$$\rho \left(u \frac{\partial w}{\partial r} + w \frac{\partial w}{\partial z} \right) = \frac{1}{r} \frac{\partial (r\tau_{rz})}{\partial r} + \frac{\partial \tau_{zz}}{\partial z}, \tag{1.47}$$

where the stress components present in the above equations are given below:

$$\tau_{rr} = 2\eta_0 \frac{\partial u}{\partial r} \left[\cfrac{1}{1 + \left\{ \Gamma^2 \left(\begin{array}{c} 4\left(\frac{\partial u}{\partial r}\right)^2 + 4\left(\frac{u}{r}\right)^2 \\ +\left(\frac{\partial w}{\partial r} + \frac{\partial u}{\partial z}\right)^2 + 4\frac{u}{r}\left(\frac{\partial u}{\partial r}\right) \end{array} \right) \right\}^{\frac{m}{2}}} \right], \qquad (1.48)$$

$$\tau_{rz} = \tau_{zr} = \eta_0 \left(\frac{\partial w}{\partial r} + \frac{\partial u}{\partial z} \right) \left[\cfrac{1}{1 + \left\{ \Gamma^2 \left(\begin{array}{c} 4\left(\frac{\partial u}{\partial r}\right)^2 + 4\left(\frac{u}{r}\right)^2 \\ +\left(\frac{\partial w}{\partial r} + \frac{\partial u}{\partial z}\right)^2 + 4\frac{u}{r}\left(\frac{\partial u}{\partial r}\right) \end{array} \right) \right\}^{\frac{m}{2}}} \right], \qquad (1.49)$$

$$\tau_{rz} = \tau_{zr} = \eta_0 \left(\frac{\partial u}{\partial z} + \frac{\partial w}{\partial r} \right) \left[\cfrac{1}{1 + \left\{ \Gamma^2 \left(\begin{array}{c} 4\left(\frac{\partial u}{\partial r}\right)^2 + 4\left(\frac{u}{r}\right)^2 \\ +4\frac{u}{r}\left(\frac{\partial u}{\partial r}\right) + \left(\frac{\partial w}{\partial r} + \frac{\partial u}{\partial z}\right)^2 \end{array} \right) \right\}^{\frac{m}{2}}} \right], \qquad (1.50)$$

$$\tau_{\theta\theta} = 2\eta_0 \frac{u}{r} \left[\cfrac{1}{1 + \left\{ \Gamma^2 \left(\begin{array}{c} 4\left(\frac{\partial u}{\partial r}\right)^2 + 4\left(\frac{u}{r}\right)^2 \\ +4\frac{u}{r}\left(\frac{\partial u}{\partial r}\right) + \left(\frac{\partial w}{\partial r} + \frac{\partial u}{\partial z}\right)^2 \end{array} \right) \right\}^{\frac{m}{2}}} \right], \qquad (1.51)$$

$$\tau_{zz} = 2\eta_0 \frac{\partial w}{\partial z} \left[\cfrac{1}{1 + \left\{ \Gamma^2 \left(\begin{array}{c} 4\left(\frac{\partial u}{\partial r}\right)^2 + 4\left(\frac{u}{r}\right)^2 \\ + 4\frac{u}{r}\left(\frac{\partial u}{\partial r}\right) + \left(\frac{\partial w}{\partial r} + \frac{\partial u}{\partial z}\right)^2 \end{array} \right) \right\}^{\frac{m}{2}}} \right].$$ (1.52)

Consequently the $r-$ and $z-$ components of momentum equation can be written as:

$$\rho\left(u\frac{\partial u}{\partial r} + w\frac{\partial u}{\partial z}\right)$$

$$= -\frac{\partial p}{\partial r}$$

$$+ 2\frac{\eta_0}{r}\frac{\partial}{\partial r}\left[r\frac{\partial u}{\partial r}\left\{ \cfrac{1}{1 + \left\{ \Gamma^2 \left(\begin{array}{c} 4\left(\frac{\partial u}{\partial r}\right)^2 + 4\left(\frac{u}{r}\right)^2 \\ + \left(\frac{\partial w}{\partial r} + \frac{\partial u}{\partial z}\right)^2 + 4\frac{u}{r}\left(\frac{\partial u}{\partial r}\right) \end{array} \right) \right\}^{\frac{m}{2}}} \right\}\right]$$

$$+ \eta_0\frac{\partial}{\partial z}\left[\left(\frac{\partial w}{\partial r} + \frac{\partial u}{\partial z}\right)\left\{ \cfrac{1}{1 + \left\{ \Gamma^2 \left(\begin{array}{c} 4\left(\frac{\partial u}{\partial r}\right)^2 + 4\left(\frac{u}{r}\right)^2 \\ + 4\frac{u}{r}\left(\frac{\partial u}{\partial r}\right) + \left(\frac{\partial w}{\partial r} + \frac{\partial u}{\partial z}\right)^2 \end{array} \right) \right\}^{\frac{m}{2}}} \right\}\right]$$

$$-2\frac{\eta_0}{r}\left[\frac{u}{r}\left\{\frac{1}{1+\left\{\Gamma^2\left(\begin{array}{c}4\left(\frac{\partial u}{\partial r}\right)^2+4\left(\frac{u}{r}\right)^2\\+4\frac{u}{r}\left(\frac{\partial u}{\partial r}\right)+\left(\frac{\partial w}{\partial r}+\frac{\partial u}{\partial z}\right)^2\end{array}\right)\right\}^{\frac{m}{2}}}\right\}\right], \quad (1.53)$$

$$\rho\left(u\frac{\partial w}{\partial r}+w\frac{\partial w}{\partial z}\right)$$

$$=-\frac{\partial p}{\partial z}$$

$$+\frac{\eta_0}{r}\frac{\partial}{\partial r}\left[r\left(\frac{\partial w}{\partial r}+\frac{\partial u}{\partial z}\right)\left\{\frac{1}{1+\left\{\Gamma^2\left(\begin{array}{c}4\left(\frac{\partial u}{\partial r}\right)^2+4\left(\frac{u}{r}\right)^2\\+\left(\frac{\partial w}{\partial r}+\frac{\partial u}{\partial z}\right)^2+4\frac{u}{r}\left(\frac{\partial u}{\partial r}\right)\end{array}\right)\right\}^{\frac{m}{2}}}\right\}\right]$$

$$+2\eta_0\frac{\partial}{\partial z}\left[\frac{\partial w}{\partial z}\left\{\frac{1}{1+\left\{\Gamma^2\left(\begin{array}{c}4\left(\frac{\partial u}{\partial r}\right)^2+4\left(\frac{u}{r}\right)^2\\+\left(\frac{\partial w}{\partial r}+\frac{\partial u}{\partial z}\right)^2+4\frac{u}{r}\left(\frac{\partial u}{\partial r}\right)\end{array}\right)\right\}^{\frac{m}{2}}}\right\}\right]. \quad (1.54)$$

With regard to boundary layer approximations, we employ the following dimensionless variables:

$$(r, z) = L(r^*, z^*), (u, w) = U(u^*, w^*) \text{ and } p = \rho U^2 p^*. \qquad (1.55)$$

Using Eq. (1.55), the radial and axial components of the momentum equation can be written in the non-dimensional forms:

$$\rho \left(u^* \frac{\partial u^*}{\partial r^*} + w^* \frac{\partial u^*}{\partial z^*} \right) = -\frac{\partial p^*}{\partial r^*}$$

$$+2 \frac{\eta_0}{r^*} \frac{\partial}{\partial r^*} \left[r^* \frac{\partial u^*}{\partial r^*} \left\{ \frac{1}{1 + \left\{ \Gamma^2 \left(\begin{array}{c} 4\left(\frac{\partial u^*}{\partial r^*}\right)^2 + 4\left(\frac{u^*}{r^*}\right)^2 \\ +4u^*\left(\frac{\partial u^*}{\partial r^*}\right) + \left(\frac{\partial w^*}{\partial r^*} + \frac{\partial u^*}{\partial z^*}\right)^2 \end{array} \right) \right\}^{\frac{m}{2}}} \right\} \right]$$

$$+\eta_0 \frac{\partial}{\partial z^*} \left[\left(\frac{\partial w^*}{\partial r^*} + \frac{\partial u^*}{\partial z^*} \right) \left\{ \frac{1}{1 + \left\{ \Gamma^2 \left(\begin{array}{c} 4\left(\frac{\partial u^*}{\partial r^*}\right)^2 + 4\left(\frac{u^*}{r^*}\right)^2 \\ +4u^*\left(\frac{\partial u^*}{\partial r^*}\right) + \left(\frac{\partial w^*}{\partial r^*} + \frac{\partial u^*}{\partial z^*}\right)^2 \end{array} \right) \right\}^{\frac{m}{2}}} \right\} \right]$$

$$-2\frac{\eta_0}{r^*}\left[\frac{u}{r^*}\left\{\frac{1}{1+\left\{\Gamma^2\left(\begin{array}{c}4\left(\frac{\partial u^*}{\partial r^*}\right)^2+4\left(\frac{u^*}{r^*}\right)^2\\+4u^*\left(\frac{\partial u^*}{\partial r^*}\right)+\left(\frac{\partial w^*}{\partial r^*}+\frac{\partial u^*}{\partial z^*}\right)^2\end{array}\right)\right\}^{\frac{m}{2}}}\right\}\right], \qquad (1.56)$$

$$\rho\left(u^*\frac{\partial w^*}{\partial r^*}+w^*\frac{\partial w^*}{\partial z^*}\right)=-\frac{\partial p^*}{\partial z^*}$$

$$+\frac{\eta_0}{r^*}\frac{\partial}{\partial r^*}\left[r^*\left(\frac{\partial w^*}{\partial r^*}+\frac{\partial u^*}{\partial z^*}\right)\left\{\frac{1}{1+\left\{\Gamma^2\left(\begin{array}{c}4\left(\frac{\partial u^*}{\partial r^*}\right)^2+4\left(\frac{u^*}{r^*}\right)^2\\+4u^*\left(\frac{\partial u^*}{\partial r^*}\right)+\left(\frac{\partial w^*}{\partial r^*}+\frac{\partial u^*}{\partial z^*}\right)^2\end{array}\right)\right\}^{\frac{m}{2}}}\right\}\right]$$

$$+2\eta_0\frac{\partial}{\partial z^*}\left[\frac{\partial w^*}{\partial z^*}\left\{\frac{1}{1+\left\{\Gamma^2\left(\begin{array}{c}4\left(\frac{\partial u^*}{\partial r^*}\right)^2+4\left(\frac{u^*}{r^*}\right)^2\\+4u^*\left(\frac{\partial u^*}{\partial r^*}\right)+\left(\frac{\partial w^*}{\partial r^*}+\frac{\partial u^*}{\partial z^*}\right)^2\end{array}\right)\right\}^{\frac{m}{2}}}\right\}\right]. \qquad (1.57)$$

where the dimensionless parameters ϵ_1 and ϵ_2 are defined as:

$$\epsilon_1 = \frac{\eta_0/\rho}{LU} \text{ and } \epsilon_2 = \frac{\Gamma^2}{\left(L/U\right)^2}. \qquad (1.58)$$

In usual boundary layer approximations, the order of r and u are taken to be 1 while z and w are of order δ. Moreover, the dimensionless parameters ϵ_1 and ϵ_2 are of order δ^2. Consequently, we get the following boundary layer equations in dimensional form:

$$\frac{\partial u}{\partial r} + \frac{u}{r} + \frac{\partial w}{\partial z} = 0, \qquad (1.59)$$

$$u\frac{\partial u}{\partial r} + w\frac{\partial u}{\partial z} = -\frac{1}{\rho}\frac{\partial p}{\partial r} + \vartheta\frac{\partial}{\partial z}\left[\frac{\frac{\partial u}{\partial z}}{1 + \left\{\Gamma\left(\frac{\partial u}{\partial z}\right)\right\}^m}\right], \qquad (1.60)$$

$$0 = -\frac{1}{\rho}\frac{\partial p}{\partial z}, \qquad (1.61)$$

where $\vartheta \left(= \eta_0/\rho\right)$ defines the kinematic viscosity.

1.4 Numerical Schemes

The differential equations emerging in the computation of flow and heat transfer of Cross fluid are highly complicated. The exact solution for complete system of equations seems impossible to determine. Due to this reason we solve our governing equations by employing numerical techniques namely shooting method and bvp4c technique.

1.4.1 Shooting Method

Majority of the problems in the current thesis are handled by using shooting method along with Runge-Kutta (RK) Fehlberg scheme. First, we change system of higher order differential equations into corresponding system of first order differential equations. For the solution of initial value problem (IVP) we need to find the values of missing conditions. For that we take some initial guessed values for the unknown conditions such that the far field conditions are satisfied. Better approximation to solution can be achieved by refining the initial guess by the help of Newton Raphson method. The convergence to a solution can be quickly obtained by repeatedly refining the values of the missing initial conditions. After determining missing initial conditions, the Runge-Kutta Fehlberg scheme [119] is utilized in order to get the solution of the IVP's of the form:

$$\frac{dt}{dx} = g(x,t), \qquad t(x_0) = t_0, \tag{1.62}$$

where the function $g(x,t)$ and the values x_0 and t_0 are already provided. We need to compute the continuously differentiable solution t of IVP (1.47). The formula for RK-Fehlberg scheme is given by:

$$t_{i+1} = t_i + \left(\frac{16}{135}k_0 + \frac{6656}{12825}k_2 + \frac{28561}{56430}k_3 - \frac{9}{50}k_4 + \frac{2}{55}k_5\right)h. \tag{1.63}$$

We can achieve fast convergence to the solution by selecting proper step size h. At each step we need the values of the coefficients k_0 to k_5, which can be calculated from the following formulas:

$$k_0 = g(x_i, t_i),$$

$$k_1 = g\left(x_i + \frac{1}{4}h, t_i + \frac{1}{4}hk_0\right),$$
$$k_2 = g\left(x_i + \frac{3}{8}h, t_i + \left(\frac{3}{32}k_0 + \frac{9}{32}k_1\right)h\right),$$

$$k_3 = g\left(x_i + \frac{12}{13}h, t_i + \left(\frac{1932}{2197}k_0 - \frac{7200}{2197}k_1 + \frac{7296}{2197}k_2\right)h\right),$$

$$k_4 = g\left(x_i + h, t_i + \left(\frac{439}{216}k_0 - 8k_1 + \frac{3680}{513}k_2 - \frac{845}{4104}k_3\right)h\right),$$

$$k_5 = g\left(x_i + \frac{1}{2}h, t_i + \left(-\frac{8}{27}k_0 + 2k_1 - \frac{3544}{2565}k_2 + \frac{1859}{4104}k_3 - \frac{11}{40}k_4\right)h\right)$$

$$(1.64)$$

1.4.2 bvp4c Technique

The bvp4c [120] involves a collocation method for the rapid calculation of the numerical approximate solution of the governing ordinary differential equations (ODE). Although, the deduction of solution for boundary value problem (BVP) is laborious in comparison with the IVPs but bvp4c technique is efficient even to handle to complex BVPs. It is forth order accurate solver which involves some initial guess to reach the final desired solution of the problem.

1.5 Research Objective and Strategy

The intention behind this research involves the study of flow behavior along with heat transfer of a non-Newtonian fluid and to develop mathematical modelling of

Cross fluid to predict the rheological characteristics. Due to the industrial importance of Cross fluid and its competency in predicting the flow in the power-law as well as the region of very low together with very high shear rates, the present thesis envisions to enhance the existing knowledge about a class of non-Newtonian fluids. Thus, the work reported in this thesis is based on mathematical modelling considering two-dimensional boundary layer flows and transfer of heat in Cross fluid under various flow situations, by incorporating different boundary conditions and considering different stretching surfaces. In fact, the boundary layer equations for Cross fluid are modelled and investigated for the first time. The thesis body consists of *ten chapters* with a chapter wise brief description provided below:

Chapter 1 presents a comprehensive literature survey covering all the possible aspects and situations for better understanding the work in the thesis. Two-dimensional boundary layer equations are also formulated for Cross fluid exploring different coordinate systems. Basic conservation laws are exhibited and a short summary of each chapter is bestowed.

In **Chapter 2,** the boundary layer flow along with heat transfer of Cross fluid towards a planar stretching surface is investigated. By taking adequate transformations, the governing partial differential equations (PDEs) are converted to ordinary differential equations (ODEs). The reduced problem is numerically solved by shooting technique. The solutions are displayed by the help of graphs and tables by varying the values of emerging parameters. The work presented in this chapter is already published in *"Thermal Science, (2017), doi: 10.2298/TSCI160919111K".*

Chapter 3 includes an analysis on mixed convection heat transfer of Cross fluid. The analysis is done in view of convective boundary condition and thermal radiation in which radiative heat flux is solved by linear Rosseland approximation. Comparative graphs are provided for assisting and opposing buoyancy effect. The contents of current investigation are published in *"International Journal of Mechanical Sciences, 138 (2018) 515-523"*.

In **Chapter 4,** the magnetohydrodynamic flow, heat and also mass transfer of Cross fluid is thoroughly discussed. Unlike usual no-slip conditions, the impact of velocity, thermal and solutal slips on the surface is taken into account. The consequence of first order chemical reaction and variable thermal conductivity are also debated. Numerical solutions are computed by the help of bvp4c technique. The explorations made in this chapter are submitted for publication in *"Internal Journal of Heat and Mass Transfer"*.

Chapter 5 describes the Falkner-Skan flow of Cross nanofluid past a wedge. The Newtonian heat and mass conditions are utilized in the exploration. Furthermore, the impact of transverse magnetic field, heat generation/absorption and diffusion of chemically reactive species is also considered. The well-known shooting technique is applied to handle the equations and the results are demonstrated by means of graphs and tables. The analysis performed in this chapter is submitted for publication in *"Journal of the Taiwan Institute of Chemical Engineers"*.

Chapter 6 focusses on the axisymmetric flow and heat transfer of Cross fluid past a radially stretching sheet. The analysis is performed by selecting cylindrical polar

coordinate system. The governing equations are first subjected to transformation technique and afterwards solved by the help of shooting technique. The outcomes of the analysis are displayed by plotting graphs of velocity and temperature field. Additionally the tables comprising of numerical values of skin friction coefficient and Nusselt number are also exhibited. The outcomes of this chapter are published in *"Results in Physics, 7 (2017) 3767-3772"*.

Chapter 7 addresses the impact of melting phenomenon on the stagnation point flow and heat transfer of Cross fluid past a radially stretching sheet. The consequence of thermal radiation is considered by using non-linear Rosseland approximation. Comparative plots are demonstrated for the case when the velocity with which the sheet is stretched dominates the free stream velocity and vice versa. The work done in this chapter is accepted for publication in *"Journal of the Brazilian Society of Mechanical Sciences and Engineering"*.

In **Chapter 8,** the axisymmetric flow and transfer of heat in MHD Cross fluid is computed. A newly proposed boundary condition is utilized according to which the normal flux of the nanoparticles is taken zero at the surface. The governing equations obtained as a result of application of appropriate transformations are numerically solved by shooting method. The numerical analysis is displayed by means of graphs and tables for suitable values of pertinent parameters. The computations performed in this chapter are submitted for publication in *"International Journal of Thermal Sciences"*.

In **Chapter 9,** numerical analysis is performed on the mixed convective flow of Cross nanofluid past a stretching cylinder. Moreover, the consequence of activation energy, thermal radiation, convective boundary condition and chemical reaction is also considered. The boundary layer equations for flow of Cross fluid towards a stretching cylinder are first calculated and then simplified to obtain numerical solutions under the above mentioned assumptions. The results of the investigation are submitted for publication in *"AIP Advances"*.

Chapter 10 marks the final chapter of the thesis. It lists the main findings of the work presented in the thesis. Additionally, it provides recommendations for doing future research in this field.

Chapter 2

Flow and Heat Transfer to Cross Fluid

In current chapter, the two-dimensional boundary layer flow and transfer of heat in Cross fluid is studied. The flow is driven by linearly stretching sheet having constant wall temperature. The governing system of PDEs is reduced to highly non-linear ODEs by invoking suitable transformations. The stretching sheet solutions are computed via. numerical technique known as the shooting method and are expressed by means of graphs and tables. The consequence of arising parameters namely the power-law index m, the Weissenberg number We and the Prandtl number Pr on the velocity and temperature fields are thoroughly examined. The numerical values of the rate of heat transfer and skin friction coefficient are also tabulated for further understanding of the problem. An investigation on obtained results reveals that with an elevation in the Weissenberg number We, the velocity profiles display a diminishing behavior while reverse trend is shown by the temperature of the fluid. Further, a declining trend is exhibited by skin friction coefficient and a boost in the heat transfer rate is seen with an increment in power-law index m. Moreover, the results are verified by presenting comparison with available literature for limiting cases and a remarkable compatibility is attained.

2.1 Mathematical Formulation

2.1.1 Geometry of the Problem

$$u = cx, v = 0, T = T_w$$
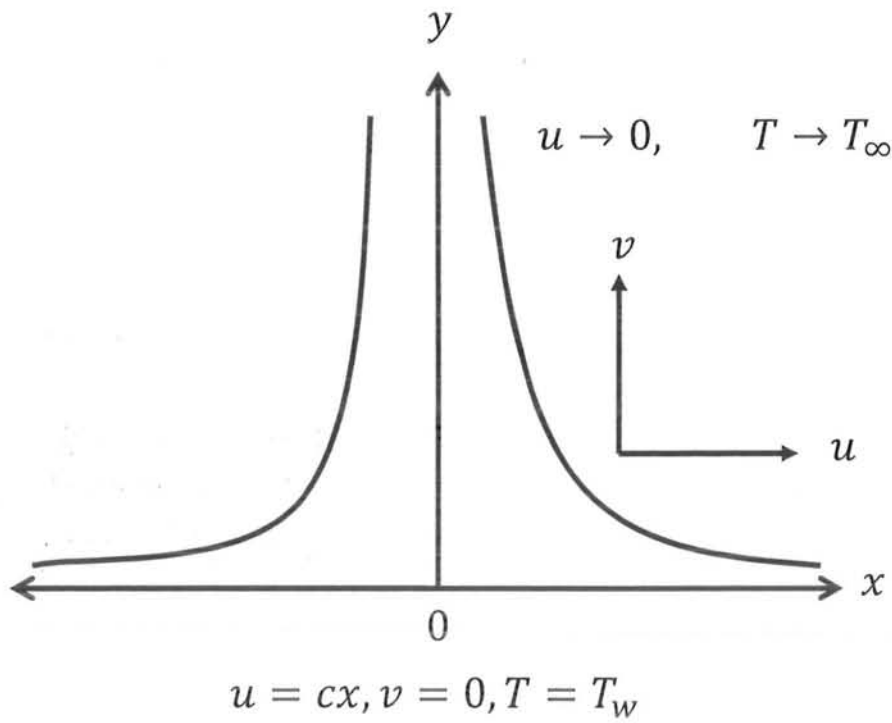
Fig. 2.1: Physical model and co-ordinate system.

2.1.2 Problem Statement

The present section endows the governing equations for two-dimensional flow of an incompressible generalized Newtonian fluid specifically the Cross fluid by incorporating the effects of stretching surface. The choice of coordinate system is made such that the stretching sheet is assumed to lie on the plane $y = 0$ while the motion of the fluid takes place in the region $y > 0$ (as demonstrated in **Fig. 2.1**). The sheet is uniformly stretched along the $x -$ axis with a velocity $U = cx$ with c (> 0) being the stretching rate of sheet. The temperature near the sheet surface is taken to

be T_w while T_∞ denotes the ambient fluid temperature. In the existing problem, the flow is driven due to stretching of sheet.

In view of above stated assumptions, the conservation equations for flow and heat transfer of Cross fluid become (cf. Chapter 1):

$$\frac{\partial u}{\partial x} + \frac{\partial v}{\partial y} = 0, \tag{2.1}$$

$$u\frac{\partial u}{\partial x} + v\frac{\partial u}{\partial y} = \vartheta \frac{\partial}{\partial y}\left[\left(\frac{\partial u}{\partial y}\right)\left(1 + \left\{\Gamma\left(\frac{\partial u}{\partial y}\right)\right\}^m\right)^{-1}\right], \tag{2.2}$$

$$u\frac{\partial T}{\partial x} + v\frac{\partial T}{\partial y} = \alpha \frac{\partial^2 T}{\partial y^2}, \tag{2.3}$$

where $\alpha \left(=\frac{k}{\rho c_p}\right)$ represents the thermal diffusivity in which k marks the thermal conductivity and c_p the specific heat at constant pressure.

The boundary conditions subjected to considered problem are:

$$u(x,y) = U(x) = cx, \; v(x,y) = 0, \; T(x,y) = T_w \; \text{at} \; y = 0, \tag{2.4}$$

$$u(x,y) \to 0, T(x,y) \to T_\infty \; \text{as} \; y \to \infty. \tag{2.5}$$

2.1.3 Non-Dimensionalization

Above system of PDEs can be turn down and corresponding system of ODEs by applying following transformations:

$$\eta = \left(\frac{cy^2}{v}\right)^{1/2}, \psi = x\sqrt{vc}f(\eta), \theta = \frac{T - T_\infty}{T_w - T_\infty}, \tag{2.6}$$

where η stands for the dimensionless independent variable, ψ the dimensional stream function such that $(u, v) = \left(\frac{\partial \psi}{\partial y}, -\frac{\partial \psi}{\partial x}\right)$. In consideration of transformations (2.6), law of conservation of mass (2.1) is identically, however, while Eqs. $(2.2) - (2.5)$ become:

$$(f f'' - f'^2)(1 + (We\, f'')^m)^2 + (1 + (1 - m)(We\, f'')^m)f''' = 0, \quad (2.7)$$

$$\theta'' + Pr f\, \theta' = 0, \tag{2.8}$$

$$f(\eta) = 0, \quad f'(\eta) = 1, \quad \theta(\eta) = 1 \quad \text{at } \eta = 0, \tag{2.9}$$

$$f'(\eta) \to 0, \quad \theta(\eta) \to 1 \quad \text{as } \eta \to \infty. \tag{2.10}$$

In aforementioned equations, prime signifies differentiation with respect to η, We symbolizes the Weissenberg number and Pr the Prandtl number, respectively, given by:

$$We = c\, \Gamma_0\, Re_L^{\frac{1}{2}}, \qquad Pr = \frac{\eta_0\, c_p}{k}, \tag{2.11}$$

where $Re_L\left(= \frac{cL^2}{\vartheta}\right)$ stands for the Reynolds number and $\Gamma = \left(\frac{x}{L}\right)^{-1} \Gamma_0$.

2.1.4 Substantial Physical Quantities

The physical quantities of keen interest are the skin friction coefficient, commonly known as surface drag and the Nusselt number which describes rate of heat transfer on wall. The expressions for these quantities are defined as:

$$C_f = \frac{\tau_w}{\frac{1}{2}\rho U^2}, \qquad Nu = \frac{L q_w}{k(T_w - T_\infty)}, \tag{2.12}$$

where τ_w gives the local wall shear stress while q_w the wall heat flux, formulated as:

$$\tau_w = \tau_{xy}\big|_{y=0} = \left[\eta_0 \frac{\frac{\partial u}{\partial y}}{1 + \left\{\Gamma\left(\frac{\partial u}{\partial y}\right)\right\}^m}\right]_{y=0}, q_w = -k\left.\frac{\partial T}{\partial y}\right|_{y=0}. \tag{2.13}$$

Upon using transformations (2.6), the dimensionless representation of the skin friction coefficient and Nusselt number can are stated as:

$$\frac{1}{2}Re_L^{\frac{1}{2}}C_f = \frac{f''(0)}{1 + (Wef''(0))^m}, -Re_L^{-\frac{1}{2}}Nu = \theta'(0), \tag{2.14}$$

where $Re_L\left(=\frac{cL^2}{\vartheta}\right)$.

2.2 Verification of Numerical Results

The modeled problem consisting of the non-linear equations (2.7) and (2.8) with boundary conditions (2.9) and (2.10) is numerically solved by the help of well-known shooting technique. The authenticity of achieved solutions is guaranteed by providing comparison with existing literature for special case as exhibited in **Tables 2.1** and **2.2**. The numeric values of skin friction coefficient are provided in **Table 2.1** for special case when $We = 0$. Comparative analysis is done with the values determined by Cortell [104], Cortell [105] and Hamad and Ferdows [106] and an outstanding compatability is achieved. Moreover, **Table 2.2** displays an appropriate comparison of rate of heat transfer among present study and results reported by Wang [107], Gorla and Sidawi [108] and Hamad [109] for the limiting case ($We = 0$). These comparisons validate the credibility of our employed numerical methodology.

Table 2.1: Comparison for the variation of $-f''(0)$ when $We = 0$.

	Cortell [104]	Cortell [105]	Hamad and Ferdows [106]	Present result
$-f''(0)$	1.0	1.0	1.0043	1.00001

Table 2.2: Comparison for the variation of $-\theta'(0)$ when $We = 0$ for different values of Pr.

Pr	$-\theta'(0)$			
	Wang [107]	Gorla and Sidawi [108]	Hamad [109]	Present results
0.07	0.0656	0.0656	0.0656	0.065526
0.2	0.1691	0.1691	0.1691	0.164037
0.7	0.4539	0.4539	0.4539	0.418299
2	0.9114	0.9114	0.9114	0.826827
7	1.8954	1.8905	1.8954	1.80433
20	3.3539	3.3539	3.3539	3.25603
70	6.4622	6.4622	6.4622	6.36662

2.3 Discussion on Obtained Results

The physical insight to the governing problem is made by performing numerical computations and the outcomes are displayed by the help of graphs and tables. **Figs. 2.2** to **2.4** provide the graphical illustration of velocity and also of temperature fields for changing the values of parameters. Moreover, a detail analysis is made on the current problem by exploring the trend of skin friction coefficient and Nusselt number as shown in **Fig. 2.5** and also in in **Tables 2.3** and **2.4**.

The impact of the power-law index m on velocity and also for temperature fields is demonstrated in **Figs. 2.2 (a, b)**. A careful analysis regarding **Fig. 2.2 (a)** discloses that as m shifts towards unity, a boost in the fluid velocity occurs as the shear-thinning nature is increased. The momentum boundary layer structure also thickens correspondingly. **Fig. 2.2 (b)** reveals that a decline in temperature field is seen for incremented values of m. Furthermore, the corresponding thermal boundary layers thickness shows a diminishing trend. These findings can be physically answered since the shear-thinning fluid renders less resistance to fluid motion because of lesser viscosity and thus fluids velocity enlarges while temperature reduces.

Figs. 2.3 (a, b) exhibit the behavior of the velocity along with temperature profiles relative to a boost in Weissenberg number We. **Fig. 2.3 (a)** displays the declining trend observed by velocity profiles and related thickness of boundary layer corresponding to growing values of the Weissenberg number. An examination of **Fig. 2.3 (b)** discloses that an elevation in fluids temperature and associated boundary layer structure occurs for an enhancement in We. Physically this trend can be justified from the fact that a growth in Weissenberg number We causes an enlargement in the

relaxation time which results in lowering fluids velocity while fluids temperature enhances.

Further investigation about heat transfer process is done by sketching temperature profiles for progressing values of Prandtl number Pr. A decline in temperature distribution and in corresponding thickness of boundary layer is seen as demonstrated in **Fig. 2.4**. Prandtl number actually determines a ratio of momentum diffusivity to thermal diffusivity. For a growth in Pr, thermal diffusivity gets weaker as a consequence of which the flow of heat into the fluid is restrained and thus lowering the thermal boundary layer structures. In fluids having low Prandtl number the heat diffuses faster from the wall on account of high thermal conductivity. Thus, Prandtl number regarded as a controlling factor in conducting flows for monitoring the rate of cooling.

Figs. 2.5 (a, b) are plotted to establish the behavior of skin friction coefficient and Nusselt number against Weissenberg number We against variation in power-law index m. It is analyzed from graphical trend that skin friction coefficient along with Nusselt number give opposite response corresponding to growth in m. **Fig. 2.5 (a)** reveals that the skin friction coefficient is a declining function of m as well as We. **Fig. 2.5 (b)** demonstrates that the rate of transfer of heat enlarges corresponding to an enhancement in m while it reduces in response to growth in We.

The change in numerical values out from skin friction coefficient along with Nusselt number corresponding to variation in physical parameters including power-law index m, Weissenberg number We and Prandtl number Pr is shown in **Tables 2.3** and **2.4**, respectively. It is inferred from the data tabulated in **Table 2.3** that the magnitude of

skin friction coefficient lowers for progressive values of Weissenberg number and power-law index. Further, it is deduced from the numerical data presented in **Table 2.4** that the Nusselt number enlarges with augmenting values of Pr. It can be physically supported using the fact that growing values of Pr enhance the process of convection in comparison with the conduction due to which the rate of transfer of heat increases. Opposite trend is disclosed for growth in We. Additionally, the rate of transfer of heat is raised by growing m.
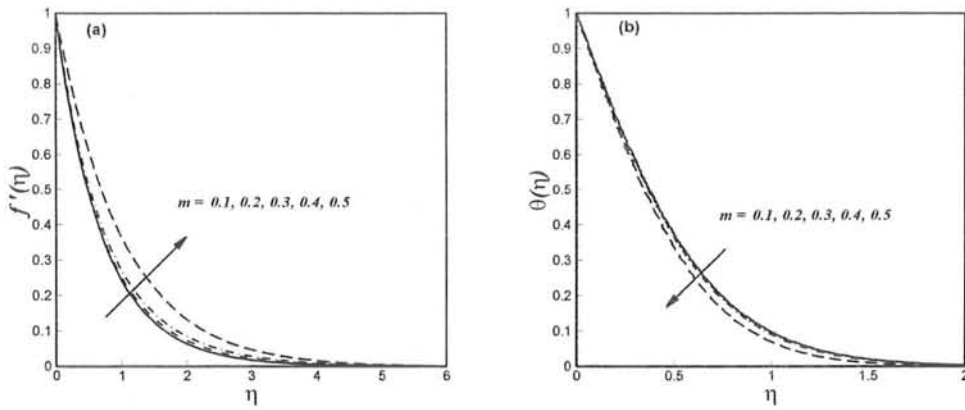
Fig. 2.2: Graphical behavior of $f'(\eta)$ and $\theta(\eta)$ for growth in m when $We = 2$ and $Pr = 5$.
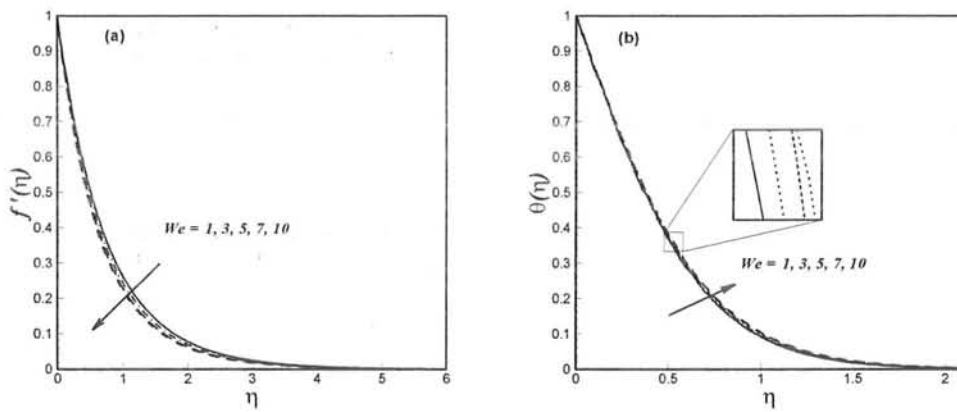
Fig. 2.3: Graphical behavior $f'(\eta)$ and $\theta(\eta)$ for growth in We when $m = 0.2$ and $Pr = 5$.
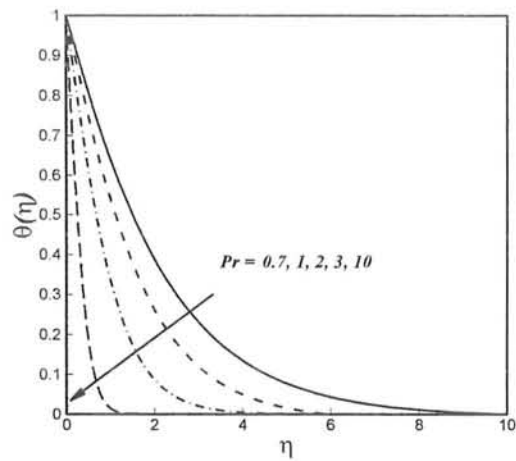
Fig. 2.4: Graphical behavior of $\theta(\eta)$ for growth in Pr when $We = 2$ and $m = 0.2$.
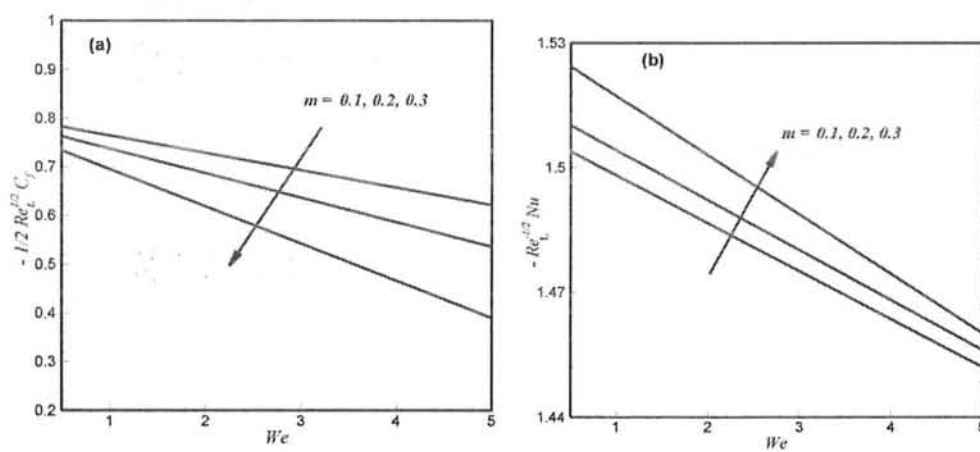
Fig. 2.5: Graphical behavior of skin friction coefficient along with Nusselt number for variation in m and We when $Pr = 5$.

Table 2.3: Numerical valuation of skin friction coefficient for growth in m and We.

Parameters (fixed values)	Parameters		$-\frac{1}{2}Re_L^{\frac{1}{2}}C_f$
$We = 2$	m	0.1	0.684867
		0.2	0.635007
		0.3	0.549867
		0.4	0.433523
		0.5	0.318336
$m = 0.2$	We	1	0.661872
		2	0.635007
		3	0.615357
		4	0.601791
		5	0.589208

Table 2.4: Numerical valuation of heat transfer rate subject to growth in m, We and Pr.

Parameters (fixed values)	Parameters		$-Re_L^{-\frac{1}{2}}Nu$
$We = 2, Pr = 5$	m	0.1	1.473410
		0.2	1.477390
		0.3	1.493460
		0.4	1.525000
		0.5	1.572540
$m = 0.2, Pr = 5$	We	1	1.488060
		2	1.477390
		3	1.470620
		4	1.46550
		5	1.459620
$m = 0.2, We = 2$	Pr	0.7	0.407252
		1	0.515167
		2	0.827280
		3	1.077400
		4	1.289770

Chapter 3

Mixed Convection Heat Transfer in Cross Fluid Flow with Thermal Radiation

This chapter presents the numerical simulations on mixed convective and radiative heat transfer considering Cross fluid by examining the effect of assisting as well as opposing buoyancy. Moreover, the flow is induced due to vertically stretching surface by taking into account the convective boundary conditions. The non-dimensional system of ODEs is derived by the aid of transformation technique. The resultant equations are then subjected to shooting technique to investigate the significance of parameters with the corresponding ranges chosen as: the mixed convection parameter $0 \leq \lambda \leq 0.5$, the power-law index $0 \leq m \leq 1$, the Weissenberg number $1 \leq We \leq 5$, the radiation parameter $0.1 \leq R \leq 1$, the Prandtl number $0.7 \leq Pr \leq 70$, and the Biot number $0.1 \leq \gamma \leq 1.5$. In addition, the plots together with numeric values of coefficient of skin friction and also Nusselt number are provided for in depth analysis of the considered problem. Few important findings of the analysis can be listed as: (i) the thickness of thermal boundary layer is greater on considering buoyancy opposed flow $(\lambda < 0)$ as compared to buoyancy aided flow $(\lambda > 0)$, (ii) the temperature profile exhibited increasing trend corresponding to increase in Weissenberg number, the Biot number and the radiation parameter. A critical comparison is reported in order to ensure the correctness of obtained results.

3.1 Mathematical Analysis of the Problem

In the ongoing section, we identify the mixed convective flow of Cross fluid driven by a vertically stretching sheet. The process of heat transfer is investigated by the application of convective boundary condition. The coordinate frame is designed such that $x-$axis is to be measured along the surface of sheet while $y-$axis extends normal to the surface of sheet and it covers the region in which the flow takes place. The ambient value of the temperature is marked as T_∞ while the temperature of sheet is varied through convection heat transfer by hot fluid having temperature T_f placed at the bottom part of sheet which gives rise to a coefficient of heat transfer h_f. With the above mentioned consideration together with the Boussinesq approximations, we arrive at the following equations (cf. Chapter 2):

$$\frac{\partial u}{\partial x} + \frac{\partial v}{\partial y} = 0, \tag{3.1}$$

$$u\frac{\partial u}{\partial x} + v\frac{\partial u}{\partial y} = \vartheta\frac{\partial}{\partial y}\left[\left(\frac{\partial u}{\partial y}\right)\left(1 + \left\{\Gamma\left(\frac{\partial u}{\partial y}\right)\right\}^m\right)^{-1}\right] \pm g\beta(T - T_\infty), \tag{3.2}$$

$$u\frac{\partial T}{\partial x} + v\frac{\partial T}{\partial y} = \alpha\frac{\partial^2 T}{\partial y^2} - \frac{1}{\rho c_p}\frac{\partial q_r}{\partial y}, \tag{3.3}$$

where the symbols g, $\beta\left(= \beta^*\left(\frac{x}{L}\right)^{-1}\right)$ and q_r, respectively, signify the magnitude of gravitational acceleration, the coefficient of volumetric thermal expansion and radiative heat flux. Moreover, the plus and minus signs appearing in Eq. (3.2) characterize the buoyancy aiding and opposing flow situations, respectively.

Upon using Rosseland approximation for radiation [110], we simplify radiative heat flux as:

$$q_r = -\frac{4}{3}\frac{\sigma^*}{k^*}\frac{\partial T^4}{\partial y}, \tag{3.4}$$

such that σ^* stands for the Stefan-Boltzmann constant while k^* the Rosseland mean absorption coefficient.

The non-linear temperature term mentioned in Eq. (3.4) can be further simplified by Taylor series expansion about T_∞ and omitting higher order term, we eventually arrive at the following term:

$$q_r = -\frac{16}{3}\frac{\sigma^*}{k^*}T^3\frac{\partial T}{\partial y}. \tag{3.5}$$

Upon using Eq. (3.5), the energy equation (3.3) turns into:

$$u\frac{\partial T}{\partial x} + v\frac{\partial T}{\partial y} = \frac{1}{\rho c_p}\left[\left(k + \frac{16}{3}\frac{\sigma^*}{k^*}T_\infty^3\right)\frac{\partial^2 T}{\partial y^2}\right]. \tag{3.6}$$

The associated boundary conditions are of the form:

$$u(x,y) = U(x) = cx, v(x,y) = 0, -k\frac{\partial}{\partial y}T(x,y) = h_f\left[T_f - T(x,y)\right] \text{ at } y = 0, \tag{3.7}$$

$$u(x,y) \to 0, T(x,y) \to T_\infty \text{ as } y \to \infty. \tag{3.8}$$

The governing problem is further reduced to non-dimensional form by employing the dimensionless similarity variable η and the stream function ψ (cf. Chapter 2).

Further, we invoke:

$$\theta(\eta) = \frac{T - T_\infty}{T_f - T_\infty}. \tag{3.9}$$

Upon substitution of above transformations, the reduced form of governing equations is given as:

$$[ff'' - f'^2][1 + (We\,f'')^m]^2 + [1 + (1-m)(We\,f'')^m]f''' + \lambda\theta = 0, \quad (3.10)$$

$$\left(1 + \frac{4}{3}R\right)\theta'' + Prf\theta' = 0. \quad (3.11)$$

While the boundary conditions related to velocity along with temperature fields take the following non-dimensional form:

$$f(\eta) = 0, f'(\eta) = 1, \theta'(\eta) = -\gamma[1 - \theta(\eta)] \text{ at } \eta = 0, \quad (3.12)$$

$$f'(\eta) \to 0, \theta(\eta) \to 0 \text{ as } \eta \to \infty. \quad (3.13)$$

The dimensionless physical quantities arising in the aforementioned equations are: the mixed convection parameter $\lambda\left(= \pm\frac{g\beta^* L(T_f - T_\infty)}{U^2}\right)$, the thermal radiation parameter $R\left(= \frac{4\sigma^*}{kk^*}T_\infty^3\right)$ and the Biot Number $\gamma\left(= \frac{h_f}{k}\left(\frac{v}{c}\right)^{1/2}\right)$. It is noteworthy that the range of λ characterizes that the flow is either assisting (for $\lambda > 0$) or opposing (for $\lambda < 0$). Specifically, for the limit $\lambda \to 0$ the heat transfer occurs by forced convection while for $\lambda \to \infty$, it takes place by free convection.

Physical quantities having utmost importance are the skin friction coefficient (cf. Chapter 2) and the Nusselt number. By incorporating radiative heat flux, the expression of wall heat flux gets:

$$q_w = -k\left(\frac{\partial T}{\partial y}\right)_{y=0} + q_r|_{y=0}. \quad (3.14)$$

Thus, Nusselt number can be calculated from:

$$Nu = \frac{Lq_w}{T_f - T_\infty} \text{ with } q_w = -\left[\left(k + \frac{16}{3}\frac{\sigma^*}{k^*}T_\infty^3\right)\frac{\partial T}{\partial y}\right]_{y=0}. \tag{3.15}$$

The resulting expression in dimensionless form can be expressed as:

$$Re_L^{-\frac{1}{2}}Nu = -\theta'(0)\left(1 + \frac{4}{3}R\right). \tag{3.16}$$

3.2 Assurance of Numerical Results

The leading equations are numerically integrated by turning them down to first order ODEs and seeking result by shooting technique. The results thus achieved are certified by displaying a comparison with already stated results by other authors for special cases. **Table 3.1** demonstrates comparative numeric values of Nusselt number in forced convective flow of Newtonian fluid by excluding the thermal radiation effect. The comparative analysis reveals an outstanding compatibility of our results and already tabulated results by Rahman *et al.* [48], Wang [107], Gorla and Sidawi [108] and Khan and Pop [111].

Table 3.1: A comparison of Nusselt number $-\theta'(0)$ for Newtonian fluid $(We = 0)$ with $\lambda = R = 0$ and $\gamma \to \infty$.

Pr	Wang [107]	Gorla and Sidawi [108]	Khan and Pop [111]	Rahman et al. [48]	Present study
0.7	0.4539	0.5349	0.4539	0.4539	0.4542
7	1.8954	1.8954	1.8954	1.8954	1.8918
70	6.4622	6.4622	6.4621	6.4622	6.4207

3.3 Graphical Discussion

The principal target of this chapter is to explore mixed convection flow along with heat transfer of Cross fluid past a stretching sheet by considering the effect of radiation and convective boundary condition. The main interest behind this work is to scrutinize the behavior of velocity together with temperature profiles for developing values of parameters viz. the power-law index m, Weissenberg number We, Biot number γ, thermal radiation parameter R and the Prandtl number Pr on the velocity and temperature profiles. Comparative graphs for buoyancy aided flow $(\lambda > 0)$ and buoyancy opposed flow $(\lambda < 0)$ are constructed for all cases. Furthermore, the flow and heat transfer mechanism is further probed by contributing the numeric values considering skin friction coefficient along with Nusselt number. Moreover, achieved numerical results are authenticated by making comparison with existing literature as special case and excellent compatibility is obtained.

Figs. 3.1 (a, b), respectively, display the graphical behavior of velocity and temperature profiles subject to rise in power-law index m. In addition, comparative plots are provided for assisting $(\lambda > 0)$ and opposing buoyancy $(\lambda < 0)$. It is analyzed from **Fig. 3.1 (a)** that the progressive values of m leads to an up rise in fluids velocity for assisting and also for opposing buoyancy. However, the boundary layer thickness is larger for buoyancy aided flow $(\lambda > 0)$ as compared to buoyancy opposed flow $(\lambda < 0)$. On inspection of **Fig. 3.1 (b)**, it is deduced that the pattern of thermal boundary layer decay for increase in m for assisting buoyancy $(\lambda = 0.5)$ and also for opposing buoyancy $(\lambda = -0.5)$. It is observed that temperature profiles and corresponding boundary layer structures are thicker for buoyancy opposed flow $(\lambda < 0)$. Physically, due to shear-thinning nature of Cross fluid less resistance is faced due to low viscosity as a result of which the fluid velocity enlarges while the temperature of fluid diminishes corresponding to growing values of m.

The variation in velocity along with temperature field is monitored for growing values of the Weissenberg number We, as portrayed in **Figs. 3.2 (a, b)**, respectively. A comparative study is done by incorporating the effect of buoyancy aided flow $(\lambda > 0)$ and buoyancy opposed flow $(\lambda < 0)$. It evident from **Fig. 3.2 (a)** that fluids velocity accompanied with corresponding boundary layer lessens by uplifting values of the Weissenberg number We. Moreover, the comparative plots for assisting $(\lambda > 0)$ and opposing buoyancy $(\lambda < 0)$ reveal that the momentum boundary layer thickness is larger for buoyancy aided flow while thinner for buoyancy opposed flow. **Fig. 3.2 (b)** discloses the role of the Weissenberg number We in the development of temperature profile for aiding along with opposing flows. It is graphically displayed

that temperature profile is a growing function of We. Physical reason behind this graphical behavior is that the relaxation time is raised for increasing values of the Weissenberg number We which causes a decline in velocity profile and boost in the fluid temperature.

Fig. 3.3 (a) portrays the consequence of the Biot number γ on velocity of fluid. It is analyzed that fluids velocity and momentum boundary layer diminishes for increasing values of Biot number. **Fig. 3.3 (b)** exhibits the dependence of the temperature profile on the Biot number γ for assisting buoyancy $(\lambda > 0)$ and also for opposing buoyancy $(\lambda < 0)$. It is clear from the graphical behavior that the temperature profile rises rapidly near the wall with a growth in γ. It is visualized that the thermal boundary layer structures are thicker for buoyancy opposed flow $(\lambda < 0)$ in comparison with buoyancy aided flow $(\lambda > 0)$. It is due to the fact that an enlargement in Biot number increases the surface convection and thus reduces the sheet thermal resistance which in turn leads to rise in fluids temperature near sheet surface.

The impact of thermal radiation parameter R on velocity along with temperature fields corresponding to both the aiding/opposing flows is demonstrated in **Figs. 3.4 (a, b)**. An inspection of **Fig. 3.4 (a)** reveals that the impact of R on velocity profile is opposite for aiding and opposing cases. A development in velocity profile is seen with an increase in R for buoyancy aided flow $(\lambda > 0)$ while a decreasing trend is demonstrated for buoyancy opposed flow $(\lambda < 0)$. **Fig. 3.4 (b)** displays that the fluid temperature grows for escalating values of the thermal radiation parameter R for the case of assisting as well as opposing flows. Further, we can observe that the influence

of the thermal radiation parameter R is much prominent for assisting flow as compared to opposing flow. Physically, surface heat flux is enlarged with an increase in R which corresponds to development of the temperature of fluid.

Figs. 3.5 (a, b) are sketched to exhibit the dependence of Prandtl number Pr on velocity along with temperature field, respectively. Besides this, graphs are also presented corresponding to buoyancy aided flow $(\lambda > 0)$ and buoyancy opposed flow $(\lambda < 0)$. **Fig. 3.5 (a)** depicts the declining trend observed by velocity profiles pertaining to aiding/opposing flows. It can be visualized that the developing values of Pr lowers the momentum boundary layer structures for assisting $(\lambda > 0)$ as well as opposing $(\lambda < 0)$ flows. It is demonstrated in **Fig. 3.5 (b)** that the Prandtl number plays important role in thinning corresponding thermal boundary layer structures for assisting together with opposing flows. It is disclosed that thickness of thermal boundary layer is greater for buoyancy opposed flow $(\lambda < 0)$ in comparison with buoyancy assisted flow $(\lambda > 0)$ for same Prandtl number.

Figs. 3.6 (a-d) reveal the graphical behavior of coefficient of skin friction and Nusselt number corresponding to increment in radiation parameter, Biot number and Prandtl number. The coefficient of skin friction is strongly influenced for assisting flow compared with opposing flow. It is inferred that the consequence of mixed convection parameter on Nusselt number is much notable for buoyancy opposed flow $(\lambda < 0)$.

Table 3.2 illustrates the numerical values of coefficient of skin friction and rate of heat transfer when the values of Weissenberg number We, power-law index m, thermal radiation parameter R, Biot number γ and the Prandtl number Pr are varied. Moreover, this table also bestows the values for assisting and also for opposing flows

for each case. It is indicated that coefficient of skin friction is higher for opposing flow ($\lambda < 0$) as compared to assisting flow ($\lambda > 0$) while reverse behavior is seen in rate of heat transfer. For assisting flow, a decline in coefficient of skin friction is observed corresponding to augmenting values of We, m, R and γ while an increasing trend is seen for rise in the values of Pr. For opposing flow, the coefficient of skin friction reduces with We, m and Pr while an increasing function of R and γ. The rate of transfer of heat at the wall grows with a rise in R, m, γ and Pr while it decreases for growing values of We for both assisting and opposing flows.
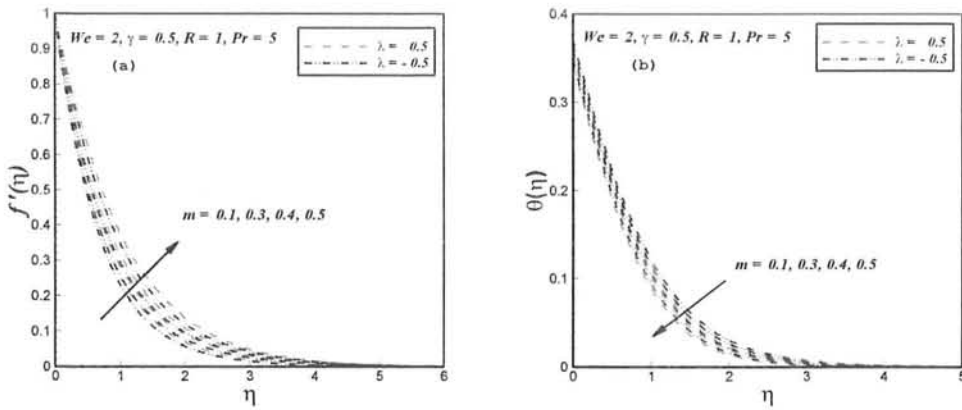
Fig. 3.1: Variation of $f'(\eta)$ and $\theta(\eta)$ corresponding to growth in power-law index m for aiding/opposing flows.

Fig. 3.2: Variation of $f'(\eta)$ and $\theta(\eta)$ corresponding to growth in Weissenberg number We for aiding/opposing flows.

Fig. 3.3: Variation of $f'(\eta)$ and $\theta(\eta)$ corresponding to growth in Biot number γ for aiding/opposing flows.

Fig. 3.4: Variation of $f'(\eta)$ and $\theta(\eta)$ corresponding to growth in radiation parameter R for aiding/opposing flows.
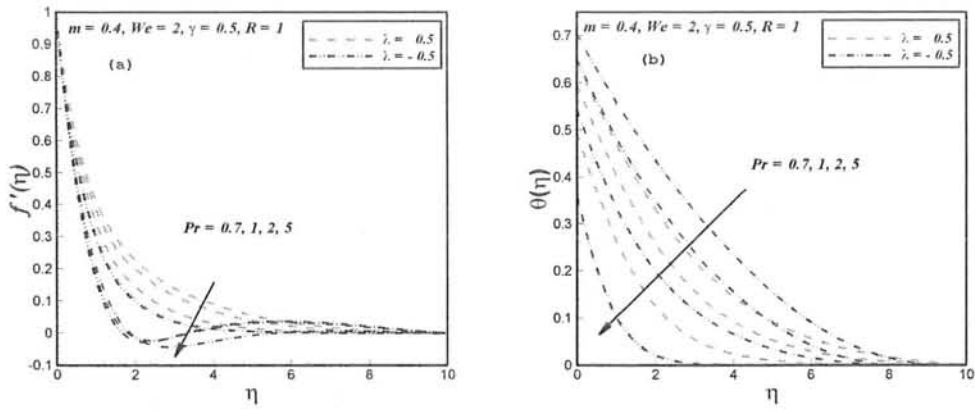
Fig. 3.5: Variation of $f'(\eta)$ and $\theta(\eta)$ corresponding to growth in Prandtl number Pr for aiding/opposing flows.
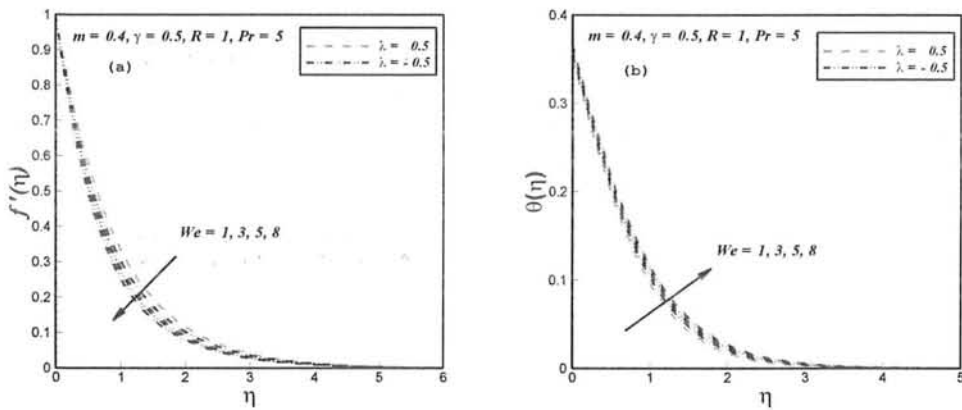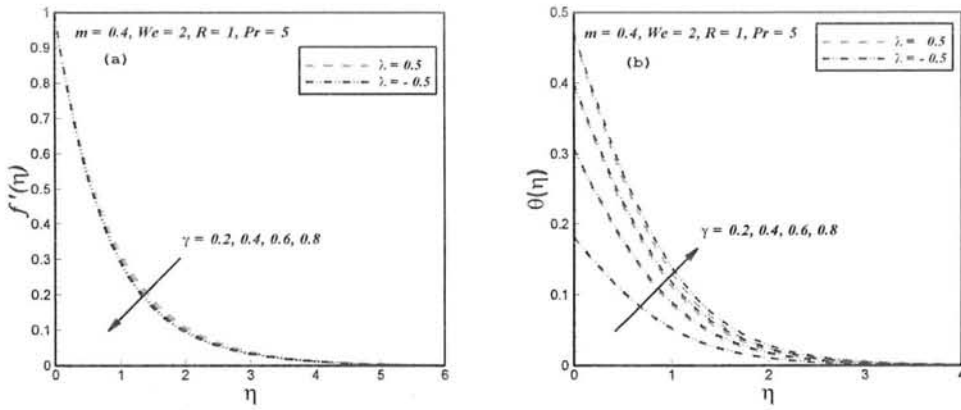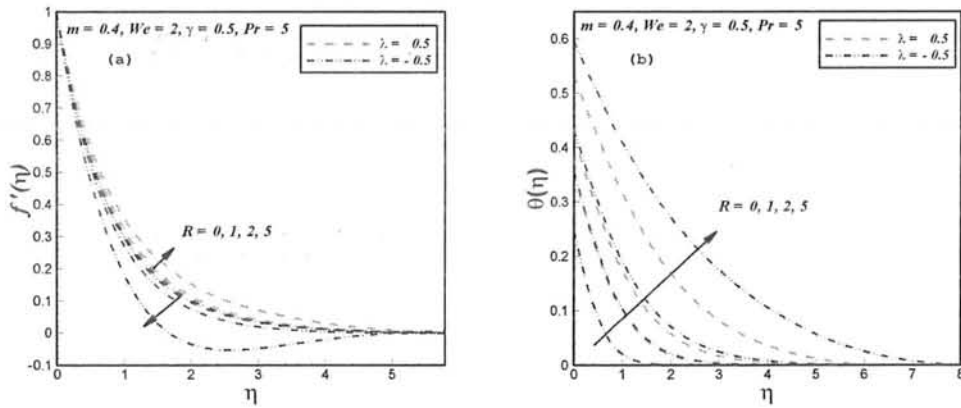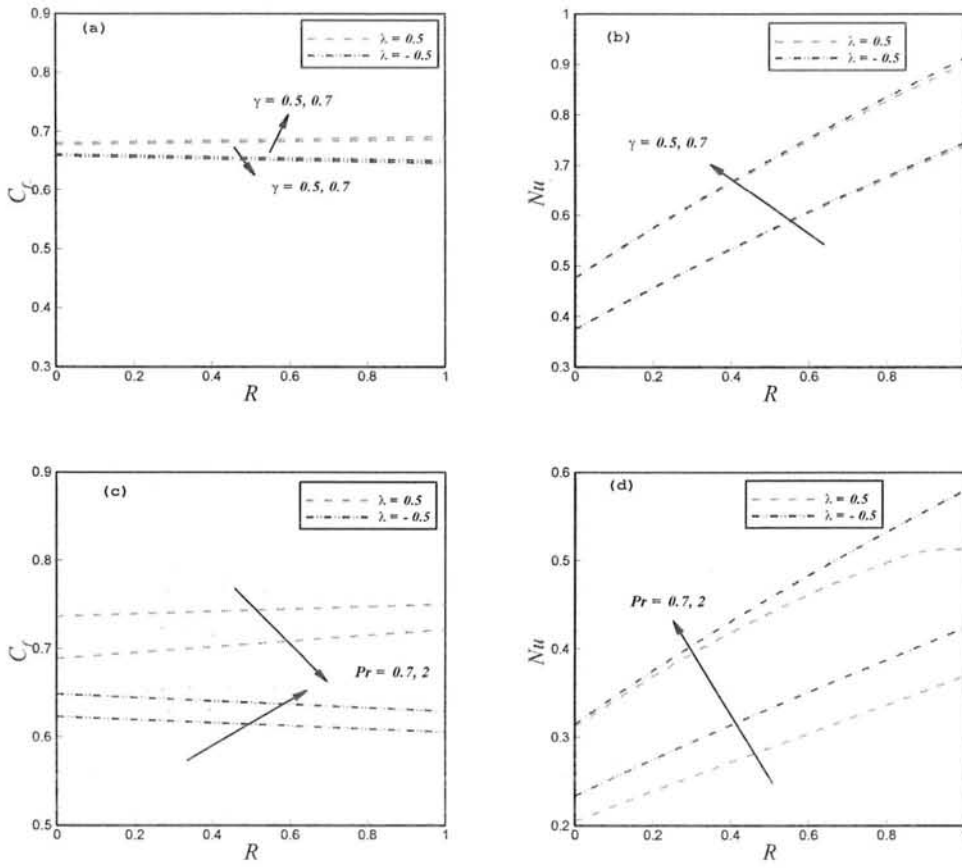
Fig. 3.6: Impact of the radiation parameter R on the skin friction coefficient along with Nusselt number corresponding to growth in γ and Pr.

Table 3.2: Skin friction coefficient along with Nusselt number considering variation of physical parameters by considering assisting as well as opposing flows.

We	m	Pr	R	γ	$\lambda = 0.5$ (Assisting flow)		$\lambda = -0.5$ (Opposing flow)	
					$-\frac{1}{2}Re_L^{\frac{1}{2}}C_f$	$-Re_L^{\frac{1}{2}}Nu$	$-\frac{1}{2}Re_L^{\frac{1}{2}}C_f$	$-Re_L^{\frac{1}{2}}Nu$
2	0.2	5	1	1.5	0.607467	1.29548	0.662641	1.26346
1					0.637788	1.30474	0.700642	1.27223
3					0.590385	1.28957	0.644656	1.25791
	0.1				0.655700	1.28948	0.715922	1.25941
	0.3				0.523040	1.30847	0.576986	1.27731
		0.7			0.558727	0.52282	0.721055	0.46120
		2			0.586989	0.86451	0.693555	0.75238
			1.5		0.602061	1.50104	0.671863	1.43007
			2		0.597570	1.68090	0.690445	1.50565
				0.3	0.624214	0.520907	0.644961	0.51884
				0.5	0.612796	0.742447	0.650382	0.73652

Chapter 4

Multiple Slip Effects on Chemically Reactive Flow of Cross Fluid with Heat and Mass Transfer

In current section, the main task is to understand flow, heat and also mass transfer aspects of Cross fluid considering a stretching surface. The hydromagnetic effects are also investigated along with the impact of variable thermal conductivity and first order chemical reaction. Additionally, instead of usual no-slip boundary conditions, we explore the combined behavior of velocity, temperature and solutal slips on sheet surface. The concerned equations are numerically handled via the bvp4c technique and emerging factors are in depth scrutinized by the help of graphs and tables. The solution methodology is authenticated by presenting comparison with already existing results for limiting cases. One of the appealing observations is that the coefficient of skin friction, rate of heat and also mass transfer get lower by increasing the values of the velocity, thermal and solutal slip parameters. A growth in Schmidt number along with chemical reaction parameter resulted in a decay of concentration field.

4.1 Problem Development

4.1.1 Momentum, Thermal and Concentration Boundary Layer Equations

In the current section, we analyze the two-dimensional flow, heat together with mass transfer features of Cross fluid towards a stretching surface. The analysis is done regarding implementation of magnetic field and further about the impact of variable thermal conductivity and chemical reacting species. Present analysis is made by taking slip boundary conditions in consideration. An applied magnetic field having uniform strength B_0 is considered normal to sheet (i.e. $y > 0$) and the induced part of magnetic field is ignored by taking considerably small magnetic Reynolds number. The model of first order chemical reaction is selected for the analysis such that rate of reaction is in direct proportion to concentration of species [85]. The above stated assumptions enable us to write the continuity, momentum, energy and mass diffusion as (cf. Chapter 1):

$$\frac{\partial u}{\partial x} + \frac{\partial v}{\partial y} = 0, \tag{4.1}$$

$$u\frac{\partial u}{\partial x} + v\frac{\partial u}{\partial y} = \vartheta\frac{\partial}{\partial y}\left[\left(\frac{\partial u}{\partial y}\right)\left(1 + \left\{\Gamma\left(\frac{\partial u}{\partial y}\right)\right\}^m\right)^{-1}\right] - \frac{\sigma B_0^2}{\rho}u, \tag{4.2}$$

$$u\frac{\partial T}{\partial x} + v\frac{\partial T}{\partial y} = \frac{1}{\rho c_p}\frac{\partial}{\partial y}\left[k(T)\frac{\partial T}{\partial y}\right], \tag{4.3}$$

$$u\frac{\partial C}{\partial x} + v\frac{\partial C}{\partial y} = D\frac{\partial^2 C}{\partial y^2} - R_r(C - C_\infty). \tag{4.4}$$

Here, C symbolizes fluids concentration, D the solutal diffusivity, R_r the chemical reaction parameter and C_∞ represents ambient value of concentration.

In the energy equation, $k(T)$ stands for the thermal conductivity that is dependent upon temperature and varies linearly with it as proposed by Chiam [73] in the following form:

$$k(T) = k_\infty \left[1 + \varepsilon \left(\frac{T - T_\infty}{T_w - T_\infty} \right) \right],$$

(4.5)

where k_∞ indicates the ambient value of thermal conductivity while ε signify a considerably small parameter recognized as thermal conductivity parameter.

4.1.2 Associated Boundary Conditions

The related conditions on boundary are:

$$u = U_w + U_{slip}, v = 0, T = T_w + T_{slip}, C = C_w + C_{slip} \text{ at } y = 0,$$

(4.6)

$$u \to 0, T \to T_\infty, C \to C_\infty \text{ as } y \to \infty,$$

(4.7)

such that:

$$U_{slip} = L_1 \frac{\partial u / \partial y}{1 + \left(\Gamma \frac{\partial u}{\partial y} \right)^m}, T_{slip} = L_2 \frac{\partial T}{\partial y} \text{ and } C_{slip} = L_3 \frac{\partial C}{\partial y},$$

(4.8)

such that L_1, L_2 and L_3 represent the velocity, temperature along with concentration slip factors, respectively. Interestingly, the no slip boundary conditions can be retrieved by letting $L_1 = L_2 = L_3 = 0$.

4.1.3 Dimensionless Investigation

The non-dimensional form of this governing system of equations is obtained by invoking suitable transformations consisting of dimensionless variables f, θ and η (cf. Chapter 2) while the dimensionless concentration field is defined as:

$$\phi(\eta) = \frac{C - C_\infty}{C_w - C_\infty},$$

(4.9)

with C_w and C_∞ being the values of concentration on sheet surface and far off from it, respectively.

Thus, the required equations for the concerned problem can be listed as:

$$[ff'' - f'^2 - M^2 f'][1 + (We\, f'')^m]^2 + [1 + (1 - m)(We\, f'')^m]f''' = 0, \quad (4.10)$$

$$(1 + \varepsilon\theta)\theta'' + \varepsilon\theta'^2 + Pr f\theta' = 0, \quad (4.11)$$

$$\phi'' + Sc\,(f\phi' - \beta_1\phi) = 0, \quad (4.12)$$

while the boundary conditions related to new variables are:

$$f(0) = 0, f'(0) = 1 + \frac{s_1 f''(0)}{1 + (We\, f''(0))^m}, \theta(0) = 1 + s_2\theta'(0), \quad (4.13)$$

$$\phi(0) = 1 + s_3\phi'(0), \quad (4.14)$$

$$f'(\infty) \to 0, \theta(\infty) \to 0, \phi(\infty) \to 0. \quad (4.15)$$

Here M designates the magnetic parameter, Pr the Prandtl number, β_1 the chemical reaction parameter, and Sc the Schmidt number. In transformed boundary conditions, s_1, s_2 and s_3 denote the velocity, temperature and solutal slip parameters, respectively. The mathematical formulae for these dimensionless parameters are as follows:

$$M^2 = \frac{\sigma B_0{}^2}{c\rho}, Pr = \frac{\mu_0 c_p}{k_\infty}, Sc = \frac{\nu}{D}, \beta_1 = \frac{R_r}{c},$$

$$s_1 = L_1\sqrt{\frac{c}{\vartheta}}, s_2 = L_2\sqrt{\frac{c}{\vartheta}}, s_3 = L_3\sqrt{\frac{c}{\vartheta}}. \quad (4.16)$$

4.1.4 Important Physical Quantities

We now interpret some vital physical quantities namely the coefficient of skin friction C_f, Nusselt number Nu and also Sherwood number Sh, specified as:

$$C_f = \frac{\tau_w}{\frac{1}{2}\rho U_w{}^2}, Nu = \frac{Lq_w}{k(T)(T_w - T_\infty)}, Sh = \frac{Lq_m}{D(C_w - C_\infty)}, \tag{4.17}$$

where τ_w, q_w and q_m are the wall shear stress, wall heat and mass fluxes, respectively, formulated as:

$$\tau_w = \eta_0 \left.\frac{\partial u/\partial y}{1 + \left(\Gamma\frac{\partial u}{\partial y}\right)^m}\right|_{y=0}, \qquad q_w = -k(T)\left.\frac{\partial T}{\partial y}\right|_{y=0}, \quad q_m = -D\left.\frac{\partial C}{\partial y}\right|_{y=0}. \tag{4.18}$$

However, in terms of dimensionless variables (4.18) can be written as:

$$Re_L{}^{1/2}C_f = \frac{f''(0)}{1 + \left(We\, f''(0)\right)^m}, Re_L{}^{-1/2}Nu = -\theta'(0), Re_L{}^{-1/2}Sh = -\phi'(0). \tag{4.19}$$

4.2 Validation of Numerical Methodology

Before moving towards a detail discussion on the achieved numerical results, the authentication of these results and the applied numerical technique is requisite. For that numerical values of Nusselt number are related with those provided by Chiam [74] and Abel *et al.* [112] a displayed in **Table 4.1**. The results are compared for special case of Newtonian fluid by taking no-slip boundary condition while other parameters are taken as $M = \beta_1 = Sc = 0$ and $Pr = 1$. For changing ε, the solutions come up in excellent compatibility with previous results and thus assure the applied numerical method.

Table 4.1: Comparison of $-\theta'(0)$ for the special case of Newtonian fluid ($We = 0$) such that $M = Sc = \beta_1 = 0$ and $Pr = 1$ with the assumption of no-slip boundary conditions.

ε	Chiam [74]		Abel *et al.* [112]		Present study
	Analytical	Numerical	Analytical	Numerical	
0	0.5819767	0.5819767	0.5819767	0.5819767	0.58197676
0.01	0.5775551	0.5775650	0.5775653	0.5768627	0.57756503
0.05	0.5606327	0.5606773	0.5607232	0.5600819	0.56067756
0.1	0.5410215	0.5411268	0.5414776	0.5406564	0.54112736
0.2	0.5058168	0.5064329	0.5090105	0.5061888	0.50643362
0.3	0.4740012	0.4765327	0.4845751	0.4764906	0.47653350
0.4	0.4432131	0.4504452	0.4681716	0.4505875	0.45044583
0.5	0.4110909	0.4274450	0.4597999	0.4277759	0.42744552

4.3   Discussion on Results

Combined consequence of velocity slip parameter s_1 and magnetic parameter M on fluid velocity, temperature and also on concentration profiles is graphically demonstrated through **Figs. 4.1 (a-c)**. It is visualized in **Fig. 4.1 (a)** that both magnetic parameter and velocity slip parameter imparts same decreasing trend on fluid velocity. The magnetic parameter offers resistive flow within the boundary layer and physical reason behind this decline in velocity is because as the magnetic field gets stronger, the Lorentz forces offer strong resistance to the motion of the fluid.

Besides, this figure also discloses that the magnitude of velocity is improved in the absence of velocity slip parameter ($s_1 = 0$). Physically, when slip takes place, the velocity close to the surface of sheet is no more just stretching velocity and hence fluid slips past the plate. As a result, fluids velocity lessens and corresponding boundary layer decays when we take the slip effects in account. **Fig. 4.1 (b)** indicates that both the slip parameter s_1 and magnetic parameter M enrich the temperature of the fluid. The structures of thermal boundary layer are higher in the presence of velocity slip ($s_1 = 1$). The same increasing trend is observed by concentration profiles corresponding to enlargement in both M and s_1 as displayed in **Fig. 4.1 (c)**.

Figs. 4.2 (a, b) show the variation of temperature profile for elevation in thermal conductivity parameter ε and Prandtl number Pr. Comparative plots are also displayed for the case of no slip condition ($s_2 = 0$) along with thermal slip condition ($s_2 = 1$). A straight forward observation reveals that an increase in thermal slip parameter resulted in decay of thermal boundary layer structures. Physical explanation behind this decline is that with an increment in s_2, the transfer of heat from the surface of sheet to nearby fluid lowers. **Fig. 4.2 (a)** indicates that the profiles of temperature expand for elevation in thermal conductivity parameter. A rise in thermal conductivity parameter causes larger amount of heat transfer from sheet to fluid due to which temperature profile progresses. **Fig. 4.2 (b)** is graphical presentation of the reliance of the fluid temperature on the Prandtl number Pr. It is disclosed that fluid temperature reduces with Pr. Physical reason behind this drop in temperature is that with an increase in Pr, the thermal diffusivity gets weaker and thus the temperature profile decays as a result of low thermal conductivity.

Figs. 4.3 (a, b) provide the variation of concentration profiles in view of elevation in Schmidt number Sc and chemical reaction parameter β_1. In addition, the graphs are contributed characterizing behavior of solutal slip on concentration field. The comparison among the plots corresponding to no slip condition ($s_3 = 0$) and solutal slip condition ($s_3 = 1$) discloses that the role of s_3 is to shrink the concentration boundary layer thickness. **Fig. 4.3 (a)** declares that growth in Sc results in reduction of the concentration profile. It is due to the fact that a rise in Sc reduces the mass diffusion. Thus, higher values of Sc corresponds to decay of molecular diffusivity which leads to diminution of solutal boundary layer thickness. The role of β_1 on concentration profile is depicted in **Fig. 4.3 (b)**. It can be viewed that concentration profile along with solutal boundary layer thickness descends as a result of boost in β_1. An enlargement in β_1 lowers the chemical molecular diffusivity and hence due to lesser diffusion, the concentration distribution decays.

The variation of magnitude of skin friction coefficient, Nusselt number along with Sherwood number is exhibited in **Table 4.2**. The numerical values reveal that the coefficient of skin friction is enhanced with an increment in the strength of magnetic field while it lessens by growth in velocity slip parameter. Further, the heat transfer rate enhances with Pr while a reduction is seen in s_2 and ε. It is revealed that a growth in Sc and β_1 resulted in an increment of Sherwood number while it decays with increase in s_3.

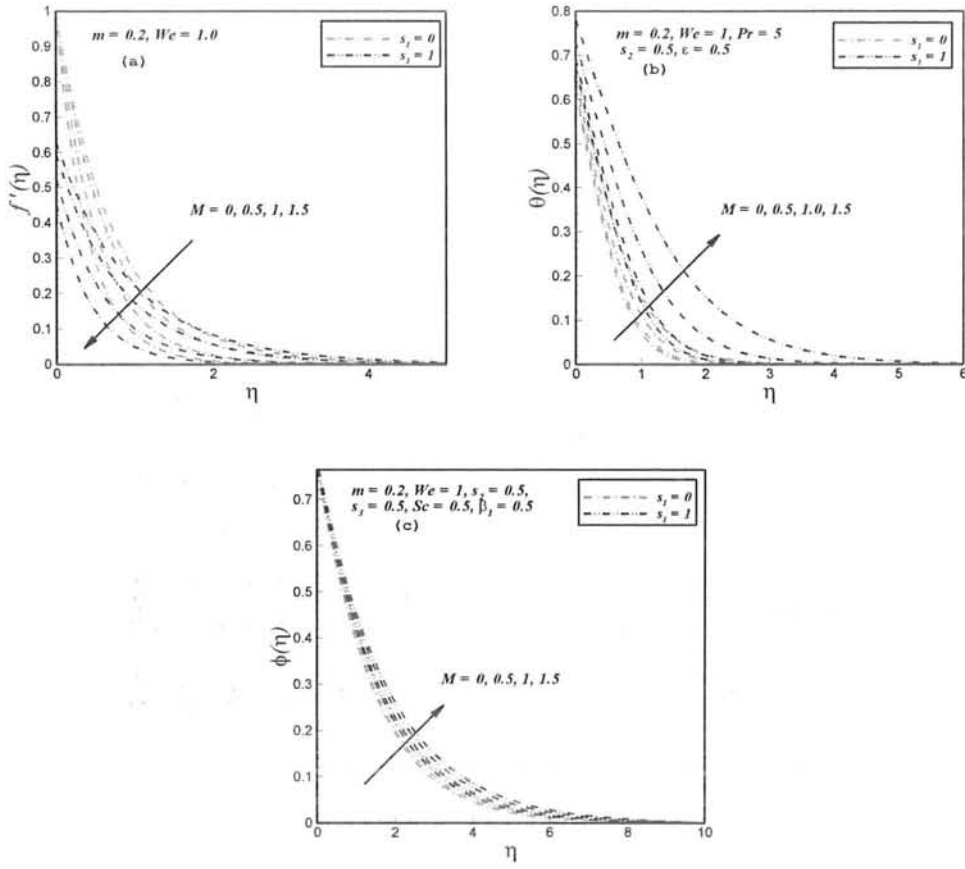**Fig. 4.1:** Dependence of magnetic parameter M and velocity slip parameter s_1 on $f(\eta)$, $\theta(\eta)$ and $\phi(\eta)$.
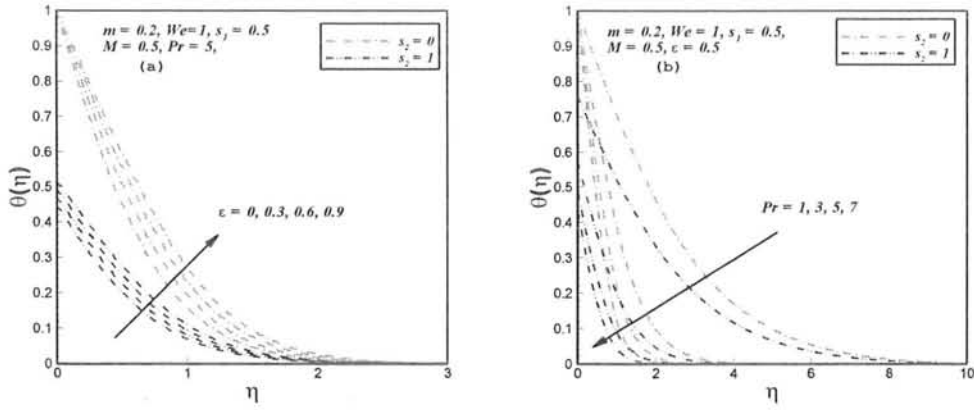
Fig. 4.2: Dependence of variable thermal conductivity ε, Prandtl number Pr and thermal slip parameter s_2 on $\theta(\eta)$.
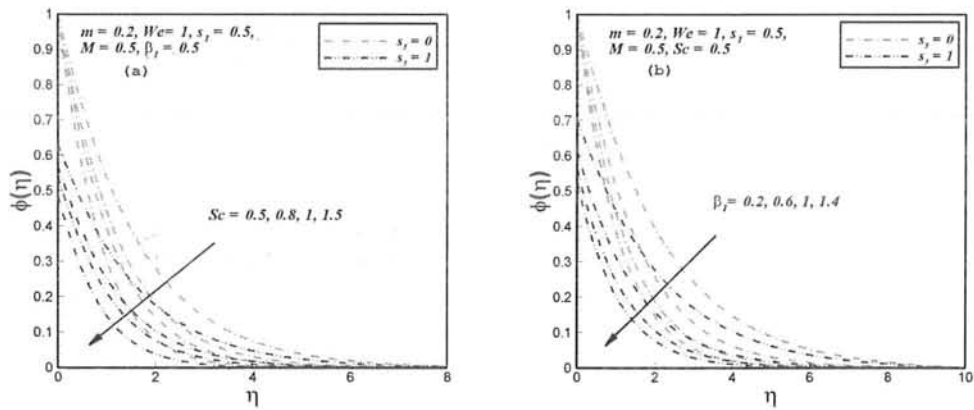

Fig. 4.3: Dependence of Schmidt number Sc, chemical reaction parameter β_1 and solutal slip parameter s_3 on $\phi(\eta)$.

Table 4.2: Numeric values of coefficient of skin friction and rate of heat and mass transfer considering growth in physical parameters.

m	We	M	s_1	ε	Pr	s_2	Sc	β_1	s_3	$-\dfrac{1}{2}Re_L{}^{1/2}C_f$	$-Re_L{}^{1/2}Nu$	$-Re_L{}^{1/2}Sh$
0.2	1	0.2	0.2	0.2	5	0.2	0.2	0.2	0.2	0.575969	1.00103	0.251510
0.3										0.553155	1.00863	0.253774
0.4										0.511168	1.02366	0.256586
	3									0.539761	0.994164	0.249521
	5									0.520575	0.990464	0.248591
		0.4								0.601891	0.986639	0.248650
		0.6								0.649569	0.964242	0.244591
			0.4							0.494012	0.959239	0.247949
			0.6							0.435550	0.924093	0.245162
				0.4						0.575969	0.926772	0.251510
				0.6						0.575969	0.863850	0.251510
					2					0.578434	0.607548	0.251511
					3					0.578463	0.767224	0.251507
						0.4				0.575969	0.843655	0.251510
						0.6				0.575969	0.727049	0.251510
							0.4			0.577286	1.00083	0.363789
							0.6			0.577286	1.00083	0.453952
								0.4		0.575969	1.00103	0.314960
								0.6		0.575969	1.00103	0.365601
									0.4	0.575969	1.00103	0.239465
									0.6	0.575969	1.00103	0.228521

Chapter 5

Falkner-Skan Flow of Chemically Reactive Cross Nanofluid with Heat Generation/Absorption

The inspiration behind the current chapter is to explore the Falkner-Skan flow of MHD Cross nanofluid across a wedge surface. The consequence of heat generation/absorption along with diffusion of chemically reactive species is also observed. Unlike the conventional no-slip conditions at the surface of the wedge, Newtonian heat and mass conditions are applied. Appropriate transformations are subjected to governing problem comprising of PDEs and resultant ODEs are accordingly handled by legendary shooting technique. The findings thus reveal that an up rise in the fluids velocity occurs by an enlargement in wedge angle parameter while the temperature along with concentration fields demonstrated a decaying trend. The heat generation/absorption parameter caused a diminution in Nusselt number. Moreover, by the application of Newtonian heat and mass conditions, enrichment in temperature plus nanoparticle concentration profiles is exhibited. Additionally, the findings of numerical investigation are validated by results already reported in literature for special case.
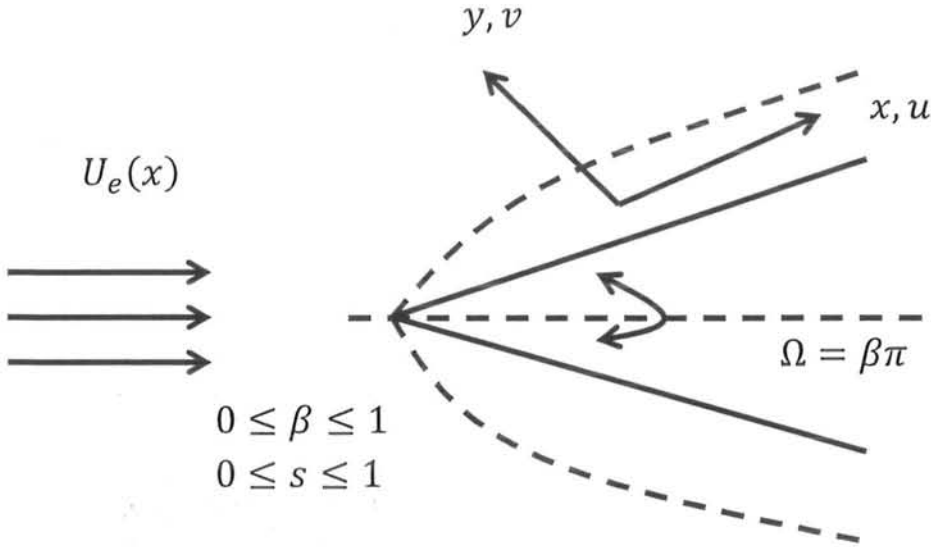
5.1 Mathematical Description

Fig. 5.1: Geometry of the problem.

5.1.1 Governing Equations

We look at the two-dimensional Falkner-Skan flow of Cross nanofluid past a wedge surface. The coordinate system is selected by choosing $x-$ axis across the wedge surface while positive $y-$axis is taken normal to surface of wedge. The wedge angle is assumed to be $\Omega = \beta\pi$, where β symbolizes the Hartee pressure gradient parameter commonly known as the wedge angle parameter. It is further assumed that $U_e = cx^s$ is the free stream velocity with which fluid passed over the wedge surface. Here, the exponent s is associated with the wedge angle $\beta\pi$ in a way that $s = \frac{\beta}{2-\beta}$ such that $0 \leq s \leq 1$. The impact of transverse magnetic field is also taken into account. Newtonian heating model for temperature and concentration is employed. Moreover,

the effect of heat generation (absorption) and chemically reactive species is investigated. In view of aforementioned assumptions, the governing equations (cf. Chapter 1) become:

$$\frac{\partial u}{\partial x} + \frac{\partial v}{\partial y} = 0, \tag{5.1}$$

$$u\frac{\partial u}{\partial x} + v\frac{\partial u}{\partial y} = -\frac{1}{\rho_f}\frac{\partial p}{\partial x} + \vartheta\frac{\partial}{\partial y}\left[\left(\frac{\partial u}{\partial y}\right)\left(1 + \left\{\Gamma\left(\frac{\partial u}{\partial y}\right)\right\}^m\right)^{-1}\right]$$
$$+ \frac{\sigma}{\rho_f}B_0{}^2(U_e - u), \tag{5.2}$$

$$u\frac{\partial T}{\partial x} + v\frac{\partial T}{\partial y} = \frac{k_f}{(\rho c_p)_f}\frac{\partial^2 T}{\partial y^2} + \tau\left[D_B\frac{\partial C}{\partial y}\frac{\partial T}{\partial y} + \frac{D_T}{T_\infty}\left(\frac{\partial T}{\partial y}\right)^2\right] + \frac{Q_0}{(\rho c_p)_f}(T - T_\infty), \tag{5.3}$$

$$u\frac{\partial C}{\partial x} + v\frac{\partial C}{\partial y} = D_B\frac{\partial^2 C}{\partial y^2} + \frac{D_T}{T_\infty}\frac{\partial^2 T}{\partial^2 y} + R_r(C - C_\infty). \tag{5.4}$$

In the above equations, ρ_f and k_f, respectively, stand for the density and thermal conductivity of the fluid, $\tau\left(= \frac{(\rho c)_p}{(\rho c)_f}\right)$ denotes the ratio of effective heat capacity of the nanoparticle to that of the fluid. D_B and D_T are the Brownian diffusion coefficient and thermophoresis diffusion coefficient, respectively. The symbols, $Q_0\left(= Q_0^*\left(\frac{x}{L}\right)^{s-1}\right)$ and $R_r\left(= R_r^*\left(\frac{x}{L}\right)^{s-1}\right)$, respectively, characterize the heat generation/absorption coefficient and the chemical reaction rate constants. It is to be noted that for the case of boundary layer flow driven by a free stream; the pressure gradient is set up by the external flow velocity (i.e. outside the boundary layer). Thus we have:

$$-\frac{1}{\rho_f}\frac{dp}{dx} = U_e \frac{dU_e}{dx}. \tag{5.5}$$

Hence, Eq. (5.2) acquires the following form:

$$\frac{\partial u}{\partial x} + v\frac{\partial u}{\partial y} = U_e \frac{dU_e}{dx} + \vartheta \frac{\partial}{\partial y}\left[\left(\frac{\partial u}{\partial y}\right)\left(1 + \left\{\Gamma\left(\frac{\partial u}{\partial y}\right)\right\}^m\right)^{-1}\right] + \frac{\sigma}{\rho_f}B_0^2(U_e - u). \tag{5.6}$$

5.1.2 Relevant Boundary Conditions

The boundary conditions for this problem can be designed as:

i) On the surface of wedge (at $y = 0$):

$$u = 0, \qquad v = 0, \qquad \frac{\partial T}{\partial y} = -h_s T, \qquad \frac{\partial C}{\partial y} = -h_c C, \tag{5.7}$$

ii) Far away from the surface (as $y \to \infty$):

$$u = U_e(x) = cx^s, \qquad T \to T_\infty, \qquad C \to C_\infty, \tag{5.8}$$

where $h_s \left(= h_s^* \left(\frac{x}{L}\right)^{-\frac{1}{2}}\right)$ and h_c depict the coefficients of heat and mass transfer, respectively.

5.1.3 Transformation into Non-Dimensional Form

The mathematical formulation is expedited with the aid of appropriate transformations which help in further simplification of the analysis. We make use of the following transformations:

$$\eta = y\sqrt{\frac{c\,(s+1)}{2v}}x^{\frac{s-1}{2}}, \psi = \sqrt{\frac{2vc}{s+1}}x^{\frac{s+1}{2}}f(\eta), \theta = \frac{T-T_\infty}{T_\infty}, \phi = \frac{C-C_\infty}{C_\infty}. \tag{5.9}$$

The resulting non-dimensional forms of momentum, energy and concentration equations become:

$$f f'' + \frac{[1 + (1 - m)(We f'')^m] f'''}{[1 + (We f'')^m]^2} + \beta[1 - (f')^2] + M^2(1 - f') = 0, \quad (5.10)$$

$$\theta'' + Pr f \theta' + Pr N_b \theta' \phi' + Pr N_t \theta'^2 + Pr \lambda_1 \theta = 0, \quad (5.11)$$

$$\phi'' + \frac{N_b}{N_t} \theta'' + Sc(f \phi' - \beta_s \phi) = 0. \quad (5.12)$$

In the above equations, the parameters λ_1, N_b, N_t, Sc and β_s specify the heat generation or absorption parameter, the Brownian motion parameter, thermophoresis parameter, the Schmidt number and the chemical reaction parameter, respectively, defined as:

$$\lambda_1 = \frac{2 Q_0^* L^{1-s}}{(\rho c)_f (1+s)c}, N_b = \frac{C_\infty D_B \tau}{\nu}, N_t = \frac{D_T \tau}{\nu}, Sc = \frac{\nu}{D_B} \text{ and } \beta_s = \frac{2 R_r^* L^{1-s}}{(1+s)c}. \quad (5.13)$$

Accordingly, the boundary conditions in dimensionless form can be stated as:

$$f(0) = 0, f'(0) = 0, \theta'(0) = -\gamma_1(1 + \theta(0)), \phi'(0) = -\gamma_2(1 + \phi(0)), \quad (5.14)$$

$$f'(\infty) \to 1, \theta(\infty) \to 0, \phi(\infty) \to 0, \quad (5.15)$$

where $\gamma_1 \left(= h_s \sqrt{\frac{2\nu x}{(s+1)U_e}} \right)$ and $\gamma_2 \left(= h_c \sqrt{\frac{2\nu x}{(s+1)U_e}} \right)$, respectively, interpret the thermal and solutal conjugate parameter.

A significant observation discloses that λ_1 determine heat generation while negative values determine heat absorption. Further, $\beta < 0$ characterizes an adverse pressure

gradient leading to decelerating flow while $\beta > 0$ indicates a favorable pressure gradient in a flow over a wedge indicating an accelerated flow. Moreover, for $\beta = 0$ $(\Omega = 0^0)$ we get the case of flow past horizontal flat plate while $\beta = 1$ $(\Omega = 180^0)$ corresponds to stagnation point flow past a vertical plate.

5.1.4 Quantities of Engineering Usance

i. **Skin friction coefficient:** It physically describes the surface drag which results due to friction of fluid against the surface of the wedge.

Conventionally, skin friction coefficient can be described as:

$$C_f = \frac{\tau_w}{\frac{1}{2}\rho U_e^2}, \tag{5.16}$$

In view of variables mentioned in Eq. (5.9), it can be transformed into the following dimensionless form:

$$Re_L^{\frac{1}{2}} C_f = \frac{2}{\sqrt{2-\beta}} \left[\frac{f''(0)}{1 + \left(We f''(0)\right)^m} \right]. \tag{5.17}$$

ii. **Nusselt Number:** It is the ratio concerning convective to conductive heat transfer. It actually depicts the rate at which heat is transferred at the wall.

The Nusselt number can be formulated as:

$$Nu = \frac{L q_w}{k(T - T_\infty)}. \tag{5.18}$$

The dimensionless form of Eq. (5.18) is given by:

$$Re_L^{-\frac{1}{2}} Nu = \frac{\gamma_1}{\sqrt{2-\beta}} \left(1 + \frac{1}{\theta(0)} \right). \tag{5.19}$$

iii.   **Sherwood number:** It accounts for amount of mass transfer at the wall.

Mathematically, it is possible to state that:

$$Sh = \frac{Lq_m}{D_B(C - C_\infty)},$$ (5.20)

where $q_m \left(= -D_B \left(\frac{\partial C}{\partial y}\right)\Big|\right)_{y=0}$ denotes the wall mass flux. The non-dimensional form

of the Sherwood number is written as:

$$Re_L^{-\frac{1}{2}}Sh = \frac{\gamma_1}{\sqrt{2-\beta}}\left(1 + \frac{1}{\phi(0)}\right).$$ (5.21)

5.2   Authentication of Numerical Manipulations

The developed non-linear equations $(5.10 - 5.12)$ with boundary conditions (5.14) and (5.15) are integrated by shooting method. Before proceeding towards the graphical discussion and making in depth analysis of the concerned problem, we first demonstrate a comparative study in order to verify our numerical approach. **Table 5.1** renders a comparative study between present and previously published solutions by Rajagopal *et al.* [96], Kuo [113], Ishaq *et al.* [114] and Hashim *et al.* [98]. The numeric values of the coefficient of skin friction are displayed corresponding to increase in wedge angle parameter β considering Newtonian fluid $(We = 0)$. An outstanding compatibility is seen and thus the legitimacy of the present numerical solution is achieved.

Table 5.1: Comparison of $f''(0)$ by variation in β when $We = M = m = 0$.

β	Rajagopal et al. [96]	Kuo [113]	Ishaq et al. [114]	Hashim et al. [98]	Present study
0.0	-	0.469600	0.4696	0.469600	0.46960049
0.1	0.587035	0.587080	0.5870	0.587035	0.58703534
0.3	0.774755	0.774724	0.7748	0.774755	0.77475459
0.5	0.927680	0.927905	0.9277	0.927680	0.92768004
1.0	1.232585	1.232589	1.2326	1.232588	1.2325877

5.3 Analysis of Results

The boundary layer equations for the Falkner-Skan flow along with heat transfer in MHD Cross nanofluid past a wedge surface are examined. The consequence of heat generation/absorption, chemical reaction and Newtonian heat and mass conditions are also assumed. The concerned problem is integrated by the help of shooting method and the numerical solutions are expressed via. graphs and tables.

Figs. 5.2 (a-c) are sketched to visualize the impact of the wedge angle parameter β on the velocity, temperature and concentration of nanofluid. The results are demonstrated for two distinct values of the power-law index i.e. $m = 0.1$ and $m = 0.3$. It is revealed from **Fig. 5.2 (a)** that with the increment in the wedge angle parameter β, the fluid velocity enhances while the thickness of momentum boundary decreases. From the physical prospective, the wedge angle parameter actually measures the pressure gradient. The positive and negative values of β correspond to

accelerated and decelerated flows, respectively. However, for the present work we only consider the accelerated flows. An increment in wedge shape effect corresponds to accelerated flow due to favorable pressure gradient. However, this boost in velocity results in decay of thickness of corresponding momentum boundary layer. It is visualized that with an enhancement in β, the velocity curve gradually squeeze near the surface of the wedge and overshoot phenomenon is not possible. Moreover, it is depicted form **Figs. 5.2 (b)** and **(c)** that temperature and nanofluid concentration profiles decline for growth in m and β. Decay in the thermal along with concentration boundary layer thickness is visualized. A decline in temperature at the surface of the wedge is due to the reason that with an increment in the values of wedge angle parameter, the driving force i.e. the pressure gradient escalates causing more flow of heat from the surface of the wedge to the fluid. Besides this, we can further interpret from the plots that the temperature as well as the nanoparticle concentration profiles is decreasing function of m.

The graphical trend for velocity, temperature and concentration fields corresponding to growing values of the thermophoresis parameter N_t is indicated in **Figs. 5.3 (a)** and **(b)**, respectively. Comparative plots are also presented for heat generation ($\lambda_1 > 0$) and absorption ($\lambda_1 < 0$). It can be seen that temperature and concentration fields are increasing function of N_t. It is further revealed that the plots are comparatively high for the heat absorption case ($\lambda_1 = -0.5$) as compared to heat generation case ($\lambda_1 = 0.5$) with much prominent impact on the temperature profile as compared to nanoparticle profiles. Physically, by an increment in thermophoresis parameter, a boost in thermophoretic force occurs as a result of which the fluid temperature and

also concentration of nanoparticle enhances due to motion of nanoparticles beginning from hot towards cold region.

The influence of thermal conjugate parameter γ_1 on temperature and concentration profiles is graphically shown in **Figs. 5.4 (a)** and **(b)**, respectively. Comparative plots for varied values of the Prandtl number Pr are also demonstrated. It is determined that temperature and also concentration boundary layer structure expands near the wall as a result of growing values of thermal conjugate parameter and gradually decays away from wall. Additionally, the plots reveal that the Prandtl number has a decreasing impact on the fluid temperature as well as the concentration of nanoparticles. However, the behavior is much prominent in the case of temperature profiles. The reason for this behavior is that the coefficient of heat transfer enhances by increasing γ_1 and as a result of which more heat transports from the surface of the wedge to the fluid causing an increment in fluid temperature. Moreover, for $\gamma_1 = 0$, we achieve the insulated wall problem while for $\gamma_1 \to \infty$, we get the case of constant wall temperature. Furthermore, it is fascinating to mention that the Prandtl number can be used as a cooling agent as it regulates the rate of cooling.

Figs. 5.5 (a, b) are presented to exhibit the dependence of the nanofluid temperature and nanoparticle concentration profile on the solutal conjugate parameter γ_2 and the Brownian motion parameter N_b. It is deduced from the plots that the temperature and also nanoparticle concentration are enhances with γ_2. Additionally, the Brownian motion parameter boosts temperature along with nanoparticle concentration fields as well as their corresponding boundary layers thickness. It is due to the fact that an

enhancement in N_b leads to rise in effective motion of nanoparticles and thus the kinetic energy increases which further enriches fluids temperature.

Figs. 5.6 (a, b) express the variation of temperature along with nanoparticle concentration profiles corresponding to lift in chemical reaction parameter β_s and Schmidt number Sc. **Fig. 5.6 (a)** delineates that Sc and β_s has decaying impact on the temperature field and corresponding thermal boundary structures. However, the effect on thermal boundary layer is minimum relative to concentration boundary layer. **Fig. 5.6 (b)** exhibits decreasing trend observed by nanoparticle concentration field corresponding to escalating values of Sc and β_s. The physical reason behind this decline in concentration boundary layer through increment in Sc is due to decline in the mass diffusion. Moreover, incremented values of chemical reaction parameter results in lowering the chemical molecular diffusivity which in turns leads to lesser diffusion.

Table 5.2 gives the data portraying values of the coefficient of skin friction, Nusselt number and Sherwood number for variation in physical parameters. It is observed that the skin friction coefficient decays by increment in power-law index m, Weissenberg number We and the magnetic parameter M while it ascends for boost in β. The magnitude of heat transfer at wedge surface can be enhanced by escalating values of Pr, N_b, Sc, β_s and γ_1. However, it is reduced for increasing values of thermophoresis parameter N_t and the heat generation/absorption parameter λ_1. Moreover, Sherwood parameter is found to increase for uplifting values of Sc, γ_2 and β_s.
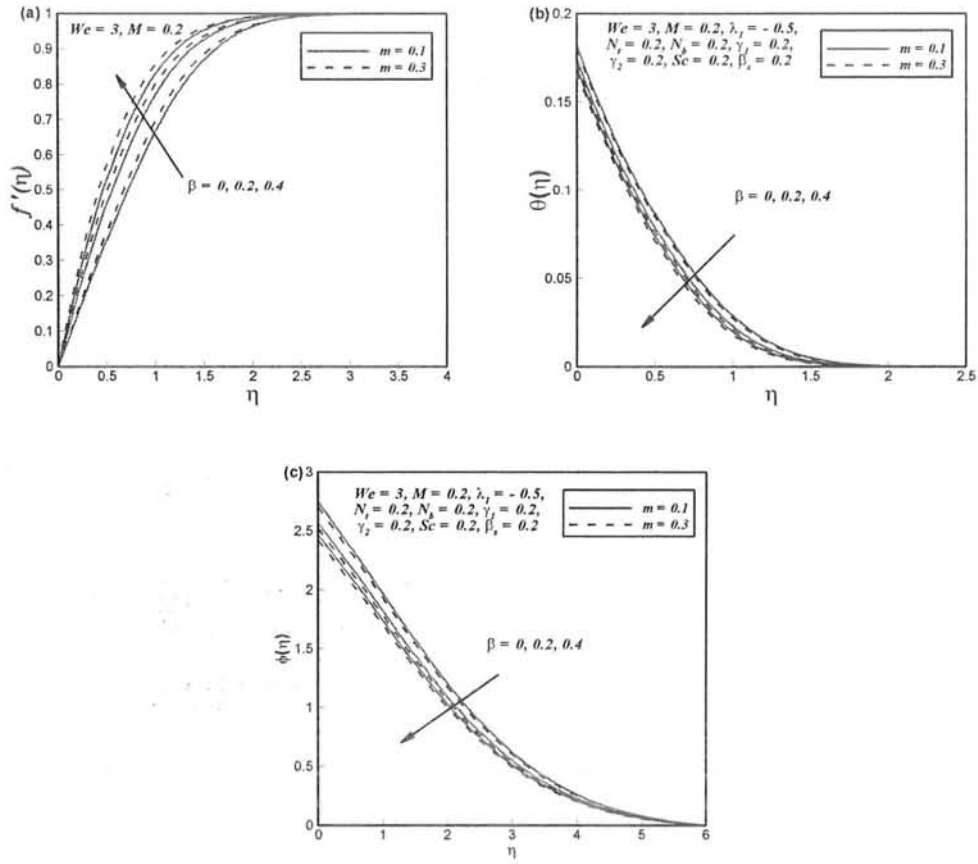
Fig. 5.2: Dependence of β and m on (a) velocity, (b) temperature and (c) concentration profiles.
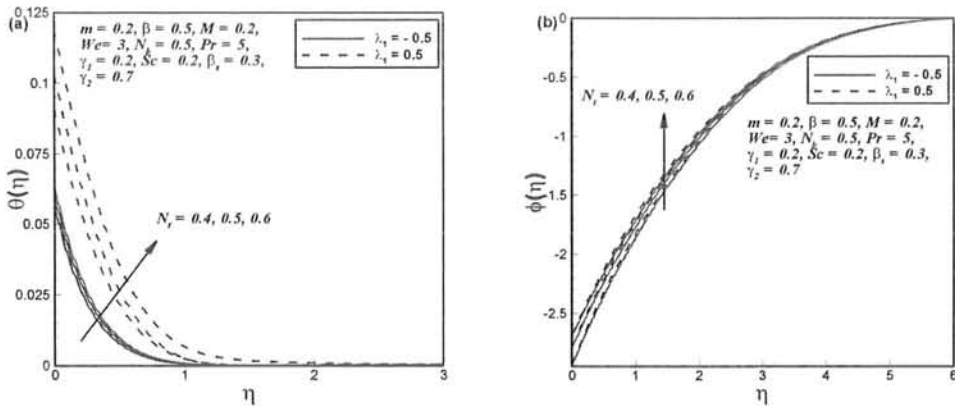
Fig. 5.3: Dependence of N_t and λ_1 on (a) temperature and (b) concentration profiles.

Fig.5.4: Dependence of γ_1 and Pr on (a) temperature and (b) concentration profiles.

Fig. 5.5: Effect of γ_2 and N_b on (a) temperature and (b) concentration profiles.

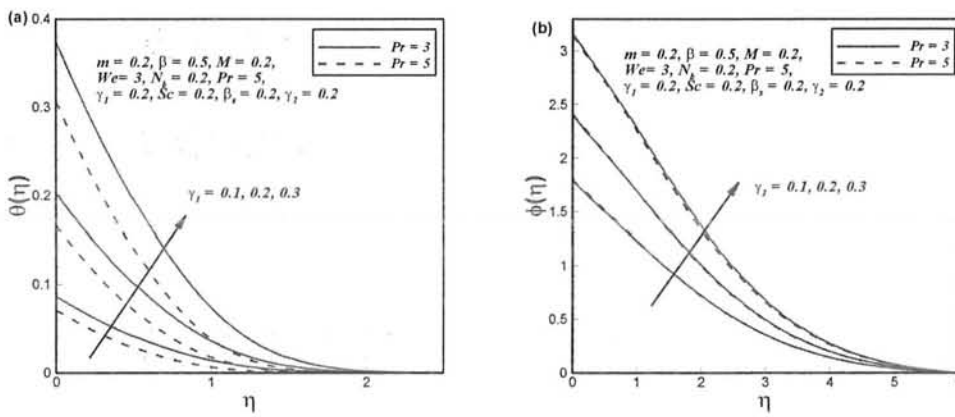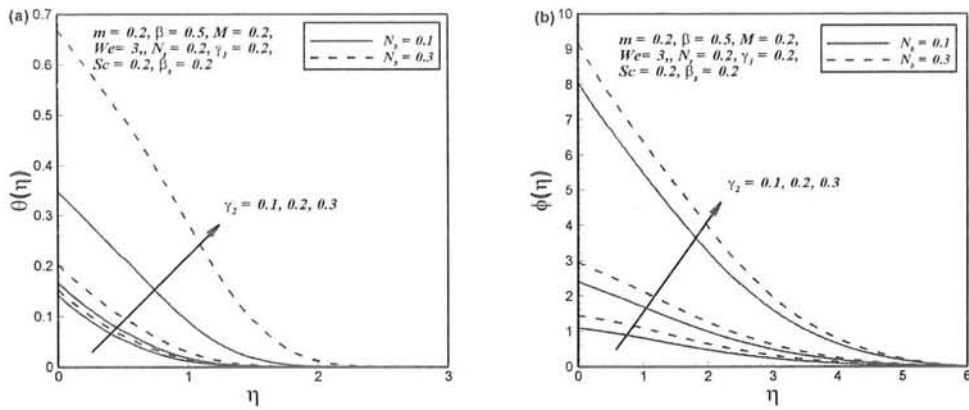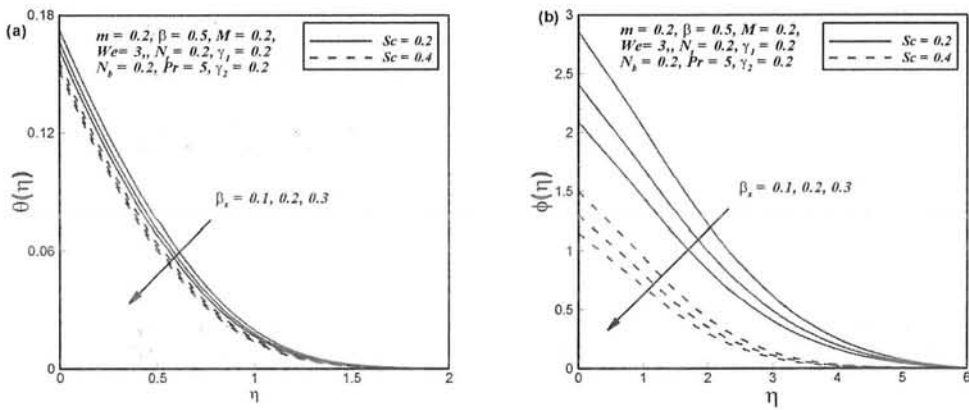**Fig. 5.6:** Dependence of β_s and Sc on (a) temperature and (b) concentration profiles.

Table 5.2: The values of skin friction coefficient and rate of heat and mass transfer at wall.

m	We	M	β	Pr	N_b	N_t	λ_1	γ_1	Sc	β_s	γ_2	$Re_L^{\frac{1}{2}}C_f$	$Re_L^{-\frac{1}{2}}Nu$	$Re_L^{-\frac{1}{2}}Sh$
0.2	2	0.2	0.5	5	0.5	0.4	-0.5	0.2	0.2	0.3	0.7	1.06240	3.02737	0.37705
0.3												1.04268	3.05174	0.37767
0.4												1.02078	3.06866	0.37845
	3											1.03805	3.03958	0.37754
	5											1.00679	3.05568	0.37818
		0.5										1.17178	3.07026	0.37856
		0.7										1.28469	3.10816	0.38001
			0.6									1.17321	3.15824	0.39150
			0.7									1.28867	3.31233	0.40734
				2								1.06240	1.52851	0.37529
				3								1.06240	2.04392	0.37612
					0.6							1.06240	3.58007	0.38684
					0.7							1.06240	3.89637	0.39568
						0.5							2.85783	0.36650
						0.6							2.73154	0.35883
							-0.3						2.84498	0.37692
							0.5						1.94640	0.37587
								0.3					3.30604	0.40075
								0.4					3.60467	0.42000
									0.3				4.04240	0.42216

0.5			8.55555	0.49309
	0.4		3.25642	0.39045
	0.5		3.52011	0.40338
		0.8	2.75242	0.38918
		0.9	2.58913	0.39915

Chapter 6

Axisymmetric Flow and Heat Transfer to Cross Fluid across a Radially Stretching Sheet

The main objective behind current chapter is to examine the axisymmetric flow together with heat transfer of an incompressible Cross fluid past a radially stretching surface. The boundary layer equations, derived in cylindrical polar coordinates, are numerically investigated to inspect flow characteristics. The non-linear ODEs acquired by applying certain transformations are simplified by well-known shooting technique. The profiles of velocity along with temperature are graphically demonstrated against variation in governing parameters. Also, numerical data is presented for skin friction coefficient together with Nusselt number for further understanding of problem. One of the interesting finding of the analysis is that the power-law index helps in elevation of the momentum boundary layer structure while the thermal boundary layer structure lowered. Comparison is bestowed relating existing literature with our results for a subcase an the legitimacy of current solutions is ensured.
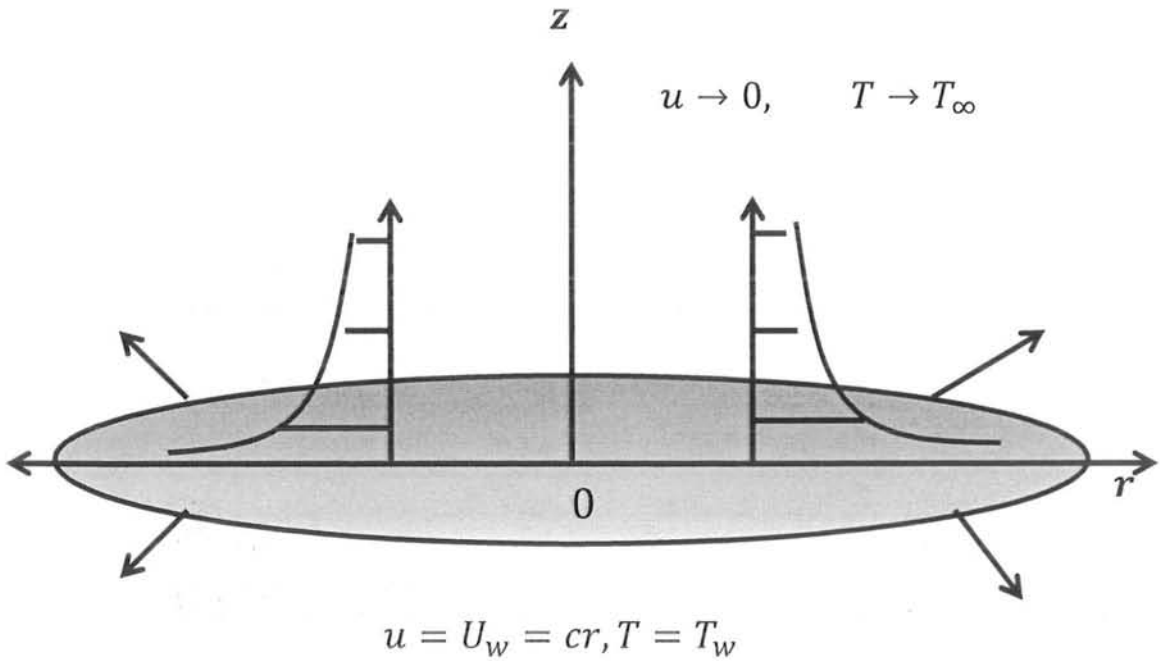
6.1   Mathematical Analysis

Fig. 6.1: Schematic diagram of the problem with coordinate system.

6.1.1 Interpretation of Flow Dynamics

The aim of this section is to visualize the two dimensional axisymmetric flow by considering Cross fluid subjected to radially stretching sheet. The sheet is supposed to align with $r\theta -$ plane while the fluid lies in the region $z > 0$ of the vertical axis (as shown in **Fig. 6.1**). The sheet is linearly stretched within its own plane having velocity $U = cr$ along the radial direction. All physical quantities will be treated independent of the azimuthal component θ due to rotational symmetry.

The conservation equations related to mass and linear momentum considering axisymmetric flow of Cross fluid (cf. Chapter 1) are given below:

$$\frac{\partial w}{\partial z} + \frac{\partial u}{\partial r} + \frac{u}{r} = 0, \tag{6.1}$$

$$u\frac{\partial u}{\partial r} + w\frac{\partial u}{\partial z} = \vartheta\frac{\partial}{\partial z}\left[\left(\frac{\partial u}{\partial z}\right)\left(1 + \left\{\Gamma\left(\frac{\partial u}{\partial z}\right)\right\}^m\right)^{-1}\right]. \tag{6.2}$$

The relevant velocity boundary conditions are:

$$u(r,0) = U(r) = cr, w(r,0) = 0, \tag{6.3}$$

$$u(r,\infty) \to 0. \tag{6.4}$$

The dimensional stream function ψ for the present problem is selected as:

$$\psi = -r^2\sqrt{vc}f(\eta), \tag{6.5}$$

with

$$\eta = z\sqrt{\frac{c}{v}}. \tag{6.6}$$

The equation of continuity will be identically satisfied by choosing ψ as:

$$(u,w) = \left(-\frac{1}{r}\frac{\partial\psi}{\partial z}, \frac{1}{r}\frac{\partial\psi}{\partial r}\right). \tag{6.7}$$

On making use of Eqs. $(6.5 - 6.7)$, the momentum equation (6.2) is transformed as below:

$$\left(2ff'' - f'^2\right)(1 + (We\,f'')^m)^2 + (1 + (1-m)(We\,f'')^m)f''' = 0, \tag{6.8}$$

while the boundary conditions become:

$$f(0) = 0, f'(0) = 1, f'(\infty) \to 0. \tag{6.9}$$

The dimensionless physical quantity having physical importance is the coefficient of skin friction:

$$C_f = \frac{\tau_{rz}|_{z=0}}{\frac{1}{2}\rho u_w^2},$$
(6.10)

such that $\tau_{rz}\left(= \left[\eta_0 \frac{\frac{\partial u}{\partial z}}{1+\left\{\Gamma\left(\frac{\partial u}{\partial z}\right)\right\}^m}\right]_{z=0}\right)$ is local wall shear stress.

In terms of dimensionless variables, the skin friction coefficient turns into:

$$\frac{1}{2}Re_L^{\frac{1}{2}}C_f = \frac{f''(0)}{1 + \left(Wef''(0)\right)^m},$$
(6.11)

such that $Re_L\left(= \frac{cr^2}{\vartheta}\right)$

6.1.2 Heat Transfer Mechanism

Let us take an isothermal radially stretching sheet kept at constant temperature T_w while ambient fluid is assumed to have temperature T_∞ under the assumption $T_w > T_\infty$. Considering the aforementioned presumptions, the energy equations under the usual thermal boundary layer approximation is explained by:

$$u\frac{\partial T}{\partial r} + w\frac{\partial T}{\partial z} = \alpha\frac{\partial^2 T}{\partial z^2},$$
(6.12)

while the thermal boundary conditions are:

$$T(r,0) = T_w, T(r,\infty) \to T_\infty.$$
(6.13)

Transforming Eqs. (6.12) and (6.13) based on dimensionless temperature $\theta \left(= \frac{T - T_\infty}{T_w - T_\infty}\right)$ as

$$\theta'' + 2Prf\theta' = 0, \tag{6.14}$$

$$\theta(0) = 1, \theta(\infty) \to 0 \cdot \tag{6.15}$$

where $Pr \left(= \frac{\eta_0 c_p}{k}\right)$ is the Prandtl number.

The expression for the heat transfer rate commonly recognized as Nusselt number is contributed by:

$$Nu = \frac{Lq_w}{k(T_w - T_\infty)}, \tag{6.16}$$

with $q_w \left(= -k \left.\frac{\partial T}{\partial z}\right|_{z=0}\right)$ being the surface heat flux. Eq. (6.16) can be written in terms of dimensionless temperature at the wall as follows:

$$-Re_L^{-\frac{1}{2}} Nu = \theta'(0). \tag{6.17}$$

6.2 Affirmation of Numerical Technique

The governing problem of flow and transfer of heat in Cross fluid across a radially stretching sheet is numerically analyzed by incorporating shooting technique. The numerical scheme is certified by taking a special case and comparing our obtained numerical results by the results already calculated with the homotopy analysis method (HAM). **Table 6.1** demonstrates an excellent agreement among the numerical solution of the present paper with the HAM solution reported by Khan and Shahzad [115] for the case of viscous fluid ($We = 0$).

Table 6.1: Comparison embodying the values of skin friction coefficient for Newtonian fluid $(We = 0)$.

Khan and Shahzad [115]	Present study
HAM solution	Numerical solution
-1	-0.9998

6.3. Interpretation of Numerical Results

The governing problem embodying the phenomenon of flow and transfer of heat in Cross fluid near radially stretching sheet is numerically solved and the solutions are graphically illustrated through **Figs.** $(6.2 - 6.4)$ for emerging parameters. The numeric values are presented for the skin friction coefficient and Nusselt number as displayed in **Table 6.2**.

The demonstration of the consequence of the power-law index m on the fluid velocity together with temperature is presented in **Fig. 6.2 (a, b)**. The examination of **Fig. 6.2 (a)** reveals that the velocity profiles along with momentum boundary layer thickness show a progressive trend for shear-thinning regime $(m < 1)$. Besides this, it is noticed from **Fig. 6.2 (b)** that temperature profiles along with its corresponding boundary layer structure lower corresponding to increase in m. The physical reason for this behavior is that less resistance is faced by shear-thinning fluid due to low viscosity which enlarges the fluid velocity and lowers its temperature.

Fig. 6.3 (a, b) portray the relationship between Weissenberg number We and fluid velocity along with temperature, respectively. The analysis of these figures imparts that We leads to lessening of fluid velocity and enhancement of fluid temperature. **Fig. 6.3 (a)** exposes that the growing values of We results in reduction of momentum boundary layer structures. However, the thermal boundary layer structures rises corresponding to enlargement in We as shown in **Fig. 6.3 (b)**. Physically, an uplift in We causes boost in relaxation time resulting the fluid velocity to diminish and fluid temperature to escalate.

Fig. 6.4 depicts the graphical behavior of Prandtl number Pr on temperature field for fixed values of m and We. It is manipulated that the fluid temperature diminishes with increase in Pr. It further discloses that thermal boundary layer structures gradually decreases by growth in Pr. Physically, an up rise in Pr causes reduction in thermal diffusivity resulting in restriction of the flow of heat into the fluid. Thus, the boundary layer structures get thinner with a rise in the Prandtl number.

Numeric results for skin friction coefficient also for Nusselt number are listed in **Table 6.2** for variation in m, We and Pr. It is clear that skin friction coefficient declines with m for fixed value of We. Similarly, a decreasing behavior in $-\frac{1}{2}Re^{\frac{1}{2}}C_{f_r}$ is observed for growing values of We. Moreover, it is observed that the rate of transfer of heat on wall enhances for growth in m. Additionally, Nusselt number is increasing function of Pr while it decreases with a rise in We.
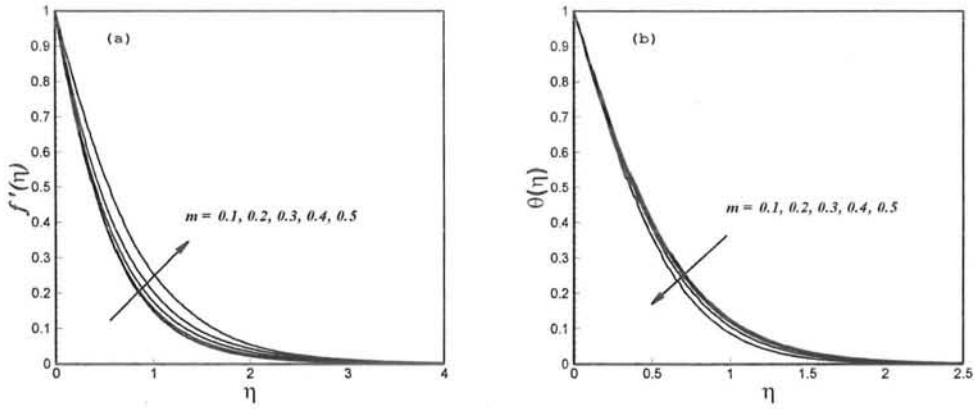
Fig. 6.2: Plots of velocity together with temperature for several values of m when $We = 2$ and $Pr = 5$.
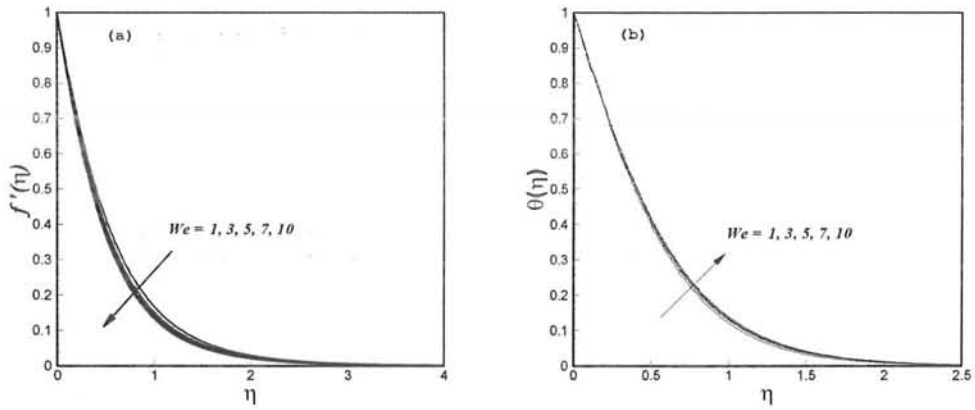

Fig. 6.3: Plots of velocity together with temperature for several values of We when $m = 0.2$ and $Pr = 5$.
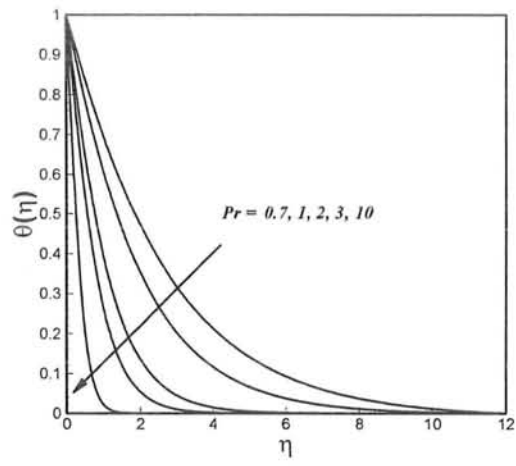
Fig. 6.4: Plots of temperature for several values of Pr when $m = 0.2$ and $We = 2$.

Table 6.2: Numeric values of skin friction coefficient $\left(-\frac{1}{2}Re_L^{\frac{1}{2}}C_f\right)$ and Nusselt number $\left(-Re_L^{-\frac{1}{2}}Nu\right)$ subject to increment in $We,\ m$ and Pr.

Parameters (fixed values)	Parameters		$-\dfrac{1}{2}Re_L^{\frac{1}{2}}C_f$	$-Re_L^{\frac{1}{2}}Nu$
$We = 2, Pr = 5$	m	0.1	0.799019	1.389500
		0.2	0.733602	1.393680
		0.3	0.630492	1.413910
$m = 0.2, Pr = 5$	We	1	0.769758	1.408150
		3	0.711423	1.385700
		5	0.683958	1.372780
$m = 0.2, We = 2$	Pr	0.7		0.359731
		2		0.744336

Chapter 7

Melting and Non-linear Radiative Heat Transfer in Stagnation Point Flow of Cross Fluid

This chapter endows an extensive analysis on the melting phenomenon in stagnation point flow of Cross fluid subject to non-linear thermal radiation. Flow process is initiated through a radially stretching sheet in view of rotational symmetry. Transformation approach is picked to achieve the non-linear ODEs from standard conservation equations of mass, linear momentum and energy. Numerical results of the concerned problem are computed via the shooting technique. Characteristics of flow features are comprehensively analyzed through graphical behavior. In addition, comparative analysis is presented for the cases when the velocity of free stream dominates the velocity of stretching surface and vice versa. The outcomes are verified by taking special cases and excellent compatibility is achieved with the existing literature. The detail analysis anticipates that the boundary layer structures could be strengthened by raising the melting parameter. The temperature profiles and the thermal boundary layer structures behaved oppositely corresponding to rise in non-linear radiation parameter and temperature ratio parameter.

7.1 Formulation of the Problem

7.1.1 Problem Development

In the current section, an analysis is done on the melting heat transfer on flow of Cross fluid in region of stagnation point. We suppose an axisymmetric flow situation by considering a radially stretching sheet having stretched velocity $u_w(r) = cr$ while the velocity of the external flow is taken to be $u_e(r) = dr$ such that c and d are positive constants. The temperature of melting sheet is considered to be T_m while temperature of fluid at the free stream is T_∞ in a way that $T_m < T_\infty$. Further the heat transfer process is investigated in view of non-linear thermal radiations. Keeping in view the above mentioned assumptions, the boundary layer equations (cf. Chapter 1) take the following form:

$$\frac{\partial w}{\partial z} + \frac{\partial u}{\partial r} + \frac{u}{r} = 0,\tag{7.1}$$

$$u\frac{\partial u}{\partial r} + w\frac{\partial u}{\partial z} = u_e\frac{du_e}{dr} + \vartheta\frac{\partial}{\partial z}\left[\left(\frac{\partial u}{\partial z}\right)\left(1 + \left\{\Gamma\left(\frac{\partial u}{\partial z}\right)\right\}^m\right)^{-1}\right],\tag{7.2}$$

$$u\frac{\partial T}{\partial r} + w\frac{\partial T}{\partial z} = \frac{k}{\rho c_p}\frac{\partial^2 T}{\partial z^2} - \frac{1}{\rho c_p}\left(\frac{\partial q_r}{\partial z}\right),\tag{7.3}$$

where q_r being the radiative heat flux in $z-$direction will be simplified by non-linear Rosseland approximation [116], by the help of which we can get the results for both small and also for large temperature differences among temperature of plate and far away from it. Thus, we simplify q_r as:

$$q_r = -\frac{4\,\sigma^*}{3\,k^*}\frac{\partial T^4}{\partial z} = -\frac{16\,\sigma^*}{3\,k^*}T^3\frac{\partial T}{\partial z}.\tag{7.4}$$

By virtue of Eq. (7.4), the energy equation (7.3) becomes:

$$u\frac{\partial T}{\partial r} + w\frac{\partial T}{\partial z} = \frac{\partial}{\partial z}\left[\left(\alpha + \frac{16}{3}\frac{\sigma^*}{k^*\rho c_p}T^3\right)\frac{\partial T}{\partial z}\right].$$

(7.5)

7.1.2 Corresponding Boundary Conditions

The boundary conditions subjected to current situation are:

$$u(r,0) = u_w(r) = cr, \; w(r,0) = 0, \; T(r,0) = T_m,$$

(7.6)

$$k\frac{\partial T}{\partial z} = \rho[\lambda + c_s(T_m - T_0)]w(r,0),$$

(7.7)

$$u(r,\infty) = u_e(r) \to dr, \; T(r,\infty) \to T_\infty,$$

(7.8)

where λ stands for fluids latent heat and c_s the heat capacity of solid surface. The physical interpretation of Eq. (7.7) is that the heat conducted to melting surface equals the heat of melting plus the sensible heat needed to boost solid temperature T_0 to melting temperature T_m [66].

7.1.3 Non-Dimensional Analysis

We invoke suitable transformations to reduce our problem into respective ordinary differential equations. For this, we take the dimensionless independent variable η and the dimensional stream function ψ as defined is previous chapter (cf. Chapter 6). However, the dimensionless temperature for the present case is defined as:

$$\theta = \frac{T - T_m}{T_\infty - T_m}.$$

(7.9)

Moreover, $T = T_m[1 + (\theta_m - 1)\theta]$, such that $\theta_m\left(= \frac{T_\infty}{T_m}\right)$ is the temperature ratio parameter with $\theta_m > 1$.

Based on these transformations, the continuity equation is satisfied identically while Eq. (7.2) and (7.5) are reduced into the following form:

$$\left(2 f f'' - f'^2 + A^2\right)(1 + (We\, f'')^m)^2 + (1 + (1 - m)(We\, f'')^m)f''' = 0, \quad (7.10)$$

$$\theta'' + 2\, Pr\, f\, \theta' + \frac{4}{3\, N_R}\frac{d}{d\eta}[\{1 + (\theta_m - 1)\theta\}^3 \theta'] = 0. \quad (7.11)$$

The transformed boundary conditions are organized as:

$$f'(0) = 1, \quad Pr\, f(0) + Me\, \theta'(0) = 0, \quad \theta(0) = 0, \quad (7.12)$$

$$f'(\infty) = A, \qquad \theta(\infty) = 1, \quad (7.13)$$

where A turns into velocity ratio parameter, N_R the non-linear radiation parameter and Me the melting parameter, formulated as:

$$A = \frac{d}{c}, \quad N_R = \frac{k\, k^*}{4\, \sigma^* T_m^3}, \quad Me = \frac{c_p(T_\infty - T_m)}{\lambda + c_s(T_m - T_0)}. \quad (7.14)$$

The melting parameter Me is actually the ratio of the Stefan number for liquid phase $\frac{c_p(T_\infty - T_m)}{\lambda}$ to the Stefan number for solid phase $c_s(T_m - T_0)$.

7.1.4 Effective Engineering Quantities

The dimensional representation of skin friction coefficient along with Nusselt number is specified as:

$$C_f = \frac{\tau_{rz}|_{z=0}}{\frac{1}{2}\rho u_w^2}, \qquad Nu = \frac{rL}{k(T_\infty - T_m)}, \quad (7.15)$$

where τ_{rz} and q_w are defined as:

$$\tau_{rz}|_{z=0} = \left[\eta_0 \frac{\frac{\partial u}{\partial z}}{1 + \left\{\Gamma\left(\frac{\partial u}{\partial z}\right)\right\}^m}\right]_{z=0} \quad , \qquad q_w = -k \left.\frac{\partial T}{\partial z}\right|_{z=0} + q_r|_{z=0} \,. \qquad (7.16)$$

The dimensionless form of Eq. (7.15) is given by:

$$\frac{1}{2} Re_L^{\frac{1}{2}} C_f = \frac{f''(0)}{1 + \left(We f''(0)\right)^m} \,,$$

$$-Re_L^{-\frac{1}{2}} Nu = \theta'(0)\left[1 + \frac{4}{3\,N_R}[\{1 + (\theta_m - 1)\theta\}^3]\right]. \qquad (7.17)$$

7.2 Correctness of Results

The legitimacy of the obtained numerical solutions is proved by bestowing comparison with already published results for special case. **Table 7.1** validates the present results by showing a comparison with the results published by Khan *et al.* [117]. The value of skin friction coefficient is compared with the numerical result, HAM solution and exact solution reported for Newtonian fluid case ($We = 0$). An excellent agreement is achieved which assures our numerical solutions.

Table 7.1: Comparative analysis of coefficient of skin friction for Newtonian fluid ($We = 0$) with $Me = A = 0$.

	Khan *et al.* [117]			Present study
	HAM solution	Exact solution	Numerical solution	
$\frac{1}{2} Re_L^{\frac{1}{2}} C_f$	-1.173721	-1.173721	-1.173721	-1.1737203

7.3 Examination of Numerical Results

The numerical results of non-linear equations (7.10) and (7.11) specified by boundary conditions (7.12) and (7.13) are computed by the help of shooting technique. The influence of pertinent parameters on the velocity along with temperature fields, skin friction coefficient and Nusselt number is presented through graphs and tables. The obtained solutions are validated by bestowing a comparison with already existing results for a sub case.

Fig. 7.1 (a,b) demonstrate the dependence of the power-law index m on the velocity and also on temperature profiles, respectively. In addition, comparative plots are displayed for the case when the velocity of free stream dominates compared with stretching velocity $(A > 1)$ and vice versa $(A < 1)$. **Fig. 7.1 (a)** exhibits a rise in the velocity profiles for increasing values of m for both cases when stretching velocity is higher than the free stream velocity and vice versa. However, much prominent impact is noticed for the case when $(A < 1)$. The examination of **Fig. 7.1 (b)** reveals that a minor increase in temperature profiles is seen for growth in m when the velocity of free stream is greater than the stretching velocity $(A > 1)$ as well as when the rate of stretching velocity dominates the rate of free stream velocity $(A < 1)$. However, the structures of thermal boundary layer are comparatively thicker when the velocity ratio parameter A has a value less than one.

The impact of the Weissenberg number We in controlling the flow behavior is displayed in **Fig. 7.2 (a,b)**. The graphical behavior exhibits both possibilities when the velocity of free stream exceeds the stretching velocity $(A > 1)$ and when the velocity concerning stretching is more than the free stream velocity $(A < 1)$. **Fig. 7.2**

(a) shows that the uplifting values of the Weissenberg number We has opposite impact on the momentum boundary layer thickness for the case when stream velocity is greater as compared to stretching velocity $(A > 1)$ and vice versa. However, the fluid velocity rises for elevating values of We for both cases $A > 1$ and $A < 1$. The inspection of **Fig. 7.2 (b)** also reveals that the profiles of temperature behaves oppositely for increase in We relating to two cases that are $A > 1$ and $A < 1$. The fluid temperature increases for the case when $A < 1$ while the corresponding boundary layer thickness is larger for the state when $A < 1$.

Fig. 7.3 (a) and **Fig. 7.3 (b)** reveal the graphical trend of velocity along with temperature fields under the effect of velocity ratio parameter A. **Fig. 7.3 (a)** discloses that the fluid velocity increases for increment in A for both cases i.e. $A > 1$ and $A < 1$. However, the momentum boundary structures show opposite trend in both cases. The momentum boundary layer thickens for the case when the rate of stretching velocity is higher compared to the rate of free stream velocity $(A < 1)$ and decays for the converse situation $(A > 1)$. **Fig. 7.3 (b)** displays that for rise in the values of velocity ratio parameter, the fluids temperature boosts while corresponding thermal boundary layer thickness reduces.

The graphical trend of profiles of fluids velocity along with temperature subject to escalating values of the melting parameter Me is demonstrated in **Fig. 7.4 (a)** and **Fig. 7.4 (b)**, respectively. It is quite obvious that the melting parameter improves the boundary layer structures by strengthening them. The momentum boundary layer thickness enlarges analogous to growing melting parameter for both situations when the velocity ratio parameter has values greater than or less than unity $(A < 1$ and

$A > 1$) as indicated in **Fig. 7.4 (a)**. Likewise, **Fig. 7.4 (b)** declares that fluids temperature descends with increase in Me while corresponding structures of boundary layer ascend. Moreover, the boundary layer structures shrinks. The melting boundary condition behaves like a blowing boundary condition on sheet surface and due to that boundary layer structures thicken up as the melting parameter enlarges. Furthermore, with the increases in the melting temperature the difference in temperature among melting surface and ambient fluid increases which results in the reduction of fluid temperature.

The impact of the temperature ratio parameter θ_m on velocity and also on temperature fields is disclosed in **Fig. 7.5 (a,b)**. It is evident that the velocity profile is a growing function of the temperature ratio parameter for $A < 1$ but opposite trend is seen for the case when $A > 1$ as displayed in **Fig. 7.5 (b)**. It is determined through **Fig. 7.5 (b)** that the temperature of the fluid gradually drops for both cases when $A > 1$ and $A < 1$. The thermal boundary layer structures rises with increase in temperature ratio parameter θ_m having significantly prominent impact in the case when $A < 1$.

Fig. 7.6 (a) and **Fig. 7.6 (b)** express the dependence of the Prandtl number Pr on velocity together with temperature of fluid, respectively. It is obvious from **Fig. 7.6 (a)** that fluid velocity declines as a result of elevated values of the Prandtl number for $A < 1$ while opposite trend is visualized when $A < 1$. **Fig. 7.6 (b)** displays that the temperature profiles show elevation under increased Prandtl number and thermal boundary layer thickness is greater whenever $A < 1$.

Fig. 7.7 exhibits the consequence of the non-linear parameter N_R on the temperature field in the case when free stream velocity over steps the stretching velocity ($A > 1$)

and when the rate of stretching velocity dominates the rate of free stream velocity ($A < 1$). A growth in fluid temperature is visualized in response to elevation in N_R while a diminution in boundary layer structures is seen.

Table 7.2 is tabulated to monitor the relationship between the emerging parameters and skin friction coefficient along with Nusselt number. It is clear from the values that the skin friction coefficient together with Nusselt number elevates with rise in the velocity ratio parameter and Prandtl number. However, decay in the skin friction coefficient and Nusselt number is visualized for growth in We, Me and N_R.
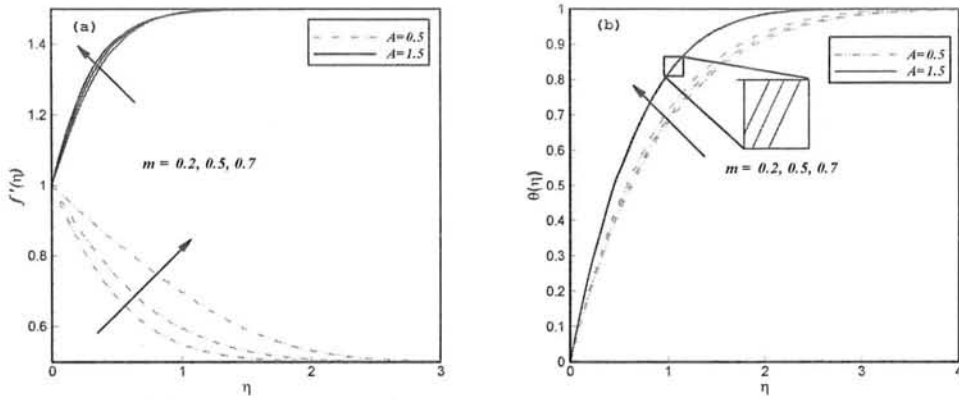
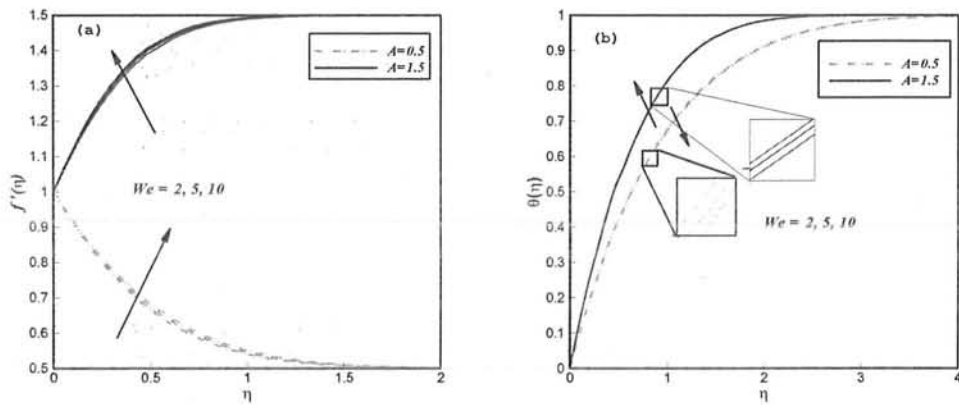**Fig. 7.1:** Profiles of $f'(\eta)$ and $\theta(\eta)$ subject to rise in m.

Fig. 7.2: Profiles of $f'(\eta)$ and $\theta(\eta)$ subject to rise in We.

Fig. 7.3: Profiles of $f'(\eta)$ and $\theta(\eta)$ subject to rise in A.

Fig. 7.4: Profiles of $f'(\eta)$ and $\theta(\eta)$ subject to rise in Me.

Fig. 7.5: Profiles of $f'(\eta)$ and $\theta(\eta)$ subject to rise in θ_m .
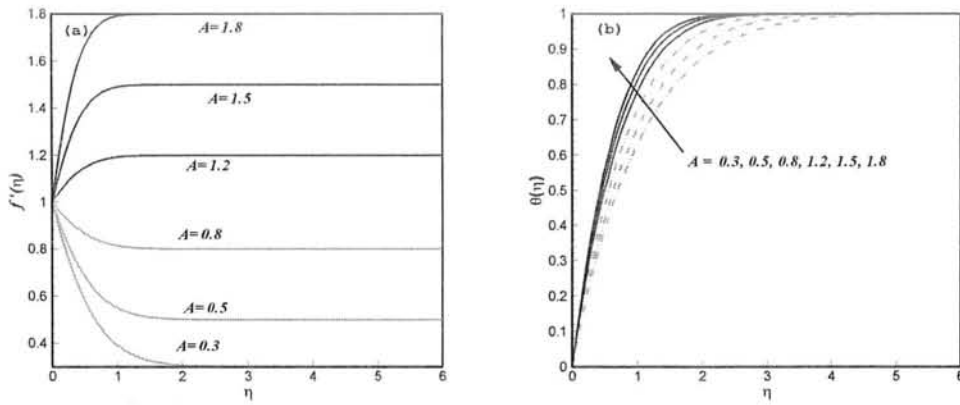

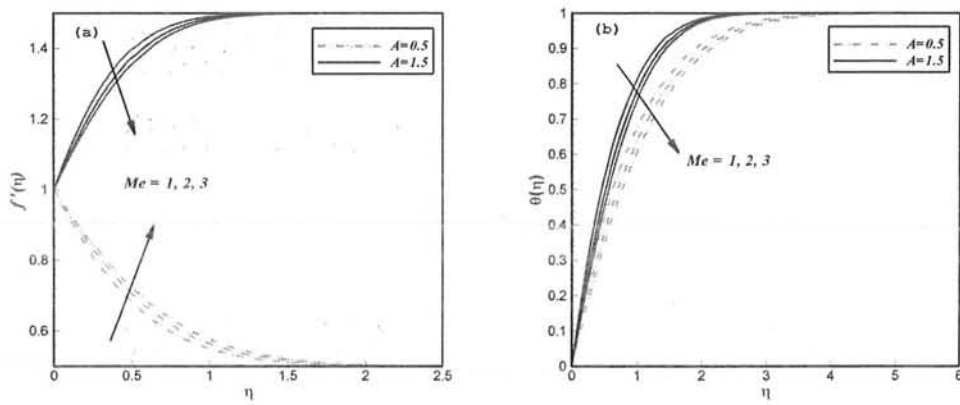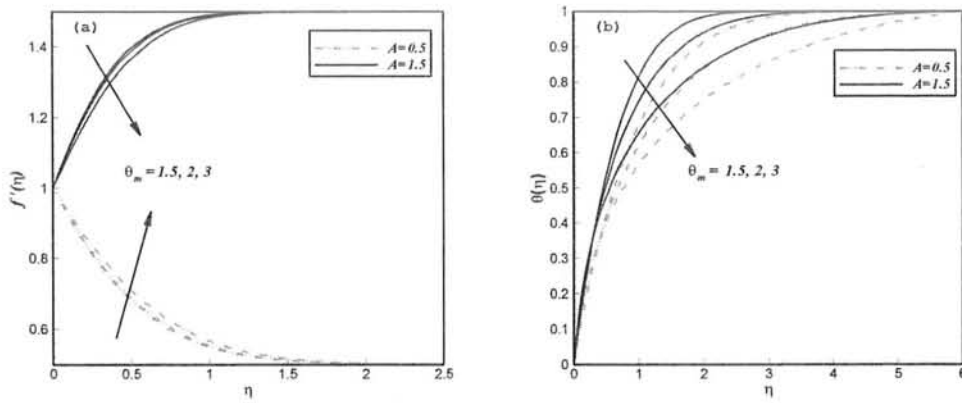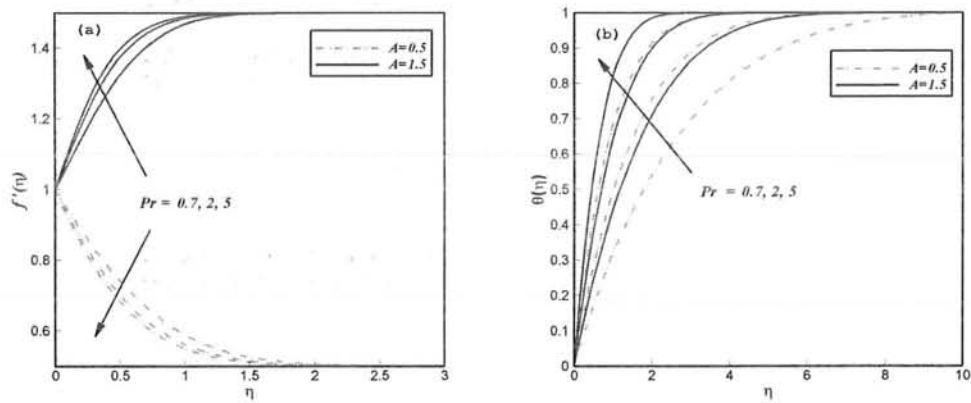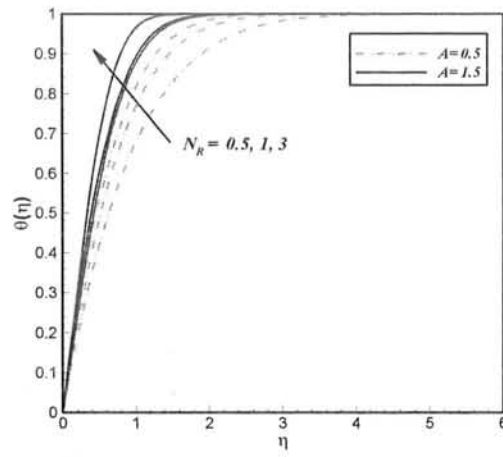**Fig. 7.6:** Profiles of $f'(\eta)$ and $\theta(\eta)$ subject to rise in Pr.

Fig. 7.7: Profiles of $f'(\eta)$ and $\theta(\eta)$ subject to rise in N_R.

Table 7.2: Numeric values of skin friction coefficient along with Nusselt number in response to emerging parameters.

We	m	A	Me	θ_m	N_R	Pr	$\frac{1}{2}Re_L{}^{\frac{1}{2}}C_f$	$-Re_L{}^{-\frac{1}{2}}Nu$
2							0.400387	3.75790
3							0.386829	3.75105
4							0.378181	3.74643
5							0.370854	3.74259
	0.3						0.364255	3.77548
	0.4						0.317053	3.80847
	0.5						0.254813	3.86324
		0.8					0.189064	4.16586
		1.2					0.216667	4.63838
		1.5					0.543834	4.97503
			1.5				0.373194	3.36597
			2				0.353358	3.05749
			3				0.321598	2.59990
				2			0.385303	4.45993
				2.5			0.368905	5.26461
				3			0.351096	6.17867
					1		0.392915	2.61385
					2		0.391154	1.92104
					3		0.391636	1.66576
						2	0.359672	2.29283
						3	0.379255	2.85143
						4	0.391740	3.33059

Chapter 8

Axisymmetric Flow in Magneto-Cross Nanofluid with New Mass Flux Condition

The current chapter reports the magnetohydrodynamic (MHD) flow along with transfer of heat to Cross nanofluid near a radially stretching sheet under the assumption of rotational symmetry. Moreover, a new boundary condition is invoked in the analysis according to which the nanoparticles near wall are assumed to have zero normal flux. The modelled equations governing the current situation are subjected to suitable transformations and shooting method is utilized to seek its solution. Graphs are sketched to display the importance of emerging parameters in problem analysis. It is found through detail analysis that structures of thermal together with concentration boundary layer are improved by applying strong magnetic field while the momentum boundary layer shrinks. An elevation in power-law index lessened the temperature along with nanoparticle concentration profiles while reverse trend is seen for increasing values of Weissenberg number.

8.1 Mathematical Interpretation

In this section, we analyze the axisymmetric flow considering electrically conducting Cross nanofluid driven by a radially stretching sheet, which lies along the plane $z = 0$ while flow occurs in the region $z > 0$. A magnetic field having strength B_0 is introduced normal to (i.e along $z -$direction). The induced magnetic field can be

ignored by taking small magnetic Reynolds number. A newly proposed boundary condition is used in which the normal flux of nanoparticles is assumed to be zero at wall.

Aforementioned suppositions gave the following form to the governing equations (cf. Chapter 6):

$$\frac{\partial w}{\partial z} + \frac{\partial u}{\partial r} + \frac{u}{r} = 0, \tag{8.1}$$

$$u\frac{\partial u}{\partial r} + w\frac{\partial u}{\partial z} = \vartheta\frac{\partial}{\partial z}\left[\left(\frac{\partial u}{\partial z}\right)\left(1 + \left\{\Gamma\left(\frac{\partial u}{\partial z}\right)\right\}^m\right)^{-1}\right] - \frac{\sigma B_0^2}{\rho_f}u, \tag{8.2}$$

$$u\frac{\partial T}{\partial r} + w\frac{\partial T}{\partial z} = \frac{k_f}{(\rho c_p)_f}\frac{\partial^2 T}{\partial z^2} + \tau\left[D_B\frac{\partial C}{\partial z}\frac{\partial T}{\partial z} + \frac{D_T}{T_\infty}\left(\frac{\partial T}{\partial z}\right)^2\right], \tag{8.3}$$

$$u\frac{\partial C}{\partial r} + w\frac{\partial C}{\partial z} = D_B\frac{\partial^2 C}{\partial z^2} + \frac{D_T}{T_\infty}\frac{\partial^2 T}{\partial z^2}, \tag{8.4}$$

subject to boundary conditions:

$$u(r,z) = U = cr, w(r,z) = 0, T(r,z) = T_w, D_B\frac{\partial C}{\partial z} + \frac{D_T}{T_\infty}\frac{\partial T}{\partial z} = 0 \text{ at } z = 0, \tag{8.5}$$

$$u(r,z) \to 0, T(r,z) \to T_\infty, C(r,z) \to C_\infty \quad \text{as } z \to \infty. \tag{8.6}$$

We invoke suitable transformations as listed below:

$$f' = \frac{u}{U}, \theta = \frac{T - T_\infty}{T_w - T_\infty}, \phi = \frac{C - C_\infty}{C_\infty}, \tag{8.7}$$

with $(u,v) = \left(-\frac{1}{r}\frac{\partial \psi}{\partial z}, \frac{1}{r}\frac{\partial \psi}{\partial r}\right)$ and local similarity variable η and dimensionless function ψ defined as:

$$\eta = \sqrt{\frac{c}{v}}z, \psi = r^2\sqrt{vc}f(\eta). \tag{8.8}$$

After utilizing the above transformations, the governing equations become:

$$\left(2\,f\,f'' - f'^2\right)\left[1 + (We\,f'')^m\right]^2 + \left(1 + (1-m)(We\,f'')^m\right)f''' - M^2 f' = 0, \quad (8.9)$$

$$\theta'' + Pr\left[f\theta' + N_b\phi'\theta' + N_t\theta'^2\right] = 0, \tag{8.10}$$

$$\phi'' + PrLef\phi' + \frac{N_t}{N_b}\theta'' = 0, \tag{8.11}$$

$$f(0) = 0, f'(0) = 1, \theta(0) = 1, N_b\phi'(0) + N_t\theta'(0) = 0, \tag{8.12}$$

$$f'(\infty) \to 0, \theta(\infty) \to 0, \phi(\infty) \to 0, \tag{8.13}$$

where $M^2\left(= \frac{\sigma B_0^{\,2}}{\rho_f U}r\right)$ denotes the magnetic parameter, $N_b\left(= \frac{\tau D_B C_\infty}{\nu}\right)$ the Brownian motion parameter, $N_t\left(= \frac{\tau D_T(T_w - T_\infty)}{\nu T_\infty}\right)$ the thermophoresis parameter and $Le\left(= \frac{\alpha}{D_B}\right)$ the Lewis number. Other emerging parameters We, Pr and Re are already defined in chapter 6.

The expressions for skin friction coefficient and Nusselt number are formulated below:

$$C_f = \frac{\tau_{rz}|_{z=0}}{1/2\rho U^2}, Nu = \frac{Lq_w}{k(T_w - T_\infty)}. \tag{8.14}$$

The non-dimensional representation of above expression can be written as:

$$\frac{1}{2}Re_L^{\frac{1}{2}}C_f = \frac{f''(0)}{1 + \left(Wef''(0)\right)^m}, -Re_L^{-\frac{1}{2}}Nu = \theta'(0). \tag{8.15}$$

Note that the reduced Sherwood number which characterizes non-dimensional mass flux on the surface is identically zero for present problem.

8.2 Graphical Description of Results

The non-linear ODEs in. $(8.9 - 8.11)$ having the boundary conditions $(8.12 - 8.13)$ is numerically solved by the help of shooting method. The numerical solutions are graphically analyzed and physically discussed in the current section. Comparative plots are constructed for the hydrodynamic $(M = 0)$ as well as hydromagnetic $(M > 0)$ flows. The default inputs of various parameters are picked up as $m = 0.2$, $We = 2, Pr = 5, Le = 0.5$ and $N_b = N_t = 0.5$ unless otherwise mentioned.

Fig. 8.1 demonstrates the dependence of the power-law index m on velocity, temperature along with concentrations fields. Simultaneous effects of hydrodynamic flow $(M = 0)$ and hydromagnetic flow $(M > 0)$ are also presented. **Fig. 8.1 (a)** indicates velocity along with temperature profiles corresponding to growth in m. It is inferred through plots that velocity enhances with m while temperature declines. It is further visualized that structures of momentum boundary layer get thicker in the absence of magnetic field while the thickness of thermal boundary layer grows for stronger magnetic field. Physically, by enhancing the magnetic field strength, the Lorentz force causes stronger resistance to motion of fluid and accordingly fluids velocity diminishes and temperature is raised. **Fig. 8.1 (b)** presents the role of m on concentration profile subject to hydrodynamic $(M = 0)$ and hydromagnetic $(M > 0)$ flows. Further, nanoparticle concentration profile gets weaker for elevation in m. Moreover, concentration boundary layer structures are thicker for hydromagnetic flow compared to hydrodynamic flow.

The impact of the Weissenberg number We on the velocity, temperature and concentration profiles is portrayed in **Fig. 8.2**. In addition, comparative plots are also presented for hydrodynamic $(M = 0)$ and hydromagnetic $(M > 0)$ flows. **Fig. 8.2 (a)** indicates that the Weissenberg number We holds opposite influence on the velocity and temperature fields. Fluids velocity diminishes while temperature rises as a result of increasing Weissenberg number We. The comparison between hydrodynamic $(M = 0)$ and hydromagnetic $(M > 0)$ flows reveal that the velocity is higher for the case of hydrodynamic flow and temperature is more for the case of hydromagnetic flow. **Fig. 8.2 (b)** discloses the dependence of the nanoparticle concentration profiles on the Weissenberg number We. The thickness of concentration boundary layer gets greater by uplifting values of We. A further rise in concentration profiles is observed for hydromagnetic flow compared with hydrodynamic flow.

Fig. 8.3 (a) renders the behavior of the temperature along with concentration profiles against Lewis number Le for hydrodynamic $(M = 0)$ and hydromagnetic $(M > 0)$ flows. It is displayed through the plots that the temperature and concentration fields show opposite trend corresponding to rising values of Lewis number. A further rise in this trend is determined by applying magnetic field. Le is basically the ratio of thermal diffusivity to mass diffusivity. The growing values of Lewis number enhance the thermal diffusivity causing a reduction in mass diffusivity and consequently thermal boundary layer structures are raised and concentration boundary layers are declined. The influence of the Prandtl number Pr on temperature and concentration fields is depicted through **Fig. 8.3 (b)**. Furthermore, the comparative plots for hydrodynamic $(M = 0)$ and hydromagnetic $(M > 0)$ flows are provided. It is

identified that the temperature and also concentration profiles falls with Prandtl number. Moreover, this effect is greater for hydromagnetic flows $(M > 0)$.

Fig. 8.4 (a) presents the consequence of Brownian motion parameter N_b on concentration profile corresponding to hydrodynamic $(M = 0)$ and hydromagnetic $(M > 0)$ flows. The ascending values of N_b results in reduction of nanoparticle concentration profiles and its corresponding boundary layer shrinks accordingly. Observation of the graph reveals that nanoparticle volume fraction is higher when MHD is present compared with the case when MHD is absent $(M = 0)$. The physical cause behind this trend is that with the increase in N_b, the Brownian motion gets weaker causing hindrance in diffusion of nanoparticles in flow regime. Due to manipulation of boundary condition suggested by Kuznetsov and Nield [29], the Brownian motion parameter imparts negligible change in thermal boundary layer structures. The dependence of N_t on temperature along with nanoparticle concentration profiles is highlighted through **Fig. 8.4 (b)**. Examination of this plot leads that developing values of N_t escalates the temperature and also nanoparticles concentration fields. Comparative plots for hydrodynamic $(M = 0)$ and hydromagnetic $(M > 0)$ flows help us to conclude that thermal along with concentration boundary layer structures elevate by applied magnetic field. It can be physically answered because by increasing N_t, the thermophoretic force gets stronger. These forces move the nanoparticles in the reverse direction to temperature gradient causing thermal and also concentration boundary layers to get thicker.

Table 8.1 provides the numerical data corresponding to coefficient of skin friction and also Nusselt number for numerous values of emerging parameters. The skin

friction coefficient descends with We and m while enhances with M. However, opposite trend is shown by Nusselt number. The rate of transfer of heat at sheet is enhanced corresponding to increase in Pr while it diminishes for growing values of N_b, N_t and Le.
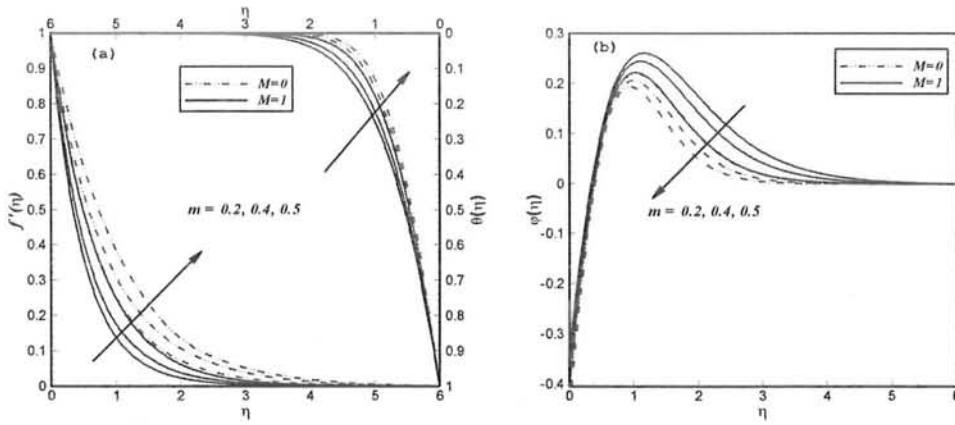
Fig. 8.1: Graphical illustration of velocity, temperature and concentration profiles against m for hydrodynamic and hydromagnetic flows.

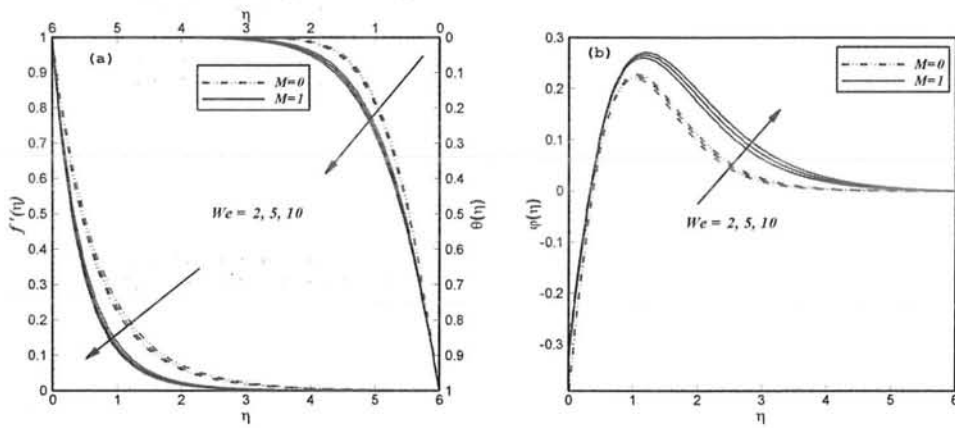**Fig. 8.2:** Graphical illustration of velocity, temperature and concentration profiles We for hydrodynamic and hydromagnetic flows.
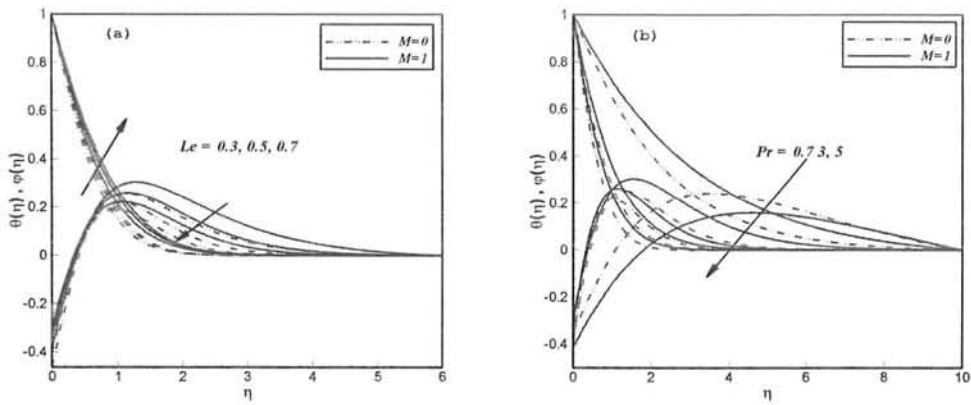
Fig. 8.3: Graphical illustration of temperature and concentration profiles against the *Le* and *Pr* for hydrodynamic and hydromagnetic flows.
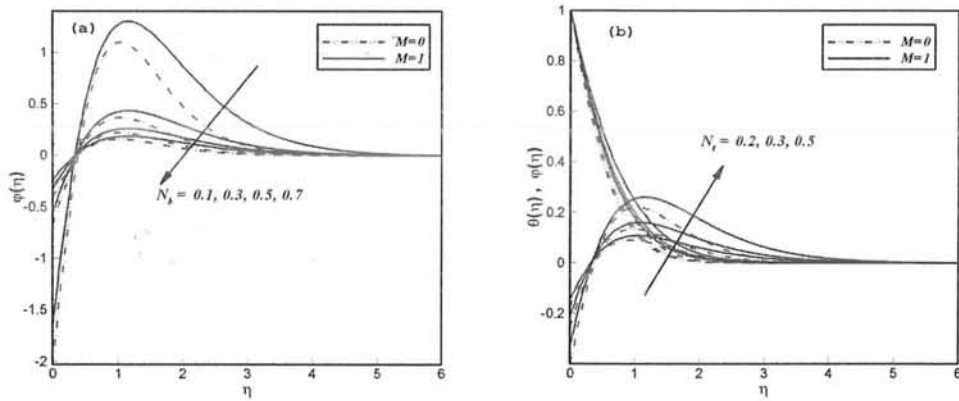

Fig. 8.4: Graphical illustration of temperature and concentration profiles against N_b and N_t for hydrodynamic and hydromagnetic flows.

Table 8.1: Values of skin friction coefficient along with Nusselt number corresponding to emerging physical parameters.

We	m	M	Pr	N_b	N_t	Le	$-\dfrac{1}{2}Re_L^{\frac{1}{2}}C_f$	$-Re_L^{\frac{1}{2}}Nu$
2	0.2	0.5	5	0.5	0.5	2	0.702871	0.903113
1							0.744789	0.914962
3							0.680894	0.896427
	0.1						0.763380	0.899871
	0.3						0.605968	0.921780
		1					0.879166	0.820930
		1.5					1.09041	0.724586
			0.7					0.335061
			2					0.646296
				0.2				0.903180
				0.3				0.905758
					0.2			1.20202
					0.3			1.09462
						1		1.04051
						1.5		0.959649

Chapter 9

Impact of Activation Energy in Mixed Convective Flow of Cross Fluid over a Cylinder

In current chapter, the boundary layer equations related to axisymmetric flow of Cross fluid past a stretching cylinder are established. Moreover, the present problem is composed of activation energy, chemical reaction, radiative heat flux, mixed convective heat transfer of Cross nanofluid by invoking practically feasible convective boundary conditions. The shooting technique is exploited for simplification of the problem and results are shown by providing graphs and tables. The analysis declares that the activation energy resulted in raising the fluid temperature while a decay in concentration profile is visualized. A growth in curvature parameter can be used to increase the coefficient of skin friction and even Sherwood number. The results achieved under current numerical implementation are ensured by presenting admissible comparison with earlier reported work.

9.1 Mathematical Formulation

9.1.1 Boundary Layer Equations

We contemplate the axisymmetric flow of Cross fluid near a stretching cylinder. We choose cylindrical polar coordinates (r, θ, z) for the mathematical analysis. We

further assume that the azimuthal component of velocity field is considered zero. We define the velocity field as:

$$V = [v(r,x), 0, u(r,x)], \tag{9.1}$$

such that v and u describe velocity components along radial and axial directions, respectively.

Keeping in mind the boundary layer equations of Cross fluid in cylindrical coordinates (cf. Chapter 1), we can write the following equations:

$$\rho\left(v\frac{\partial v}{\partial r} + u\frac{\partial v}{\partial x}\right)$$

$$= -\frac{\partial p}{\partial r} + 2\frac{\eta_0}{r}\frac{\partial}{\partial r}\left[r\frac{\partial v}{\partial r}\left\{\frac{1}{1 + \left\{\Gamma^2\left(\begin{array}{c}4\left(\frac{\partial v}{\partial r}\right)^2 + 4\left(\frac{v}{r}\right)^2 \\ + \left(\frac{\partial u}{\partial r} + \frac{\partial v}{\partial x}\right)^2 + 4\frac{v}{r}\left(\frac{\partial v}{\partial r}\right)\end{array}\right)\right\}^{\frac{m}{2}}}\right\}\right]$$

$$+ \eta_0\frac{\partial}{\partial x}\left[\left(\frac{\partial u}{\partial r} + \frac{\partial v}{\partial x}\right)\left\{\frac{1}{1 + \left\{\Gamma^2\left(\begin{array}{c}4\left(\frac{\partial v}{\partial r}\right)^2 + 4\left(\frac{v}{r}\right)^2 \\ + \left(\frac{\partial u}{\partial r} + \frac{\partial v}{\partial x}\right)^2 + 4\frac{v}{r}\left(\frac{\partial v}{\partial r}\right)\end{array}\right)\right\}^{\frac{m}{2}}}\right\}\right]$$

$$-2\frac{\eta_0}{r}\left|\frac{v}{r}\left\{\frac{1}{1+\left\{\Gamma^2\left(\begin{array}{c}4\left(\frac{\partial v}{\partial r}\right)^2+4\left(\frac{v}{r}\right)^2\\+\left(\frac{\partial u}{\partial r}+\frac{\partial v}{\partial x}\right)^2+4\frac{v}{r}\left(\frac{\partial v}{\partial r}\right)\end{array}\right)\right\}^{\frac{m}{2}}}\right\}\right|, \quad (9.2)$$

$$\rho\left(v\frac{\partial u}{\partial r}+u\frac{\partial u}{\partial x}\right)$$

$$=-\frac{\partial p}{\partial x}$$

$$+\frac{\eta_0}{r}\frac{\partial}{\partial r}\left[r\left(\frac{\partial u}{\partial r}+\frac{\partial v}{\partial x}\right)\left\{\frac{1}{1+\left\{\Gamma^2\left(\begin{array}{c}4\left(\frac{\partial v}{\partial r}\right)^2+4\left(\frac{v}{r}\right)^2\\+\left(\frac{\partial u}{\partial r}+\frac{\partial v}{\partial x}\right)^2+4\frac{v}{r}\left(\frac{\partial v}{\partial r}\right)\end{array}\right)\right\}^{\frac{m}{2}}}\right\}\right]$$

$$+2\eta_0\frac{\partial}{\partial x}\left[\frac{\partial u}{\partial x}\left\{\frac{1}{1+\left\{\Gamma^2\left(\begin{array}{c}4\left(\frac{\partial v}{\partial r}\right)^2+4\left(\frac{v}{r}\right)^2\\+\left(\frac{\partial u}{\partial r}+\frac{\partial v}{\partial x}\right)^2+4\frac{v}{r}\left(\frac{\partial v}{\partial r}\right)\end{array}\right)\right\}^{\frac{m}{2}}}\right\}\right]. \quad (9.3)$$

We employ the boundary layer assumptions, according to which the order of x, u, p are taken to be 1 while r and v are of order δ. In view of these assumptions, the

equations reduce to the following form:

$$0 = -\frac{1}{\rho}\frac{\partial p}{\partial r},$$

(9.4)

$$v\frac{\partial u}{\partial r} + u\frac{\partial u}{\partial x} = -\frac{1}{\rho}\frac{\partial p}{\partial x} + \frac{\vartheta}{r}\frac{\partial}{\partial r}\left[\left(r\frac{\partial u}{\partial r}\right)\left(1 + \left\{\Gamma\left(\frac{\partial u}{\partial r}\right)\right\}^m\right)^{-1}\right].$$
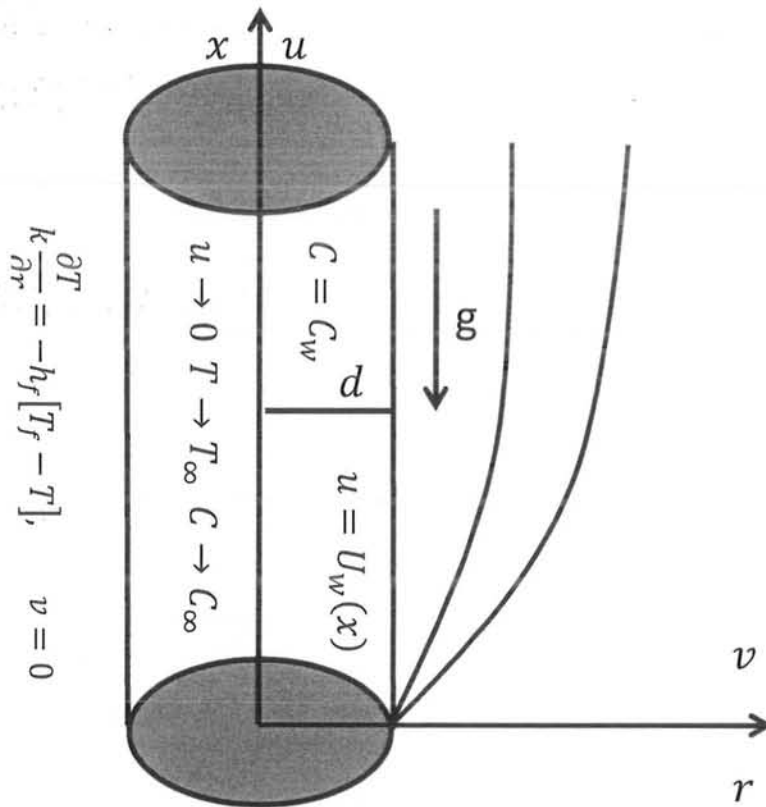
(9.5)

9.1.2 Geometry of the Problem

Fig. 9.1: Physical model of the problem.

9.1.3 Problem Development

Mixed convective heat transfer for Cross nanofluid over a vertically stretching cylinder of constant radius d is explored. The Arrhenius activation energy is also examined along with chemical reaction. The heat transfer analysis is performed on the surface of the cylinder in view of linear radiation and convective boundary conditions. The coordinate system for the axisymmetric flow is designed such that x −axis is marked along cylinders surface while r −axis is along radial direction. Considering above notions, equations of boundary layer for Cross fluid past a stretching cylinder are:

$$\frac{\partial u}{\partial x} + \frac{\partial v}{\partial r} + \frac{v}{r} = 0, \tag{9.6}$$

$$v\frac{\partial u}{\partial r} + u\frac{\partial u}{\partial x} = \frac{\vartheta}{r}\frac{\partial}{\partial r}\left[\left(r\frac{\partial u}{\partial r}\right)\left(1 + \left\{\Gamma\left(\frac{\partial u}{\partial r}\right)\right\}^m\right)^{-1}\right]$$
$$+ g[\beta_T(T - T_\infty) + \beta_C(C - C_\infty)], \tag{9.7}$$

$$v\frac{\partial T}{\partial r} + u\frac{\partial T}{\partial x} = \frac{k_f}{(\rho c_p)_f}\left(\frac{\partial^2 T}{\partial r^2} + \frac{1}{r}\frac{\partial T}{\partial r}\right) - \frac{1}{(\rho c_p)_f}\frac{1}{r}\frac{\partial}{\partial r}(rq_r)$$
$$+ \tau\left[D_B\frac{\partial C}{\partial r}\frac{\partial T}{\partial r} + \frac{D_T}{T_\infty}\left(\frac{\partial T}{\partial r}\right)^2\right], \tag{9.8}$$

$$v\frac{\partial C}{\partial r} + u\frac{\partial C}{\partial x} = D_B\left(\frac{\partial^2 C}{\partial r^2} + \frac{1}{r}\frac{\partial C}{\partial r}\right) + \frac{D_T}{T_\infty}\left(\frac{\partial^2 T}{\partial r^2} + \frac{1}{r}\frac{\partial T}{\partial r}\right)$$
$$+ k_r^2(C - C_\infty)\left(\frac{T}{T_\infty}\right)^n e^{-\left(\frac{E_a}{\kappa T}\right)}. \tag{9.9}$$

In the above equations, g denotes the gravitational acceleration, $\beta_T \left(= \beta_T^* \left(\frac{x}{L}\right)\right)$ the coefficient of thermal expansion and β_C the coefficient of concentration expansion. Moreover, in concentration equation, the last term describes the modified Arrhenius function [88] with k_r^2 representing the reaction rate, E_a the activation energy, $\kappa \; (= 8.61 \times 10^{-5} \, eV/K)$ the Boltzmann constant. Furthermore, the radiative heat flux q_r in heat equation can be written by using Rosseland approximation for radiation as:

$$q_r = -\frac{4}{3} \frac{\sigma^*}{k^*} \frac{\partial T^4}{\partial r}. \tag{9.10}$$

If the temperature difference is small, we use Taylor series about T_∞ to express T^4 as a linear function of temperature and after omitting the higher order terms, Eq. (9.8) can be modified as:

$$v \frac{\partial T}{\partial r} + u \frac{\partial T}{\partial x} = \frac{k_f}{(\rho c_p)_f} \left(\frac{\partial^2 T}{\partial r^2} + \frac{1}{r} \frac{\partial T}{\partial r}\right) - \frac{16}{3(\rho c_p)_f} \frac{\sigma^* T_\infty^3}{k^*} \frac{\partial}{r} \frac{\partial}{\partial r}(r q_r)$$

$$+ \tau \left[D_B \frac{\partial C}{\partial r} \frac{\partial T}{\partial r} + \frac{D_T}{T_\infty} \left(\frac{\partial T}{\partial r}\right)^2 \right]. \tag{9.11}$$

The associated boundary conditions of the governing problem are:

$$v(r,x) = 0, u(r,x) = U_w(x) = cx, k \frac{\partial T(r,x)}{\partial r} = -h_f \left[T_f - T(r,x) \right],$$

$$C(r,x) = C_w \quad \text{at } r = d, \tag{9.12}$$

$$u(r,x) \to 0, T(r,x) \to T_\infty, C(r,x) \to C_\infty \text{ as } r \to \infty, \tag{9.13}$$

with $c > 0$ being the stretching rate of cylinder. It is assumed that a hot fluid having temperature T_f warms up the surface of cylinder by setting up a coefficient of heat transfer h_f at the surface of cylinder.

We simplify our governing set of equations by the help of following transformations:

$$\eta = \frac{r^2 - d^2}{2d} \sqrt{\frac{U_w}{vx}}, \psi = \sqrt{U_w vx} \, d \, f(\eta), \theta(\eta) = \frac{T - T_\infty}{T_f - T_\infty}, \phi(\eta) = \frac{C - C_\infty}{C_w - C_\infty}, \tag{9.14}$$

while the stream function ψ can be determined from $(v, u) = \left(-\frac{1}{r}\frac{\partial \psi}{\partial x}, \frac{1}{r}\frac{\partial \psi}{\partial r} \right)$.

By using the above transformation, Eq. (9.6) is satisfied in identical way while Eqs. (9.7), (9.9) and (9.11) are transformed into the following equations:

$$\left[f f'' - f'^2 + \lambda(N\phi + \theta) \right] [1 + (We f'')^m]^2 + \gamma^* f'' \left[2 + (2 - m)(We f'')^m \right]$$

$$+ (1 + 2\gamma^* \eta)[1 + (1 - m)(We f'')^m] f''' = 0, \tag{9.15}$$

$$(1 + 2\gamma^* \eta)\theta'' + 2\gamma^* \theta' + \frac{Pr}{1 + R} f \theta' + \frac{Pr(1 + 2\gamma^* \eta)}{1 + R} \left[N_b \theta' \phi' + N_t \theta'^2 \right] = 0, \tag{9.16}$$

$$(1 + 2\gamma^* \eta)\phi'' + \frac{N_t}{N_b} \left[2\gamma^* \theta' + (1 + 2\gamma^* \eta)\theta'' \right] + Sc(f + 2\gamma^*)\phi'$$

$$+ Sc \, \sigma_1 \phi \, exp \left(-\frac{E}{1 + \delta_1 \theta} \right) (1 + \delta_1 \theta)^n = 0. \tag{9.17}$$

The corresponding conditions at the boundary are:

$$f(0) = 0, \, f'(0) = 1, \, \theta'(0) = -\gamma[1 - \theta(0)], \phi(0) = 1, \tag{9.18}$$

$$f'(\infty) \to 0, \theta(\infty) \to 0, \phi(\infty) \to 0, \tag{9.19}$$

where $We \left(= \frac{\Gamma_0}{d}\sqrt{\frac{c}{\vartheta}}cL\right)$ is the Weissenberg number, $\gamma^* \left(= \frac{1}{d}\sqrt{\frac{c}{\vartheta}}\right)$ the curvature

parameter, $\lambda \left(= \frac{g(T_f - T_\infty)\beta_T^*}{c^2 L}\right)$ the thermal mixed convection parameter, $N \left(= \frac{(C_w - C_\infty)\beta_C}{(T_f - T_\infty)\beta_T}\right)$ the solutal mixed convection parameter, $R \left(= \frac{16}{3}\frac{\sigma^*}{k\,k^*}T_\infty^{\,3}\right)$ the thermal

radiation parameter, $Pr \left(= \frac{\eta_0 c_p}{k}\right)$ the Prandtl number, $N_t \left(= \frac{\tau D_T(T_f - T_\infty)}{T_\infty \nu}\right)$ the

thermophoresis parameter, $N_b \left(= \frac{\tau D_B(C_w - C_\infty)}{\vartheta}\right)$ the Brownian motion

parameter, $Sc \left(= \frac{\vartheta}{D_B}\right)$ the Schmidt number, $E \left(= \frac{E_a}{\kappa T_\infty}\right)$ the dimensionless activation

energy, $\sigma_1 \left(= \frac{k_r^{\,2}}{c}\right)$ the dimensionless reaction rate, $\delta_1 \left(= \frac{(T_f - T_\infty)}{T_\infty}\right)$ the temperature

difference parameter and n the fitted rate constant.

The expressions related to coefficient of skin friction, Nusselt number and also for

Sherwood number are:

$$C_f = \frac{\tau_w}{\frac{1}{2}\rho u_w^2}, \qquad Nu = \frac{Lq_w}{k(T_f - T_\infty)}, \qquad Sh = \frac{Lq_m}{D_B(C_w - C_\infty)}, \qquad (9.20)$$

where wall shear stress τ_w, wall heat flux q_w and wall mass flux q_m are given by:

$$\tau_w = \left[\eta_0 \frac{\frac{\partial u}{\partial r}}{1 + \left\{\Gamma\left(\frac{\partial u}{\partial r}\right)\right\}^m}\right]_{r=d}, q_w = -k\left(\frac{\partial T}{\partial r}\right)\Big|_{r=d} + q_r|_{r=d},$$

$$q_m = -D_B\left(\frac{\partial C}{\partial r}\right)\Big|_{r=d}. \qquad (9.21)$$

Using relations (9.14), the dimensionless form of Eq. (9.20) can be written as:

$$\frac{1}{2}Re_L^{\frac{1}{2}}C_f = \left[\frac{f''(0)}{1 + \left(Wef''(0)\right)^m}\right], \quad Re_L^{-\frac{1}{2}}Nu = -(1 + R)\theta'(0), \qquad (9.22)$$

$$Re_L^{-\frac{1}{2}}Sh = -\phi'(0).\qquad(9.23)$$

9.2 Verification of Numerical Results

The governing system of highly non-linear ODEs is subjected to shooting technique to obtain the solutions. Before presenting a detail analysis on the numerical results, a certification of the solution technique is ensured. Due to which, the presents results are validated by comparing $f''(0)$ for Newtonian fluid past a stretching cylinder for growth in curvature parameter γ^*. **Table 9.1** reveals a remarkable agreement between our results and the results reported by Vajravelu *et al.* [118] for the case when $\lambda = N = 0$.

Table 9.1: Comparison of $f''(0)$ for different γ^* for the case of Newtonian fluid ($We = 0$) when $\lambda = N = 0$.

	$\gamma^* = 0$	$\gamma^* = 0.25$	$\gamma^* = 0.5$	$\gamma^* = 0.75$	$\gamma^* = 1.0$
Vajravelu *et al.* [118]	1.000001	1.0918256	1.182410	1.271145	1.35819
Current Results	1.0004763	1.0918255	1.1824105	1.2711465	1.3582032

9.3 Analysis of Results

The purpose of current section involves the study of emerging parameters and their dependence on the profiles of velocity, temperature and also concentration. Furthermore, the coefficient of skin friction, Nusselt number and Sherwood number are explored under the growth of various physical parameters.

Fig. 9.2 (a-c) displays the dependency of velocity, temperature and even of concentration fields on Weissenberg number We. Also the comparative plots are provided for variation in the power-law index m. It is visible from **Fig. 9.2 (a)** that fluids velocity and its corresponding boundary layer structure decline for up rise in We. **Fig. 9.2 (b)** indicates an addition in fluid temperature and related thermal boundary layer thickness with a rise in We. However, opposite trend is shown by nanoparticle concentration profiles as shown in **Fig. 9.2 (c)**. An enlargement in We causes fluids relaxation time to grow which retards the velocity and also nanoparticle concentration while boosts up the fluids temperature. Furthermore, the impact of m is to boost the momentum and concentration boundary layer structure while a decay in thermal boundary layer structure is analyzed. It is due to the fact that as m grows, the shear-thinning nature of fluid increases which leads to decay in the viscosity. As a result the velocity and concentration field increase while the temperature gradually decays.

Fig. 9.3 (a-c) are schemed to depict the importance of thermal and solutal mixed convection parameter in view of fluid velocity, temperature together with nanoparticle concentration profiles, respectively. Moreover, $\lambda > 0$ represents buoyancy aided flow, i.e., cooling of the surface of cylinder or heating of the fluid while $\lambda < 0$ indicates buoyancy opposed flow, i.e., either cooling of fluid or heating cylinder's surface. These plots further reveal that momentum and also solutal boundary layer thickness elevates as we move from buoyancy opposed flow ($\lambda = -0.2$) towards buoyancy aided flow ($\lambda = 0.2$) while the thickness of thermal boundary layer shows decreasing trend. It is spotted that the profiles of velocity,

temperature and even concentration are more compact for buoyancy aided flow in comparison with buoyancy opposed flow. Physically, λ represents the ratio of buoyancy forces to inertial forces. For higher values of λ, the buoyancy forces dominate causing fluid velocity to increase. Correspondingly, the temperature lowers due to boost in temperature difference $T_f - T_\infty$ causing convective cooling. Also, increasing values of λ cause an enlargement in the gravitational field causing an improvement in nanoparticle volume fraction. Moreover, the solutal mixed convection parameter N results in enlargement of fluid velocity and nanoparticle concentration $\lambda > 0$ while decay is observed for $\lambda < 0$. Moreover, the temperature profile rises for $\lambda < 0$ and decays for $\lambda > 0$.

Fig. 9.4 reveals the impact of curvature parameter γ^* on the fluid velocity $f'(\eta)$, temperature $\theta(\eta)$ and also nanoparticle concentration $\phi(\eta)$. An increment in γ^* causes a development in velocity and also in fluids temperature while decay is observed in concentration profile. Moreover, the momentum and thermal boundary layer thickness also increase while the solutal boundary layer diminishes gradually. Additionally, one can observe that the profiles are more elevated for the case of flow past a stretching cylinder ($\gamma^* > 0$) compared to flow over a stretching sheet ($\gamma^* = 0$) while opposite behavior is demonstrated by concentration distributions. Physically, as γ^* increases a decay in the radius d of the cylinder is observed which can be manipulated from the expression $\gamma^* = \frac{1}{d}\sqrt{\frac{c}{\nu}}$. Consequently, the contact area of cylinder with fluid also gets shrinks and less resistance is faced by fluid due to low viscosity and thus fluids velocity increases.

The variation in dimensionless temperature along with concentration subject to variation in thermal radiation R and Prandtl number Pr are exhibited through **Fig. 9.5**. The elevated values of R and Pr have opposite impact on $\theta(\eta)$ and $\phi(\eta)$. The thermal radiation parameter caused decay in boundary structures related to concentration while a lift in thermal boundary layer structure is visualized. However, the Prandtl number provoked the temperature profile to decline while the concentration profile progressed correspondingly.

The graphical illustration of the role of thermophoresis parameter N_t and Brownian motion parameter N_b corresponding to fluids temperature along with concentration is displayed in **Fig. 9.6** displays the influence of N_t on temperature together with nanoparticle concentration profiles, respectively. It is perceived that temperature along with concentration is growing function of N_t. As we increase N_t, the thermophoresis force gets stronger which results in stronger penetration of nanoparticles within ambient fluid and hence the thermal and concentration boundary layer structures elevate. Moreover, these figures also reveal that the profiles of temperature and concentration depict opposite trend corresponding to enlargement in N_b. Physically, a rise in N_b effects the Brownian motion and slows down the diffusion of nanoparticles and accordingly the temperature of fluid rises while concentration of nanoparticle volume fraction decreases.

Fig. 9.7 demonstrates the consequence of the Schmidt number Sc on temperature together with nanoparticle concentration. Comparative plots disclose the role of Biot number as well. It is evident from the plot that Sc implied a reduction in temperature field while the concentration field is strengthened as a result. Actually, a growth in Sc

provides hindrance in the mass diffusion which retards the concentration profile while temperature of the fluid grows. These plots also disclose that the Biot number γ boosts the fluid temperature and also nanoparticle concentration. Physically, growth in γ indicates large convection which leads to rise in heat near the surface of cylinder.

Fig. 9.8 is delineated to examine the dependence of activation energy parameter E and reaction rate parameter σ_1 corresponding to temperature along with concentration profiles. It is witnessed through **Fig. 9.8 (a)** that structures related to thermal boundary layer gets thicker by increasing E while they decay for increasing values of σ_1. **Fig. 9.8 (b)** reveals that the profiles of concentration descends with E while they ascend with σ_1.

Table 9.2 provides the outputs of skin friction coefficient, Nusselt number and also Sherwood number subject to change in emerging quantities. The tabulated data reveals a decay in the coefficient of skin friction coefficient against development in m, We, λ, N, R, N_b, N_t, γ, Sc, E, σ_1 and n. However, elevation is observed for growing values of γ^*, Pr and δ. The rate of transfer of heat enhances with m, λ, N, R, Pr, γ, Sc, δ, σ_1 and n while it gets weaker with We, γ^*, N_b, N_t and E. The Sherwood grows for elevation in values of m, λ, N, R, We, γ^*, N_b, E and σ_1. A decrease in Sherwood number is visualized for Pr, N_t, γ, Sc, δ and n.
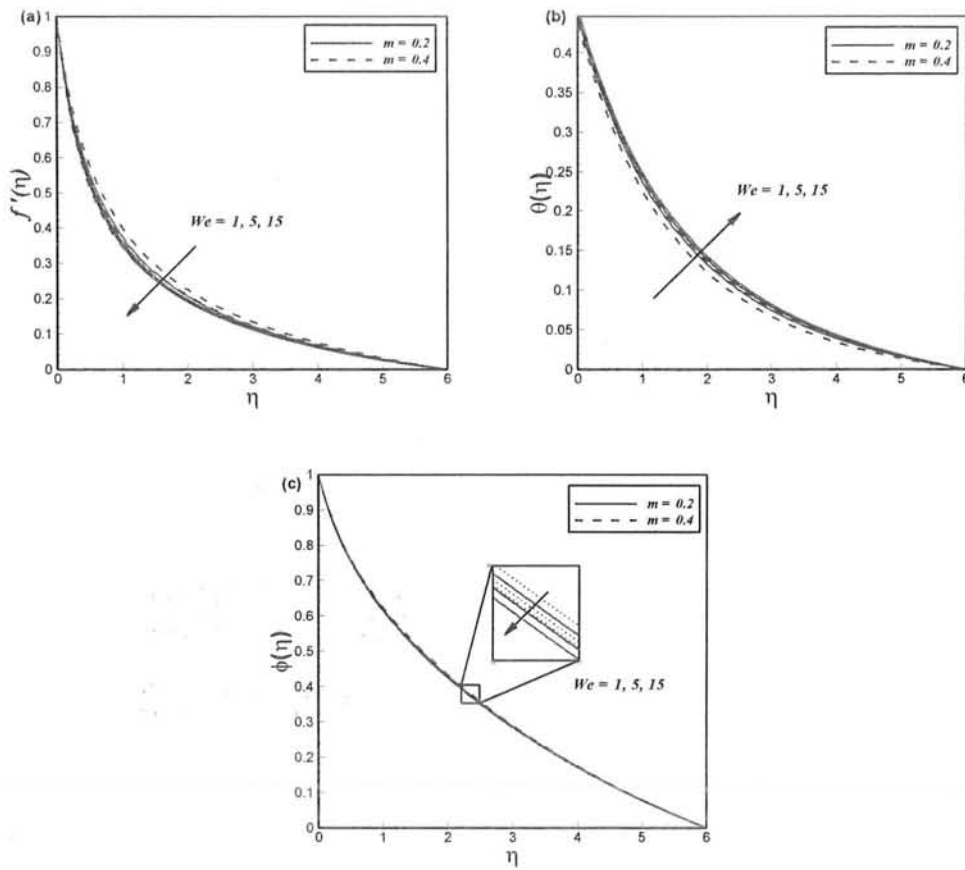
Fig. 9. 2: Impact of We on **(a)** $f'(\eta)$, **(b)** $\theta(\eta)$ and **(c)** $\phi(\eta)$ for changing m.
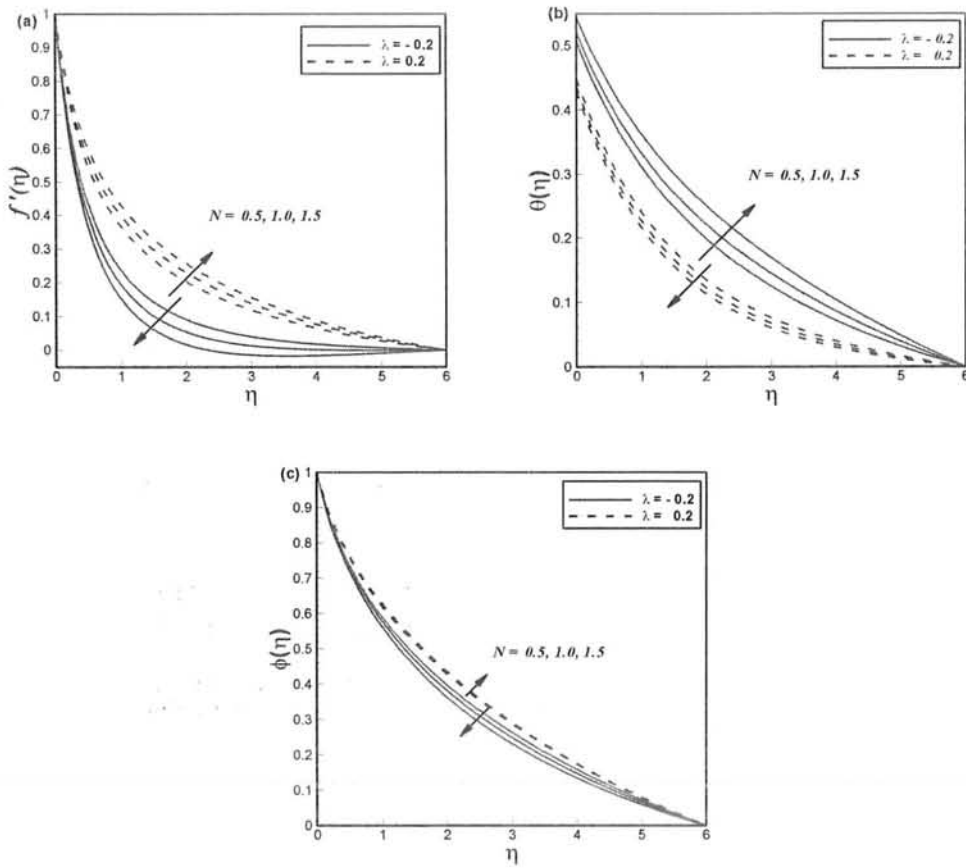
Fig. 9. 3: Impact of N on **(a)** $f'(\eta)$, **(b)** $\theta(\eta)$ and **(c)** $\phi(\eta)$ for changing λ.

Fig. 9. 4: Impact of γ^* on $f'(\eta)$, $\theta(\eta)$ and $\phi(\eta)$.
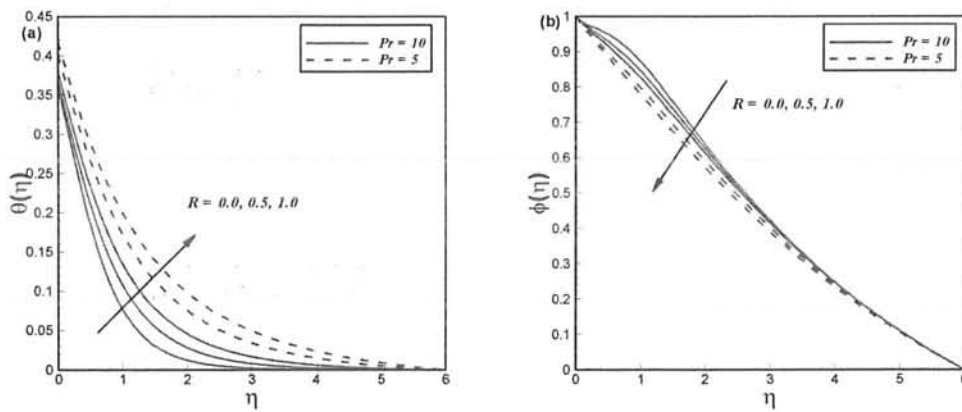
Fig. 9. 5: Impact of R on **(a)** $\theta(\eta)$ and **(b)** $\phi(\eta)$ for changing Pr.
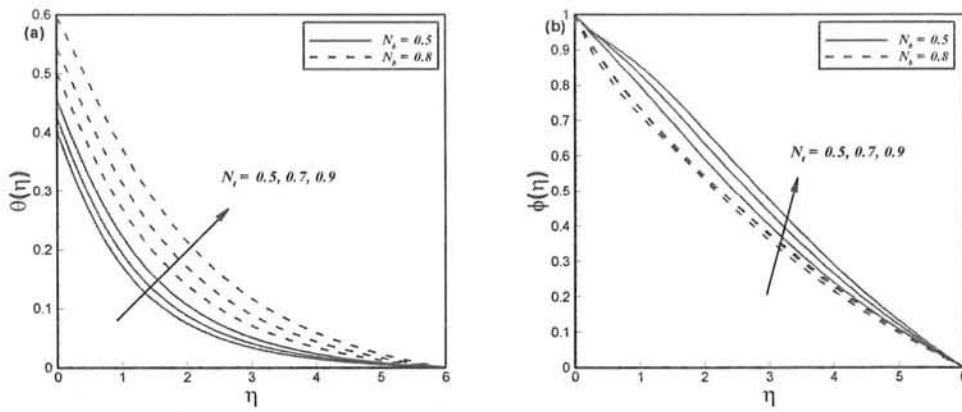
Fig. 9.6: Impact of N_t on **(a)** $\theta(\eta)$ and **(b)** $\phi(\eta)$ for changing N_b.
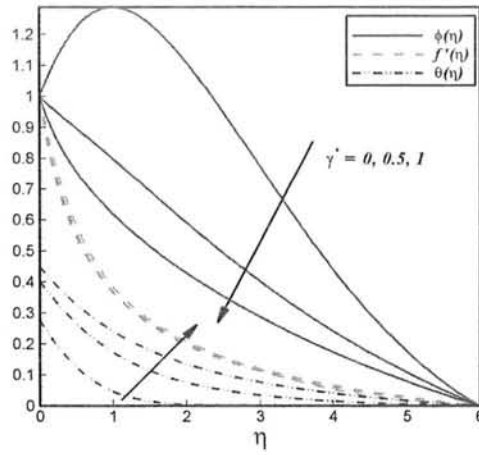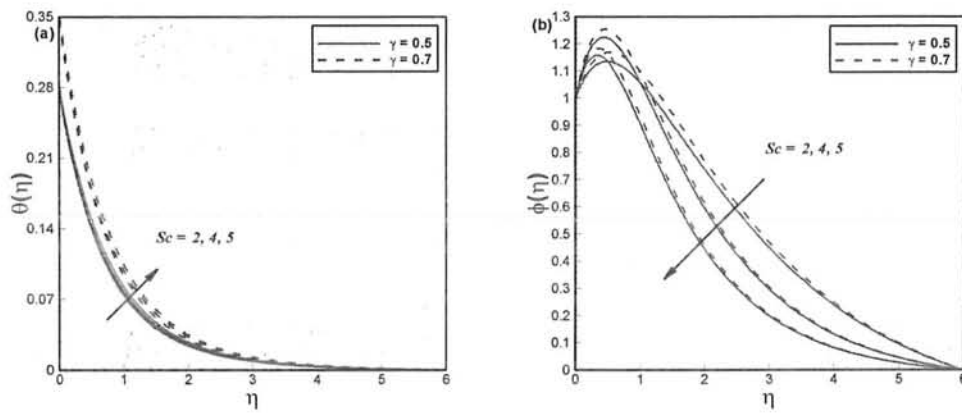

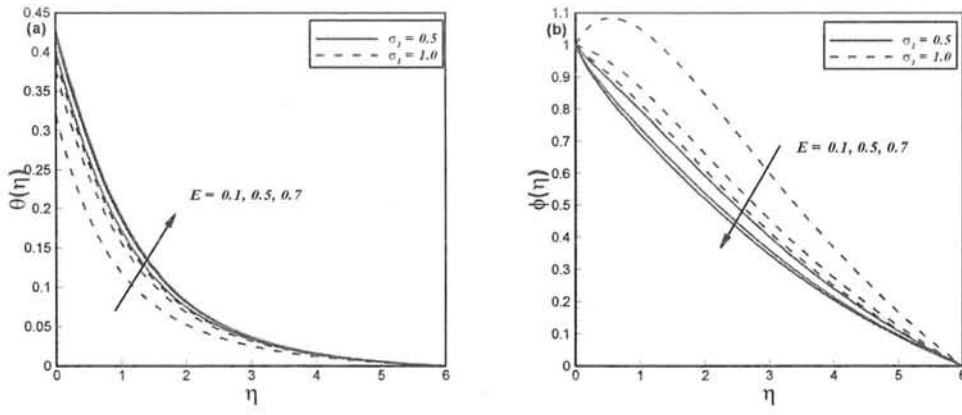**Fig. 9.7:** Impact of Sc on **(a)** $\theta(\eta)$ and **(b)** $\phi(\eta)$ for changing γ.

Fig. 9.8: Impact of E on **(a)** $\theta(\eta)$ and **(b)** $\phi(\eta)$ for changing σ_1.

Table 9.2: The outcomes of skin friction coefficient, Nusselt number and Sherwood number related to different emerging parameters.

N	γ^*	R	N_b	N_t	γ	Sc	E	δ	σ_1	n	$Re_L^{\frac{1}{2}}C_f$	$Re_L^{-\frac{1}{2}}Nu$	$Re_L^{-\frac{1}{2}}Sh$
0.5	0.5	0.5	0.5	0.5	0.5	0.5	0.1	0.1	0.5	0.5	0.628491	0.449104	0.235664
1											0.575448	0.457402	0.238496
1.5											0.522958	0.463821	0.243302
	0.7										0.659027	0.430177	0.452064
	0.9										0.696252	0.417797	0.644364
		0.6									0.626632	0.476140	0.240699
		0.7									0.625034	0.503047	0.245493
			0.6								0.620564	0.426303	0.285208
			0.7								0.619316	0.401264	0.323607
				0.6							0.625841	0.440663	0.222967
				0.7							0.624892	0.431217	0.217066
					0.6						0.619352	0.493892	0.227328
					0.7						0.615512	0.530763	0.221487
						0.6					0.628774	0.452747	0.189903
						0.7					0.628514	0.456526	0.142867
							0.5				0.630050	0.434142	0.370599
							0.7				0.628166	0.429115	0.416220
								1			0.626737	0.452151	0.198268

2			0.628447	0.455287	0.160716
	1		0.623952	0.510123	0.339487
	1.5		0.602819	0.602550	1.463077
		1	0.626581	0.449540	0.231726
		1.5	0.626527	0.449920	0.227818

Chapter 10

Concluding Remarks and

Future Research Directions

The aim behind the research work presented in the current thesis was to explore the boundary layer phenomenon during flow and heat transfer of Cross fluid. Although, literature reveals that during past few decades significant efforts have been made to explore boundary layer flow problems but unfortunately no work has been notified regarding the boundary layer flow of Cross fluid. The present thesis has opened a new door for the researchers by presenting boundary layer equations for Cross fluid in Cartesian as well as in cylindrical polar coordinates. This chapter provides a short review of the computations carried out in the thesis and thus grants the main findings of the research work. Moreover, it also bestows valuable suggestions regarding the future considerations in the field of fluid mechanics.

10.1 General Overview of the Thesis

This thesis reports the boundary layer flow and transfer of heat in Cross fluid along stretching surfaces. Current investigations can be characterized in view of different flow configurations including the planar stretching sheet, radially stretching sheet, stretching cylinder and wedge flow. Various flow situations are accounted covering the stagnation point flow, mixed convection flow, nano boundary layer flow and

Falkner-Skan flow. Moreover, the heat transfer analysis is incorporated by taking into account several effects like the variable thermal conductivity, linear and non-linear thermal radiation, heat generation/absorption and Arrhenius activation energy. In addition to conventional no-slip boundary conditions we have also applied different boundary conditions including the convective boundary condition, Newtonian heat and mass condition, melting heat transfer, zero-nanoparticle mass flux and multiple slip boundary conditions. The leading equations consisting of PDEs for each problem are initially modelled and then reduced to corresponding ODEs through appropriate transformations. The equations are numerically manipulated by invoking numerical techniques namely the shooting method and the bvp4c technique. The numerical results are validated by presenting suitable comparisons with existing solutions for special cases. The outcomes are displayed by the help of graphs for velocity, temperature and concentration distributions. Additionally, the numeric data is also provided in the form of tables of skin friction coefficient, Nusselt number together with Sherwood number.

10.2 Main Findings

The present work claimed to fill the gap in the existing literature by bestowing notable work on Cross fluid. A detail analysis of the current thesis helped us to summarize the main findings of the problems. The graphical behavior and tabulated numerical data lead us to conclude that:

- It was seen that a decline in the velocity profile occurs corresponding to growth in Weissenberg number. However, the temperature profiles indicated a progressive pattern.

- An enlargement in power-law index resulted in lifting of fluid velocity while a decline in thermal boundary layer structures was seen.

- The momentum boundary layer became thicker for buoyancy aided flow $(\lambda > 0)$ as compared to buoyancy opposed flow $(\lambda > 0)$ for the growing values of power-law index, Weissenberg number, thermal radiation parameter and also Prandtl number.

- The variable conductivity parameter elevated the structures related to thermal boundary layer while an implementation of thermal slip condition resulted in the decay of thermal boundary layer.

- The coefficient of skin friction was enhanced for growth in momentum slip parameter. While the thermal and solutal slips resulted in a decline of rat of transfer of heat and mass, respectively.

- The thermal and also solutal conjugate parameters resulted in an enhancement of fluid temperature along with concentration fields.

- The growing values of wedge angle parameter implied a boost in fluids velocity, but the thickness of momentum boundary layer gradually lowers.

- The Nusselt number and Sherwood number exhibited a declining trend corresponding to heat generation and absorption cases.

- The melting parameter resulted in strengthening the momentum and also the thermal boundary layer structures.

- By escalating the Weissenberg number, velocity and fluids temperature behaved oppositely for cases $A > 1$ and $A < 1$.

- In general, the thermal along with concentration boundary layer structures are enhanced by considering hydromagnetic flow $M > 0$ while momentum boundary layer structures exhibited diminishing trend.

- The temperature along with nanoparticle concentration profiles exhibited same ascending trend corresponding to growing thermophoresis parameter but by uplifting Brownian motion parameter the concentration boundary layer structures are lessened.

10.3 Future Suggestions

The study done in this thesis contemplates the flow along with heat transfer prospects of the Cross fluid. Although, various investigations are carried out in the present work by examining numerous effects and boundary conditions corresponding to flow together with heat transfer mechanisms but still there is a need of further work to be done in the current field. Firstly, we have solved our problems in view of assumption of steady flow case. The same analysis can be done in the light of unsteady flow case. Secondly, we have restricted our work to two-dimensional flow problems. It can be taken forward for covering three-dimensional flows regarding Cross fluid. Furthermore, the mathematical modelling of Cross fluid can be pursued by taking into account the non-zero infinite shear rate viscosity. Moreover, the Cross fluid model could be explored in consideration of curvilinear coordinates. The extension can be done regarding rotating disk, channel flow and many more.

Bibliography

[1] R.B. Bird, C.F. Curtiss, R.C. Armstrong and O. Hassager, Dynamics of Polymeric Liquids, *Wiley*, New York, (1987).

[2] R.B. Bird, Useful non-Newtonian models, *Annual Review of Fluid Mechanics*, **8** (1976) 13-34.

[3] I.A. Hassanien, A.A. Abdullah and R.S.R. Gorla, Flow and heat transfer in a power-law fluid over a non-isothermal stretching sheet, *Math. Comput. Modell.*, **28** (1998) 105-116.

[4] S. Matsuhisa and R.B. Bird, Analytical and numerical solutions for laminar flow of the non-Newtonian Ellis fluid, *AIChE. J.*, **11** (1965) 588-595.

[5] A.W. Sisko, The flow of lubricating greases, *Ind. Eng. Chem.*, **50** (1958) 1789-1792.

[6] M.M. Cross, Rheology of non-Newtonian fluids: A new flow equation for pseudoplastic systems, *J. Colloid Sci.*, **20** (1965) 417-437.

[7] H.A. Barnes, J.F. Hutton and K. Walters, An Introduction to Rheology, *Elsevier Science*, Amsterdam, (1989).

[8] M.A. Rao, Rheology of Fluid, Semisolid, and Solid Foods, *Springer*, New York, (2014).

[9] J.F. Steffe, Rheological Methods in Food Process Engineering, *Freeman*, USA, (1992).

[10] Y.X. Gan, Continuum Mechanics-Progress in Fundamentals and Engineering Applications, *InTech, China*, (2012).

[11] E.C. Bingham, Fluidity and Plasticity, *McGraw-Hill*, New York, (1922).

[12] M.P. Escudier, I.W. Gouldson , A.S. Pereira, F.T. Pinho and R.J. Poole, On the reproductivity of the rheology of shear-thinning liquids, *J. Non-Newtonian Fluid Mech.*, **97** (2001) 99-124.

[13] J. Xie and Y.C. Jin, Parameter determination for the Cross rheology equation and its application to modeling non-Newtonian flows using the WC-MPS method, *Eng. Appl. Comput. Fluid Mech.*, **10** (2015) 111-129.

[14] B.C. Sakiadis, Boundary layer behavior on continuous solid surfaces, *AICHE J.*, **7** (1961) 26-28.

[15] L.J. Crane, Flow past a stretching plate, *Z. Angew. Math. Phys.* (*ZAMP*), **21** (1970) 645-647.

[16] W.H.H. Banks, Similarity solutions of the boundary layer equations for a stretching wall, *Journal de Mecanique Theorique et Appliquee*, **2** (1983) 92-375.

[17] H.I. Andersson and K.H. Bech, Magnetohydrodynamic flow of a power-law fluid over a stretching sheet, *Int. J. Non-Linear Mech.*, **27** (1992) 929-936.

[18] T.G. Howell, D.R. Jeng and K.J.D. Witt, Momentum and heat transfer on a continuous moving surface in a power law fluid, *Int. J. Heat Mass Transf.*, **40** (1997) 1853-1861.

[19] M. Khan and M. Rahman, Flow and heat transfer to modified second grade fluid over a non-linear stretching sheet, *AIP Advs.*, **5** (2015) 087157.

[20] P.D. Ariel, Axisymmetric flow due to a stretching sheet with partial slip, *Comput. Math. Appl.*, **54** (2007) 1169-1183.

[21] M. Sajid, T. Hayat, S. Asghar and K. Vajravelu, Analytic solution for axisymmetric flow over a nonlinearly stretching sheet, *Arch. Appl. Mech.*, **78** (2008) 127-134.

[22] A. Shahzad R. Ali and M. Khan, On the exact solution for axisymmetric flow and heat transfer over a nonlinear radially stretching sheet, *Chin. Phys. Lett.*, **29** (2012) 084705.

[23] M. Khan, R. Malik and A. Munir, Mixed convective heat transfer to Sisko fluid over a radially stretching sheet in the presence of convective boundary conditions, *AIP Advs.*, **5** (2015) 087178.

[24] S.U.S. Choi, Enhancing thermal conductivity of fluids with nanoparticles, in: The Proceedings of the 1995 ASME International Mechanical Engineering Congress and Exposition, San Francisco, USA, *ASME*, FED 231/MD, **66** (1995) 99-105.

[25] S.U.S. Choi, Z.G. Zhang, W. Yu, F.E. Lockwood and E.A. Grulke, Anomalously thermal conductivity enhancement in nanotube suspensions, *Appl. Phys. Lett.*, **79** (2001) 2252-2254.

[26] J. Buongiorno, Convective transport in nanofluids, *ASME J. Heat Transf.*, **128** (2006) 240-250.

[27] W.A. Khan and I. Pop, Boundary-layer flow of a nanofluid past a stretching sheet, *Int. J. Heat Mass Transf.*, **53** (2010) 2477-2483.

[28] O.D. Makinde and A. Aziz, Boundary layer flow of a nanofluid past a stretching sheet with a convective boundary condition, *Int. J. Therm. Sci.*, **50** (2011) 1326-1332.

[29] A.V. Kuznetsov and D.A. Nield, Natural convective boundary-layer flow of a nanofluid past a vertical plate: A revised model, *Int. J. Therm. Sci.*, **77** (2014) 126-129.

[30] R.U. Haq, S. Nadeem, Z.H Khan and N.S. Akbar, Thermal radiation and slip effects on MHD stagnation point flow of nanofluid over a stretching sheet, *Physica E*, **65** (2015) 17-23.

[31] M.U. Rahman, M. Khan and M. Manzur, Boundary layer flow and heat transfer of a modified second grade nanofluid with new mass flux condition, *Results Phys.*, **10** (2018) 594-600.

[32] T. Sarpkaya, Flow of non-Newtonian fluids in a magnetic field, AIChE J., **7** (1961) 324-328.

[33] K.B. Pavlov, Magnetohydrodynamic flow of an incompressible viscous fluid caused by deformation of a plane surface, *Magninaya Gidrodinamika* (*USSR*), **4** (1974) 146-148.

[34] H.I. Andersson, MHD flow of a viscoelastic fluid past a stretching surface, *Acta Mech.*, **95** (1992) 227-230.

[35] K.V. Prasad and K. Vajravelu, Heat transfer in the MHD flow of a power law fluid over a non-isothermal stretching sheet, *Int. J. Heat Mass Transf.*, **52** (2009) 4956-4965.

[36] K. Heimenz, Die Grenzchicht an einem in den gleichformingen Flussigkeitsstrom eingetauchten graden Kreiszylinder, Dinglers *Polytech. J.*, **326** (1911) 321-324.

[37] F. Homann, Der Einfluss grosser Zahigkeit bei der Stromung um den Zylinder

und um die Kugel, *Zeitschrift für Angewandte Mathematik und Mechanik*, **16** (1936) 153-164.

[38] T.C. Chiam, Stagnation point flow towards a stretching plate, *J. Phys. Soc. Jpn.*, **63** (1994) 2443-2444.

[39] T.R. Mahapatra and A.S. Gupta, Heat transfer in stagnation-point flow towards a stretching sheet, *Heat Mass Transf.*, **38** (2002) 517-521.

[40] T.R. Mahapatra, S.K. Nandy and A.S. Gupta, Analytical solution of magnetohydrodynamic stagnation-point flow of a power-law fluid towards a stretching surface, *Appl. Math. Comput.*, **215** (2009) 1696-1710.

[41] N.S. Akbar, S. Nadeem, R.U. Haq and Z.H. Khan, Radiation effects on MHD stagnation point flow of nanofluid towards a stretching surface with convective boundary condition, *Chinese J. Aeronautics*, **26** (2013) 1389-1397.

[42] T.Y. Wang, Mixed convection heat transfer from a vertical plate to non-Newtonian fluids, *Int. J. Heat Fluid Flow*, **16** (1995) 56-61.

[43] C.H. Chen, Laminar mixed convection adjacent to vertical continuously stretching sheet, *Heat Mass Transf.*, **33** (1998) 471-476.

[44] C.H. Chen, Magneto-hydrodynamic mixed convection of a power-law fluid past a stretching surface in the presence of thermal radiation and internal heat generation/absorption, *Int. J. Non-Linear Mech.*, **44** (2009) 596-603.

[45] M. Turkyilmazoglu, The analytical solution of mixed convection heat transfer and fluid flow of a MHD viscoelastic fluid over a permeable stretching surface, *Int. J. Mech. Sci.*, **77** (2013) 263-268.

[46] S.V. Subhashini, N. Samuel and I. Pop, Effects of buoyancy assisting and

opposing flows on mixed convection boundary layer flow over a permeable vertical surface, *Int. Commun. Heat Mass Transf.*, **38** (2011) 499-503.

[47] D. Pal and G. Mandal, Influence of thermal radiation on mixed convection heat and mass transfer stagnation-point flow in nanofluids over stretching/shrinking sheet in a porous medium with chemical reaction, *Nucl. Eng. Des.*, **273** (2014) 644-652.

[48] M.U. Rahman, M. Manzur and M. Khan, Mixed convection heat transfer to modified second grade fluid in the presence of thermal radiation, *J. Mol. Liq.*, **223** (2016) 217-223.

[49] A. Aziz, A similarity solution for laminar thermal boundary layer over a flat plate with a convective surface boundary condition, *Commun. Nonlinear Sci. Numer. Simulat.*, **14** (2009) 1064-1068.

[50] O.D. Makinde and A. Aziz, MHD mixed convection from a vertical plate embedded in a porous medium with a convective boundary condition, *Int. J. Therm. Sci.*, **49** (2010) 1813-1820.

[51] S. Yao, T. Fang and Y. Zhong, Heat transfer of a generalized stretching/shrinking wall problem with convective boundary conditions, *Commun. Nonlinear Sci. Numer. Simulat.*, **16** (2011) 752-760.

[52] A. Shahzad and R. Ali, MHD flow of a non-Newtonian power law fluid over a vertical stretching sheet with the convective boundary condition, *Walailak J. Sci. Tech. (WJST)*, **10** (2012) 43-56.

[53] R. Malik, M. Khan, A. Munir and W.A. Khan, Flow and heat transfer in Sisko fluid with convective boundary condition, *PLoS ONE*, 9(10): e107989. doi:

10.1371/journal.pone.0.07989, PMID:25285822 (2014).

[54] J.H. Merkin, Natural-convection boundary-layer flow on a vertical surface with Newtonian heating, *Int. J. Heat Fluid Flow*, **15** (1994) 392-398.

[55] M.Z. Salleh, R. Nazar and I. Pop, Boundary layer flow and heat transfer over a stretching sheet with Newtonian heating, *J. Taiwan Inst. Chem. Engrs.*, **41** (2010) 651-655.

[56] M.U. Rahman, M. Khan and M. Manzur, Homogeneous-heterogeneous reactions in modified second grade fluid over a non-linear stretching sheet with Newtonian heating, *Results Phys.*, **7** (2017) 4364-4370.

[57] S. Qayyum, T. Hayat, S.A. Shehzad and A. Alsaedi, Effect of a chemical reaction on magnetohydrodynamic (MHD) stagnation point flow of Walters-B nanofluid with newtonian heat and mass conditions, *Nucl. Eng. Technol.*, **49** (2017) 1636-1644.

[58] T. Hayat, M. I. Khan, M. Waqas and A. Alsaedi, Newtonian heating effect in nanofluid flow by a permeable cylinder, *Results Phys.*, **7** (2017) 256-262.

[59] C.L.M.H. Navier, Memoire sur les lois du movement des fluids, *Men. Acad. R. Sci. Inst. France*, **6** (1827) 389-440.

[60] E. Schnell, Slippage of water over non-wettable surfaces, *J. Appl. Phy.*, **27** (1956) 1149-1152.

[61] H.I. Andersson, Slip flow past a stretching surface, *Acta Mech.*, **158** (2002) 121-125.

[62] M. Turkyilmazoglu, Exact analytical solutions for heat and mass transfer of MHD slip flow in nanofluids, *Chemical Eng. Sci.*, **84** (2012) 182-187.

[63] R. Ellahi and M. Hameed, Numerical analysis of steady non-Newtonian flows with heat transfer analysis, MHD and nonlinear slip effects, *Int. J. Numer. Methods Heat Fluid Flow*, **22** (2012) 24-38.

[64] W. Ibrahim and B. Shankar, MHD boundary layer flow and heat transfer of a nanofluid past a permeable stretching sheet with velocity, thermal and solutal slip boundary conditions, *Comput. Fluids*, **75** (2013) 1-10.

[65] L. Roberts, On the melting of a semi-infinite body of ice placed in a hot stream of air, *J. Fluid Mech.*, **4** (1958) 505-528.

[66] M. Epstein and D.H. Cho, Melting heat transfer in steady laminar flow over a flat plate, *J. Heat Transf.*, **98** (1976) 531-533.

[67] M.M. Chen, R. Farhadieh, J.L. Baker, On free convection melting of a solid immersed in a hot dissimilar fluid. *Int. J. Heat Mass Transf.*, **29** (1986) 1087-1093.

[68] A.Y. Bakier, Aiding and opposing mixed convection flow in melting from a vertical flat plate embedded in a porous medium, *Transp. Porous Media*, **29** (1997) 127-139.

[69] A. Ishak, R. Nazar, N. Bachok and I. Pop, Melting heat transfer in steady laminar flow over a moving surface, *Heat Mass Transf.*, **46** (2010) 463-468.

[70] T. Hayat, A. Shafiq and A. Alsaedi, Characteristics of magnetic field and melting heat transfer in stagnation point flow of Tangent-hyperbolic liquid, *J. Magn. Magn. Mater.*, **405** (2016) 97-106.

[71] T. Hayat, M. Farooq, A. Alsaedi and Z. Iqbal, Melting heat transfer in the stagnation point flow of Powell–Eyring fluid, *J. Thermophysics Heat Transf.*,

27 (2013) 761-766.

[72] Hashim, M. Khan and A.S. Alshomrani, Characteristics of melting heat transfer during flow of Carreau fluid induced by a stretching cylinder, *Eur. Phys. J. E*, (2017) doi: 10.1140/epje/i2017-11495-6.

[73] T.C. Chiam, Heat transfer with variable conductivity in a stagnation-point flow towards a stretching sheet, *Int. Commun. Heat Mass Transf.*, **23** (1996) 239-248.

[74] T.C. Chiam, Heat transfer in a fluid with variable thermal conductivity over a linearly stretching sheet, Acta Mech., **129** (1998) 63-72.

[75] K. Vajravelu, K.V. Prasad and C. Ng, Unsteady convective boundary layer flow of a viscous fluid at a vertical surface with variable fluid properties, *Nonlinear Anal.: Real World Appl.*, **14** (2013) 455-464.

[76] K. Vajravelu and J. Nayfeh, Hydromagnetic convection at a cone and a wedge, *Int. Comm. Heat Mass Transf.*, **19** (1992) 701-710.

[77] M. Sheikh and Z. Abbas, Effects of thermophoresis and heat generation/absorption on MHD flow due to an oscillatory stretching sheet with chemically reactive species, *J. Magnetism Magnetic Materials*, **396** (2015) 204-213.

[78] T. Hayat, T. Muhammad, S.A. Shehzad and A. Alsaedi, An analytical solution for magnetohydrodynamic Oldroyd-B nanofluid flow induced by a stretching sheet with heat generation/absorption, *Int. J. Therm. Sci.*, **111** (2017) 274-288.

[79] A.A. Mohammadein and M.F.E. Amin, Thermal radiation effects on power-law fluids over a horizontal plate embedded in a porous medium, *Int. Comm. Heat Mass Transf.*, **27** (2000) 1025-1035.

[80] S.K. Khan, Heat transfer in a viscoelastic fluid flow over a stretching surface with heat source/sink, suction/blowing and radiation, *Int. J. Heat Mass Transf.*, **49** (2006) 628-639.

[81] R. Cortell, Suction, viscous dissipation and thermal radiation effects on the flow and heat transfer of a power-law fluid past an infinite porous plate, *Chem. Eng. Res. Des.*, **89** (2011) 85-93.

[82] Pantokratoras and T. Fang, Sakiadis flow with nonlinear Rosseland thermal radiation, *Phys. Scr.*, **87** (2013) 015703.

[83] R. Cortell, Fluid flow and radiative nonlinear heat transfer over a stretching sheet, *J. King Saud University*, **26** (2014) 161-167.

[84] A. Mushtaq, M. Mustafa, T. Hayat and A. Alsaedi, Nonlinear radiative heat transfer in the flow of nanofluid due to solar energy: A numerical study, *J. Taiwan Inst. Chem. Eng.*, **45** (2014) 1176-1183.

[85] E.L. Cussler, Diffusion mass transfer in fluid systems, *Cambridge University Press*, London, (1998).

[86] K. Das, Effect of chemical reaction and thermal radiation on heat and mass transfer flow of MHD micropolar fluid in a rotating frame of reference, *Int. J. Heat Mass Transf.*, **54** (2011) 3505-3513.

[87] K. Bhattacharyya, Dual solutions in boundary layer stagnation-point flow and mass transfer with chemical reaction past a stretching/shrinking sheet, *Int. Commun. Heat Mass Transf.*, **38** (2011) 917-922.

[88] Bestman, Natural convection boundary layer with suction and mass transfer in a porous medium, *Int. J. Eng. Res.*, **14** (1990) 389-396.

[89] O.D. Makinde, P.O. Olanrewaju and W.M. Charles, Unsteady convection with chemical reaction and radiative heat transfer past a flat porous plate moving through a binary mixture, *Africka Matematika*, **22** (2011) 65-78.

[90] K.A. Maleque, Effects of binary chemical reaction and activation energy on MHD boundary layer heat and mass transfer flow with viscous dissipation and heat generation/absorption, *ISRN Thermodyn.*, 2013. http://dx.doi.org/10.1155/2013/284637. Article ID 284637.

[91] K.A. Maleque, Effects of exothermic/endothermic chemical reactions with Arrhenius activation energy on MHD free convection and mass transfer flow in presence of thermal radiation, *J. Thermodyn.*, 2013. http://dx.doi.org/10.1155/2013/692516. Article ID 692516.

[92] F.G. Awad, S. Motsa and M. Khumalo, Heat and mass transfer in unsteady rotating fluid flow with binary chemical reaction and activation energy, *PLoS ONE*, 9 (2014): e107622. http://dx.doi.org/10.1371/journal.pone.0107622.

[93] M. Mustafa, J.A. Khan, T. Hayat and A. Alsaedi, Buoyancy effects on the MHD nanofluid flow past a vertical surface with chemical reaction and activation energy, *Int. J. Heat Mass Transf.*, **108** (2017) 1340-1346.

[94] L.V.M. Falkner and S.W. Skan, Some approximate solutions of the boundary layer equations, *Philos. Mag.*, **12** (1931) 865-896.

[95] D.H. Hartree, On an equation occurring in Falkner and Skan's approximate treatment of the equations of the boundary layer, *Proc. Camb. Philos. Soc.*, **33** (1937) 223-239.

[96] K.R. Rajagopal, A.S. Gupta and T.Y. Na, A note on the Falkner-Skan flows of a

transfer of nanofluid over nonlinearly stretching sheet, *Appl. Math. Mech.*, **33** (2012) 923-930.

[107] C.Y. Wang, Free convection on a vertical stretching surface, *J. Appl. Math. Mech.*, **69** (1989) 418-420.

[108] R.S.R. Gorla and I. Sidawi, Free convection on a vertical stretching surface with suction and blowing, *Appl. Sci. Res.*, **52** (1994) 247-257.

[109] M.A.A. Hamad, Analytical solution of natural convection flow of a nanofluid over a linearly stretching sheet in the presence of magnetic field, *Int. Commun. Heat Mass Transf.*, **38** (2011) 487-492.

[110] M.Q. Brewster, Thermal Radiative Transfer Properties, John Wiley and Sons, (1972).

[111] W.A. Khan and I. Pop, Boundary-layer flow of a nanofluid past a stretching sheet, *Int. J. Heat Mass Transf.*, **53** (2010) 2477-2483.

[112] M.S. Abel, P.S. Datti and N. Mahesha, Flow and heat transfer in a power-law fluid over a stretching sheet with variable thermal conductivity and non-uniform heat source, *Int. J. Heat Mass Transf.*, **52** (2009) 2902-2913.

[113] B.L. Kuo, Application of the differential transformation method to the solutions of Falkner-Skan wedge flow, *Acta Mech.*, **164** (2003) 161-174.

[114] A. Ishaq, R. Nazar and I. Pop, Moving wedge and flat plate in a micropolar fluid, *Int. J. Eng. Sci.*, **44** (2006) 1225-1236.

[115] M. Khan and A. Shahzad, On axisymmetric flow of Sisko fluid over a radially stretching sheet, *Int. J. Non-Linear Mech.*, **47** (2012) 999-1007.

[116] S. Rosseland, Astrophysik und Atom-Theoretische Grundlagen, *Springer*

Verlag, Berlin (1931) 41-44.

[117] M. Khan, A. Munir and A. Shahzad, Convective Heat Transfer to Sisko Fluid over a Nonlinear Radially Stretching Sheet, Heat Transfer Studies and Applications; Kazi, S.N., Ed.; *Intech: Rijeka*, Croatia, (2015) 341-361.

[118] K. Vajravelu, K.V. Prasad and S.R. Santhi, Axisymmetric magneto-hydrodynamic (MHD) flow and heat transfer at a non-isothermal stretching cylinder, *Appl. Math. Comput.*, **219** (2012) 3993-4005.

[119] E. Fehlberg, Classical Runge-Kutta formulas of fourth and lower order with step-width control and their application to heat conduction problems, *Computing*, **6** (1970) 61-71.

[120] L.F. Shampine, I. Gladwell and S. Thompson, Solving ODEs with MATLAB, (1st Edn.), *Cambridge University Press*, Cambridge, (2003).